

Classifying benthic habitats and deriving bathymetry at the Caribbean Netherlands using multispectral Imagery.

Case study of St. Eustatius

P.(Paula) Nieto², C.A. (Sander) Múcher¹,
H.W.G. (Erik) Meesters, J.G.P.W (Jan) Clevers²

IMARES rapport C143/13; Alterra rapport 2467



IMARES Wageningen UR

Institute for Marine Resources & Ecosystem Studies

¹Alterra, Wageningen UR

²Laboratory of Geo-Information Science and Remote Sensing, Wageningen University

Client:

Ministry of Economic Affairs
Postbus 20401
2500 EK The Hague
The Netherlands

BO-11-011.05-002

Publication date:

September 2013

IMARES is:

- an independent, objective and authoritative institute that provides knowledge necessary for an integrated sustainable protection, exploitation and spatial use of the sea and coastal zones;
- an institute that provides knowledge necessary for an integrated sustainable protection, exploitation and spatial use of the sea and coastal zones;
- a key, proactive player in national and international marine networks (including ICES and EFARO).

This report is part of the Wageningen University BO research program (BO-11-011.05-002) and has been financed by the Ministry of Economic Affairs (EZ) under project number 43082011.08.

Name Paula Nieto
Students registration number 830603602010
Programme Master of Science Geo-Information Science and Remote Sensing
Specialisation
Department: Laboratory of Geo-Information Science and Remote Sensing, Wageningen University and Research Centre
Supervisors: Dr. ir. Jan Clevers, dr. ir. Sander Mûcher, dr. Erik Meesters
Place: Wageningen
Date: September 2013

| | | | |
|---|--|---|--|
| P.O. Box 68 1970 AB IJmuiden Phone: +31 (0)317 48 09 00 Fax: +31 (0)317 48 73 26 E-Mail: imares@wur.nl www.imares.wur.nl | P.O. Box 77 4400 AB Yerseke Phone: +31 (0)317 48 09 00 Fax: +31 (0)317 48 73 59 E-Mail: imares@wur.nl www.imares.wur.nl | P.O. Box 57 1780 AB Den Helder Phone: +31 (0)317 48 09 00 Fax: +31 (0)223 63 06 87 E-Mail: imares@wur.nl www.imares.wur.nl | P.O. Box 167 1790 AD Den Burg Texel Phone: +31 (0)317 48 09 00 Fax: +31 (0)317 48 73 62 E-Mail: imares@wur.nl www.imares.wur.nl |
|---|--|---|--|

© 2013 IMARES Wageningen UR

IMARES, institute of Stichting DLO is registered in the Dutch trade record nr. 09098104, BTW nr. NL 806511618

The Management of IMARES is not responsible for resulting damage, as well as for damage resulting from the application of results or research obtained by IMARES, its clients or any claims related to the application of information found within its research. This report has been made on the request of the client and is wholly the client's property. This report may not be reproduced and/or published partially or in its entirety without the express written consent of the client.

A_4_3_2-V13.2

Abstract

Benthic habitats (habitats occurring at the bottom of a water body) and coral reef ecosystems provide many functions. Currently, however, worldwide coral reefs are threatened by a number of factors and are degrading rapidly. Benthic maps are important for management, research and planning, but the benthic communities around St. Eustatius have not yet been accurately mapped or described.

Remote sensing imagery has been found to be a useful tool in providing timely and up-to-date information for benthic mapping and offers an approach that may complement the limitations of field sampling. Remote sensing in water, however, presents challenges mainly due to the complex physical interactions of absorption and scattering between water and light. Shorter wavelengths (~450 nm) penetrate deepest into the water column and longer wavelengths (~500-750 nm) are more rapidly absorbed and scattered. Therefore, the potential extent of use of remote sense imagery in the oceans relies more on shorter wavelengths (blue band), which have inherently noisier signals due to atmospheric effects.

This research explores the utility of multispectral imagery to identify and classify marine benthic habitats in the Dutch Caribbean island of St Eustatius. These include the comparison of two sensors with different spatial and spectral resolution, QuickBird (2.4m, 4 bands) and WorldView-2 (2.0m, 8 bands) for mapping benthic habitats. The study first investigates the existing methodologies for benthic habitat classification. The benefits of atmospheric correction, corrections for sun-glint effect and water column attenuation on the accuracy of classification maps are also assessed. Then, an object and pixel-based supervised classifications for the characterization of sea grass, sand and coral are performed. This research also evaluates the possibility to extract water depth from multispectral satellite imagery by the use of a ratio transform method. Bathymetric data is important for water column correction, to improve the classification accuracy and for the study of the ecology of the habitats.

Results showed that the best results for pixel-based image classification in QuickBird and WorldView-2 imagery were obtained after deglinting the image, with accuracies of 49.3% and 51.9% respectively. The sun-glint removal method improved the total accuracy of the benthic habitat mapping by 3.4% for QuickBird and by 6.3% for WorldView-2. Object-based classification provided slightly better classification results, with a 53.7% accuracy for QuickBird and 56.9% accuracy for WorldView-2. Therefore, it can be concluded that an object-oriented approach to image classification shows potential for improving benthic mapping. The classification accuracy did not increase after compensation for water column effects. The usefulness of the classification results of this study is still limited since almost 50% was wrongly classified, however, including additional variables (e.g. depth or exposure) in the classification algorithm may substantially increase classification success. This should be explored in follow-up research.

The effectiveness of the ratio method to calculate the bathymetry using multispectral imagery has been confirmed. Results can be useful, especially if no other bathymetric data are available. The coefficients of determination (r^2) achieved are statistically significant, 0.66 for QuickBird, and 0.41 for WorldView-2 (BG ratio) for a linear relation. The root mean square errors are 4.02 m for QuickBird and 5.11 m for WorldView-2. We show that the ratio method works better for shallow areas, with a root mean square error of 2.32 m and 2.47 m, respectively. Biologically a depth difference of 2.5m, especially in shallow areas, can however make a large difference in the composition of the benthic community. Results also indicate that the accuracy of the ratio method is sensitive to bottom type (e.g. sand gives the highest accuracy). Overall, better bathymetric values were obtained with QuickBird than with WorldView-2. Additional adjustments of the model, better ground-truthing data, and better satellite images may increase the accuracy of the estimates.

This research indicates how remote sensing can assist coral reef status and ecology assessments over large areas. At present the applicability is limited to only the coarsest habitat types, but further improvements in the classification are possible and should be explored.

Keywords: Benthic habitats, Coral reefs, Remote Sensing, QuickBird, WorldView-2, Sunlint, Water Column Correction, Pixel-based and Object-based Classification, Bathymetry.

List of acronyms

| | |
|---------|--|
| AOI | Area of Interest |
| BES | Bijzondere Eilandelijke Status |
| DCNA | The Dutch Caribbean Nature Alliance |
| DEM | Digital Elevation Model |
| DN | Digital Number (values) |
| EEZ | Exclusive Economic Zone |
| ENVI | Environment for Visualizing Images |
| GNSS | Global Navigation Satellite System |
| GPS | Global Positioning System |
| ICRI | International Coral Reef Initiative |
| IDL | Interactive Data Language |
| IMARES | Institute for Marine Resources and Ecosystem Studies |
| LIDAR | Light Detection And Ranging |
| MLC | Maximum Likelihood Classification |
| NACRI | The Netherlands Antilles Coral Reef Initiative |
| NIR | Near-Infrared Region |
| OBIA | Object-Based Image Analysis |
| QB | QuickBird |
| STENAPA | St. Eustatius National Parks Foundation |
| TNHS | The Netherlands Hydrographic Service |
| TOA | Top Of the Atmosphere |
| VHR | Very High Resolution |
| WV2 | WorldView-2 |

Table of Contents

| | |
|--|----|
| Abstract | 3 |
| List of acronyms | 5 |
| 1 Introduction | 8 |
| 1.1 Context | 8 |
| 1.2 Problem definition | 9 |
| 1.3 Objectives | 9 |
| 1.4 Research questions | 9 |
| 1.5 Structure of the report | 10 |
| 2 Literature review | 11 |
| 2.1 Remote sensing for shallow water coastal areas | 11 |
| 2.2 Remote sensing techniques for benthic mapping | 14 |
| 2.2.1 Pre-processing of imagery for benthic mapping | 14 |
| 2.2.2 Classification of imagery for benthic mapping | 20 |
| 2.2.3 Determination of water depth | 21 |
| 3 Methodology and processing | 23 |
| 3.1 Study area | 23 |
| 3.1.1 Description | 23 |
| 3.1.2 Benthic habitats of St. Eustatius | 24 |
| 3.1.3 Coral reefs status | 29 |
| 3.2 Data | 30 |
| 3.3 General Methodology | 33 |
| 3.3.1 Preparation of field data | 35 |
| 3.3.2 Pre-processing imagery | 35 |
| 3.3.3 Classification | 37 |
| 3.3.4 Comparison and accuracy assessment | 39 |
| 3.3.5 Bathymetry calculation | 39 |
| 3.3.6 Conversion to GIS | 40 |
| 4 Results | 41 |
| 4.1 Sunlint removal | 41 |
| 4.2 Water column correction | 43 |
| 4.3 Classification | 49 |
| 4.3.1 Pixel-based classification | 49 |
| 4.3.2 Object-based classification | 49 |
| 4.3.3 Comparison and accuracy assessment | 54 |
| 4.4 Bathymetry derivation | 54 |
| 5 Discussion | 64 |
| 5.1 Remote sensing of marine environments | 64 |
| 5.2 General comments about the characteristics of the data | 64 |
| 5.3 Decisions or limitations in the pre-processing methods | 65 |
| 5.4 Comparison between classification procedures | 67 |
| 5.5 Comparison between Sensors | 67 |
| 5.6 Bathymetry calculation | 68 |
| 6 Conclusions and Recommendations | 69 |
| 6.1 Conclusions | 69 |
| 6.2 Recommendations | 71 |
| 7 List of references | 73 |
| Quality assurance | 77 |
| Justification | 77 |
| Appendix 1. QuickBird and WorldView-2 files | 78 |
| Appendix 2. Final table of field data points | 79 |
| Appendix 3. Additional data | 83 |
| Appendix 4. Classifications zooms | 85 |
| Appendix 5. Validation | 93 |

1 Introduction

1.1 Context

Coral reef ecosystems provide many functions, services and goods to coastal populations (Herman, 2000) and its mapping is essential for management, research and planning (Miller et al., 2011). In 1997 coral ecosystems worldwide were estimated to provide US\$ 375 billion worth of ecological services, such as disturbance regulation, food production, recreation or cultural goods (Costanza et al., 1997). Currently, however, coral reefs are being degraded rapidly due to diverse factors such as destructive fishing practices, erosion processes inland, coral mining, marine pollution and sedimentation, global sea level and temperature rising, among others. Besides, at the global level, coral bleaching has recently become an additional major threat (Cesar, 2000). For all this, there is a need for coral reef ecologists and managers to develop a universal standard for monitoring the ecological status and trends of coral reefs (Knowlton and Jackson, 2008).

Thematic habitat maps are fundamental to characterize marine systems. For mapping purposes, habitats are defined as spatially recognizable areas where the physical, chemical and biological environment is distinctly different from surrounding areas (Kostylev, 2007). The term benthic refers to anything associated with or occurring on the bottom of a water body. Benthic habitat maps and/or coral cover maps provide useful information for the management of coastal ecosystems and are used in numerous research and monitoring activities of, for example, coral reef resiliency, sea-level change, climate change, and ocean acidification (Miller, 2010). Benthic maps facilitate describing the coral reef physical environment (Andréfouët et al., 2002a), identify connectivity to relevant land-based and marine threats (Andréfouët et al., 2002b), and set a baseline reference for change detection analysis and monitoring. The common technique to map benthic habitats has been field sampling and aerial photography. However, this has its limitations, as it requires more time, is more expensive, and is labour intensive and limited over remote areas. For all these reasons, the use of satellite imagery is becoming more widespread for coastal and marine environments.

Tropical coastal ecosystems are of high spatial complexity and temporal variability, and therefore remote sensing imagery has been found to be very useful tool in providing timely and up-to-date information for benthic and coral reef mapping and monitoring (Eakin et al., 2010). Through the development and commercialization of "Very High Resolution" (VHR) sensors, spatial capabilities of satellites have joined those of aircraft, providing information at the dominant benthos scale but over large areas (Collin et al., 2012). Many studies have used different high resolution sensors to map benthic habitats, and have proved to have accuracies of around 70% (Green et al., 2000; Sharma et al., 2008). However, the mapping of these submerged and highly heterogeneous environments also impose challenges (Chen et al., 2011). Two distinct benthic types at different depths (for example) may be spectrally indistinguishable in a remotely sensed image (Hedley et al., 2012). Therefore, bathymetric data is an essential data source required for water column corrections prior to image classification (Sterckx et al., 2005) of marine habitats. A bathymetric map is a very important document for coral reef studies (Purkis, 2005) as it helps the classification and gives an insight into coral reef ecology (Bertels et al., 2008). Some studies have shown that Object-Based Image Analysis (OBIA) improved the classification of benthic habitats in comparison with pixel-based classifications (Benfield et al., 2007; Leon and Woodroffe, 2011; Phinn et al., 2012).

1.2 Problem definition

On 10 October 2010 the Caribbean Islands of Bonaire, St. Eustatius and Saba (known as the Caribbean Netherlands) became Dutch municipalities with a distinct status. Mapping and monitoring the coastal ecosystems (including seagrasses and coral reefs) is essential for conservation in these islands, particularly because the unique biodiversity of these islands is threatened by a large number of factors. Ecological monitoring can assist in directing management actions and conservation of natural area (Economic-Affairs, 2010).

With reduced growth rates, mortalities due to disease and bleaching, and increased damage by severe weather, coral reef habitats are decreasing rapidly, as well as their value to shoreline protection. Recent studies have shown that the average live coral cover on Caribbean reefs has declined from more than 50% in the 1970s to just 8% of the reef today (Jackson, 2012). Scientists estimated that 75% of the Caribbean's coral reefs are in danger, and predicted that by 2050 virtually all of the world's coral reefs would be in risk (Jackson, 2012). One of the major threats to corals, bleaching, has been observed in the Windward Islands (including St. Eustatius) since August 2005 (Esteban et al., 2005). Benthic habitats in the islands also serve as an important corridor function for animals that use both the land and sea.

The macro-habitats and benthic communities around St. Eustatius have not been properly mapped and described. There are some in situ benthic and reef monitoring activities taking place in the islands, as well as research on the status of the reefs, water quality monitoring, etc. Nevertheless, more coral mapping and monitoring is needed for a better protection of their biodiversity. The International Coral Reef Initiative (ICRI) strives to preserve coral reefs and related ecosystems by increasing research and monitoring of reefs to provide the data for effective management. The Netherlands Antilles Coral Reef Initiative (NACRI) is a response to the call to action from ICRI to form regional and national initiatives to preserve the coral reefs in The Netherlands (NACRI, 2010). In this sense, a good coral reef and bathymetric map will contribute to these initiatives.

1.3 Objectives

The main objective of this research is to use multispectral data to map and classify benthic habitats at the Dutch island of St. Eustatius, as an accurate habitat map will be useful for the management and protection of its biodiversity. Classifying benthic habitats has been done by various researchers around the world, using different imagery and methodology. Here, the research questions will focus on finding out the best way of using the available high resolution imagery (WorldView-2 and QuickBird) and apply the best classification procedure. The 8 spectral bands of the WorldView-2 satellite might improve the classification accuracy of the 4 spectral bands of QuickBird.

Overall, the purpose of this study is to help reveal the capabilities and limitations of the available data to categorize benthic habitats based on their spectral characteristics and ground truth data over the study area. Furthermore, the use of Object-Based Image Analysis (OBIA) will be evaluated, as it has shown improved performances over pixel based classifications. This research will also evaluate the possibility of deriving bathymetry using the satellite imagery. A good bathymetric map is important not only to improve the classification accuracy of the images, but also for the study of the ecology of the habitats.

For this thesis, the case study of the island of St. Eustatius has been selected among the others islands due to the availability of data, which includes two sets of satellite imagery (QuickBird and WorldView-2) and ground truth data.

1.4 Research questions

Based on the objectives described, the following research questions are formulated:

1. To what extent can benthic habitats of St. Eustatius be classified and mapped using WorldView-2 and QuickBird imagery?

2. Do the additional bands of WorldView-2 provide any benefits to classification accuracy in comparison to QuickBird bands?
3. Does water column correction improve benthic habitat classification?
4. What benefits to classification accuracy can the application of object-oriented classification provide over standard pixel based classification techniques?
5. Can bathymetry be accurately calculated with available imagery using the ratio transform method?

To answer all these questions a literature review was performed to assess the best methodology.

1.5 Structure of the report

This thesis is organized in six major sections. Chapter 2 includes a literature review of the background of remote sensing of shallow water coastal areas and the existing methodologies for the best classification of benthic habitats and bathymetric calculation. The methodology and processing of the imagery and data is described in Chapter 3, including the methods performed for atmospheric and bathymetric correction, image classification, and accuracy assessment. Results are presented in Chapter 4, in terms of the final benthic maps, calculated bathymetry and achieved accuracy. The most important observations derived from this study and suggestions on the potential of employed imagery and evaluated methods for benthic habitat mapping are addressed in Chapter 5 Discussion and Chapter 6 Conclusions and Recommendations.

2 Literature review

2.1 Remote sensing for shallow water coastal areas

The reflected energy received by an optical remote sensor from shallow water areas is the result of the influence of the air-sea interface, atmospheric absorption and scattering, and the water column. Radiation passes through two media, the atmosphere and the water, and then back to the sensor, as shown in Figure 1.

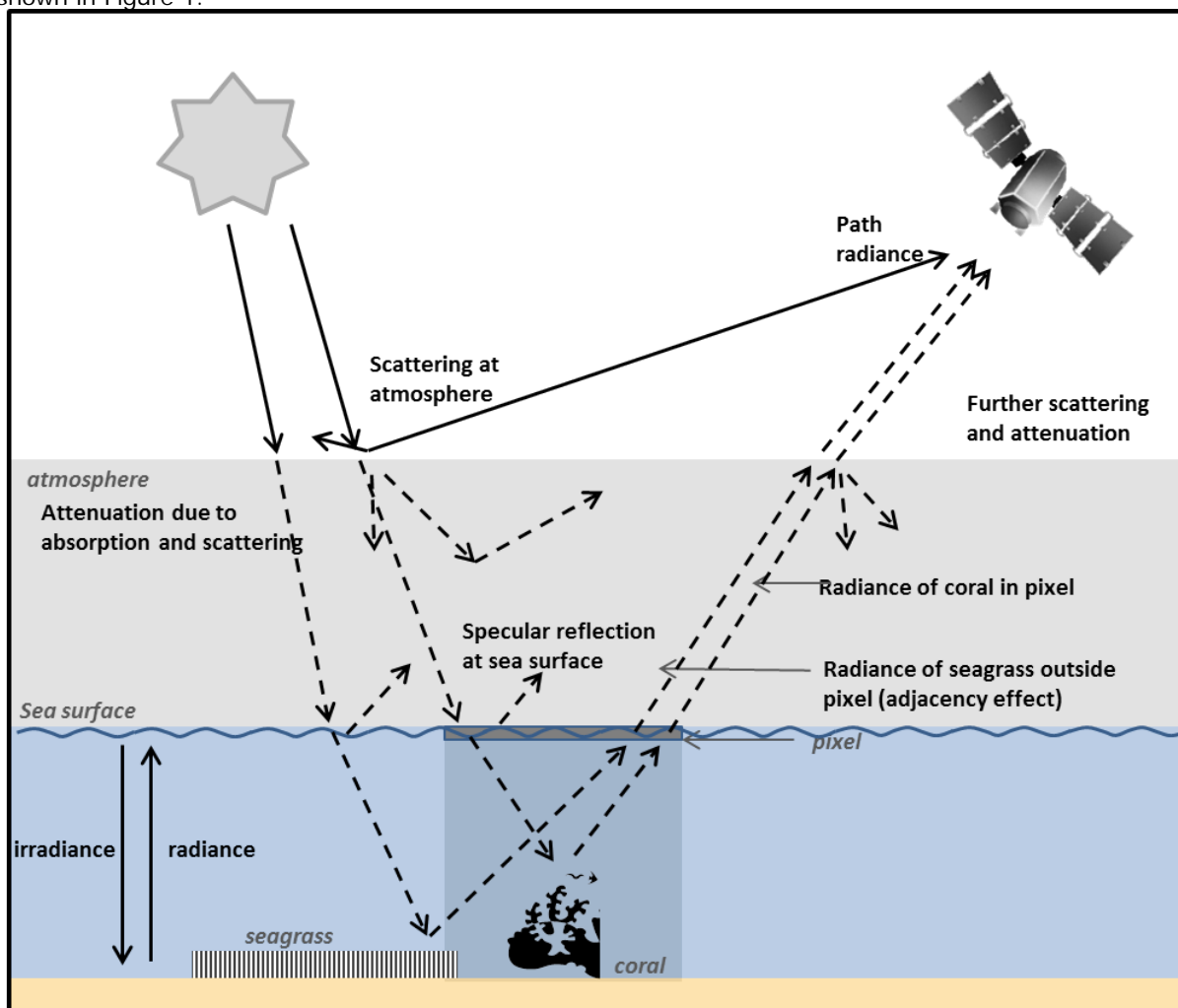


Figure 1. Factors influencing the amount of radiance reaching the sensor over a water mass (own elaboration based on Edwards, 1999).

To derive information about benthic environments from remotely sensed data, the optical processes in the water column must be taken into account, and due to the variety of interactions that take place, these are considered more complex than atmospheric interactions. The dissolved particulate matter in the sea water are optically significant and their concentration varies in the water column both spatially and temporally (Mobley, 1994).

Optical remote sensing methods typically penetrate clear waters to approximately 15–30 m (Mumby et al., 2004). Light penetration is wavelength dependent, being greater in blue wavelengths than in the red wavelengths. The precise degree of penetration in a spectral band will depend upon the optical properties

of the water (e.g. the concentration of dissolved organic matter and suspended sediments) (Mumby et al., 2004).

Spectral signatures are the variations in reflected or absorbed electromagnetic radiation at varying wavelengths, which can identify particular objects. For any given material, the amount of reflectance, absorption, or scattering will depend on wavelength (Olsen, 2007). Each substrate type has spectral characteristics that can be used to distinguish it from other objects, and so do different marine benthic environments (Lubin et al., 2001). Figure 2 illustrates spectral signatures of some common coral reef benthic substrates. It can be observed that sand has a much higher reflectance at visible wavelengths than algae.

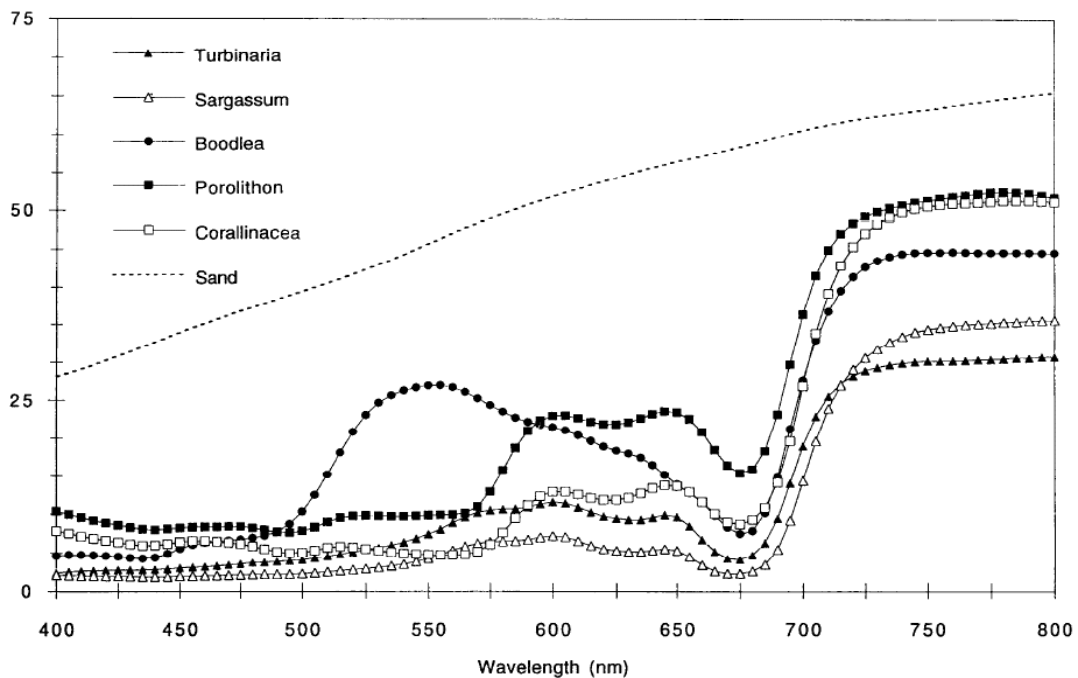


Figure 2. Spectral values of the reflectance for various algae and coral sand (Maritorena, 1996)

The number of classes distinguishable by remote sensing depends on many factors, including the platform (satellite, airborne), type of sensor (spectral, spatial and temporal resolution), atmospheric clarity, surface roughness, water clarity and water depth (Mumby et al., 2004).

Many researchers (e.g. (Andréfouët, 2003; Benfield et al., 2007; Capolsini et al., 2003; Hedley et al., 2004; Hochberg et al., 2003b; Mishra et al., 2006; Mumby and Edwards, 2002)) have used different imagery like Landsat, SPOT, IKONOS or QuickBird satellite data for mapping and classifying benthic habitats. With the launch of WorldView-2, some researchers have also used this high resolution satellite data in the last years, e.g. (Chen et al., 2011). Few multi-sensor comparisons have been accomplished until now to determine the capabilities of existing sensors in terms of their spatial and spectral resolution, and performance over various environments (Andréfouët et al., 2002a; Capolsini et al., 2003; Hochberg et al., 2003b; Mumby and Edwards, 2002). These have demonstrated some general trends when mapping coral reef habitats. For instance, some studies have shown that spectral resolution (the number and width of spectral bands) is more important than spatial resolution for discriminating between reef communities (Hochberg et al., 2003b; Mumby et al., 1997; Mumby et al., 2004). Further, some authors demonstrated the advantages of considering the reef morphology and habitat zonation at reef level (e.g. contextual knowledge) to improve image classification accuracy (Andréfouët, 2003; Capolsini et al., 2003; Mumby et al., 1998). Classification accuracy of coral reefs can be increased significantly by compensation for light attenuation in the water column and contextual editing to account for generic patterns of reef distribution. Both processes are easily implemented and collectively constitute an increment in accuracy of up to 17% for satellite sensor imagery (Mumby et al., 1998).

2.2 Remote sensing techniques for benthic mapping

2.2.1 Pre-processing of imagery for benthic mapping

A critical step of remote sensing imagery analysis for benthic habitats classification is the pre-processing of the images. This involves radiometric radiance conversion of the image from digital numbers to spectral radiance, atmospheric correction, sunglint removal, and correction for the water column. The pre-processed images can then be used for the classification and for bathymetry derivation.

In this section, the main methods for the pre-processing steps are discussed.

2.2.1.1 Atmospheric correction

There are a variety of methods for atmospheric correction above the sea surface. These, however, usually require some input parameters concerning atmospheric and sea water conditions that are difficult to be obtained (Kerr, 2012). Therefore, many researchers used the simplified method of dark pixel subtraction for this kind of application (e.g. (Green et al., 2000; Mishra et al., 2006). Some studies have concluded that correcting the atmosphere through the empirical dark object subtraction procedure led to improved bathymetry retrievals (Collin and Hensch, 2012).

In the method of dark pixel subtraction the value of an object with zero reflectance, e.g. deep water, is subtracted from all pixels to remove the effect of atmospheric scattering. Although a minimum NIR brightness over deep water might be expected to be zero, in practice the minimum NIR brightness in any image is greater than zero. This linear correction does not change the results of a statistical classification (Capolsini et al., 2003).

The procedure followed for this atmospheric correction is described in chapter 3.

2.2.1.2 Sunglint removal

Sunglint at the sea surface is a common problem in high resolution imagery over water, and many authors use techniques of sea surface roughness correction for a better classification of benthic habitats. Sunglint occurs in imagery when the water surface orientation is such that the sun is directly reflected towards the sensor; and hence is a function of sea surface state, sun position and viewing angle (Kay et al., 2009). Sunglint adds a radiation component to the signal registered by the sensor which does not carry any information about the water column, and is typically much higher than the water leaving signal in all spectral bands, saturating pixel values (Streher, 2013).

A variety of glint correction methods have been developed for high resolution coastal imagery. In all cases the principle is to estimate the glint contribution to the radiance reaching the sensor, and then subtract it from the received signal (Kay et al., 2009). Previous methods for sunglint removal were designed for ocean colour applications on pixels at large physical scales (.1 km) (Fraser et al., 1997). More recently, Hochberg et al. (2003) created a new and simple method of 'deglinting' a high spatial resolution image (Hochberg et al., 2003a).

Hochberg et al.'s (2003) method relies on two assumptions: (1) That the brightness in the NIR is composed only of sunglint and a spatially constant 'ambient' NIR component (no spatially variant benthic contribution to the NIR) and (2) That the amount of sunglint in the visible bands is linearly related to the brightness in the NIR band (Hedley et al., 2005). This method assumes that the near-infrared region (NIR) is totally absorbed by the water. Therefore, any recorded NIR upward radiance above a water body should contain the reflected sunlight as a function of geometry independent of wavelength. Assuming that the glint effect remains relatively constant independently of wavelength, pixels with glint contribution in NIR bands also have similar glint contribution in total upward radiance in visible bands. Therefore, identifying the pixels with maximum and minimum radiances in the NIR enables estimation of the percentage of glint contribution in each pixel.

The method described by Hochberg et al. (2003) in effect models a constant 'ambient' NIR brightness level which is removed from all pixels. This deglint method, however, has some limitations, as it is sensitive to outlier pixels and requires a proper masking out of land and clouds. This prior rigorous

masking is required to avoid that the brightest NIR pixel would be a land or cloud pixel, as this could be problematic.

An improvement to the deglinting method that improves the robustness of the technique was presented by Hedley et al. (2005). This modified method establishes linear relationships between NIR and visible bands using linear regression based on a sample of the image pixels (Hedley et al., 2005). One or more regions of the image are selected where a range of sunglint is evident, and where spectral brightness would be expected to be consistent (areas of deep water). For each band a linear regression is made between the NIR radiance and the band radiance, as shown in Figure 3.

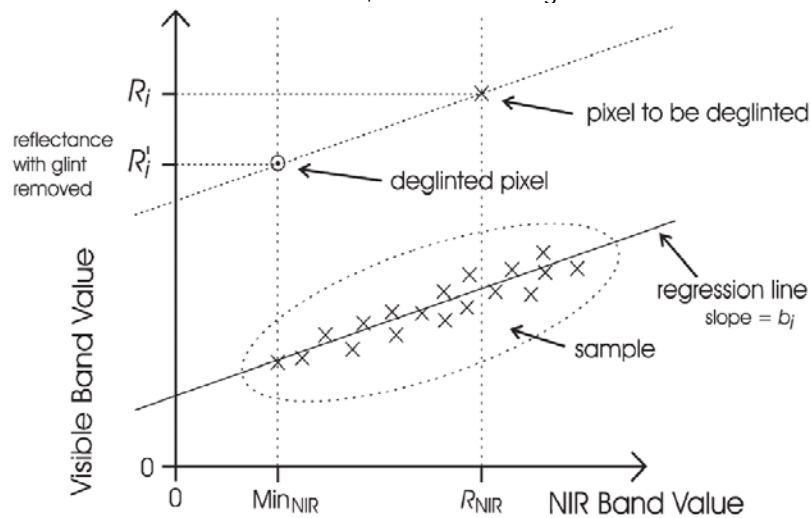


Figure 3. Deglinted method developed by Hedley et al. 2005 (Hedley et al., 2005).

Figure 3 shows the main concepts of this methodology. To deglint a visible band, a regression is performed between the NIR values and the values in the visible band using a homogenous sample set of pixels. The slope of the regression and the minimum value of the NIR band is used to predict the values for other pixels (Hedley et al., 2005).

Each pixel is corrected by assuming its glint-free NIR radiance is the same as the minimum value in the sample regions and reducing the visible band accordingly, using the least squares regression slope to give the relationship between the visible and NIR bands. The following equation is used:

$$L'_i = L_i - b_i (L_{NIR} - \text{Min}_{NIR}) \quad \text{Equation 1}$$

where L'_i is the deglinted radiance value, L_i is the radiance value in band i , b_i is the slope estimated by the linear regression, L_{NIR} is the NIR radiance value, and Min_{NIR} is the minimum value for the NIR band established from the sample. This method assumes a constant ambient signal level (Min_{NIR}), which is subtracted from each pixel of the image during the process.

The effectiveness of the method relies on the appropriate choice of the pixel samples from an image region that is relatively dark, reasonably deep, and with evident glint (Green et al., 2000; Hedley et al., 2005). Ideally, the sample pixels should be drawn from several locations in the image including (if possible) large-scale areas with no sunglint at all (Hedley et al., 2005).

WorldView-2 provides extra bands, so the definition of the proper band combination of NIR (two bands) and visible (six bands) that would be involved in the linear regression for sunglint removal is very important. Experimental results demonstrated that there was a strong linear relationship among the 'new' bands (band 1, band 4 and band 6) with the NIR2, and among the 'traditional' bands (band 2, band 3 and band 5) with the NIR1 (Doxania et al., 2012). On the other hand, Deidda and Sanna (2012) show that using the coastal band (band 1) instead of the blue band has no noticeable effects on the results.

Sunglint removal and atmospheric correction of remotely sensed data are essential processes prior to the application of a bathymetry model. There are no rules about the sequence of these two procedures.

Many researchers begin with the sunlint removal and the atmospheric correction follows, while others apply the procedures vice-versa (Kay et al., 2009).
The methodology of this process is further explained in

Methodology and processing.

2.2.1.3 Water column correction

When light penetrates water its intensity decreases exponentially (attenuates) with increasing depth because of two processes, absorption and scattering. The degree of attenuation differs with the wavelength of the electromagnetic radiation. In the region of visible light, the red part of the spectrum attenuates more rapidly than the shorter-wavelength blue part (Mumby et al., 2004).

Absorption is wavelength-dependent and involves the conversion of electromagnetic energy into other forms such as heat or chemical energy. In marine environments, the main absorbers are algae, particulate matter in suspension, dissolved organic compounds, and water itself, which strongly absorbs red light and has a smaller effect on shorter wavelength blue light.

Scattering is when the electromagnetic radiation interacts with suspended particles in the water column and change direction. This process increases with the suspended sediment load of the water, so in more turbid waters more scattering occurs.

The spectra of a benthic habitat changes with increasing depth. As depth increases, the separability of habitat spectra declines, as shown in Figure 4 with the example of seagrass.

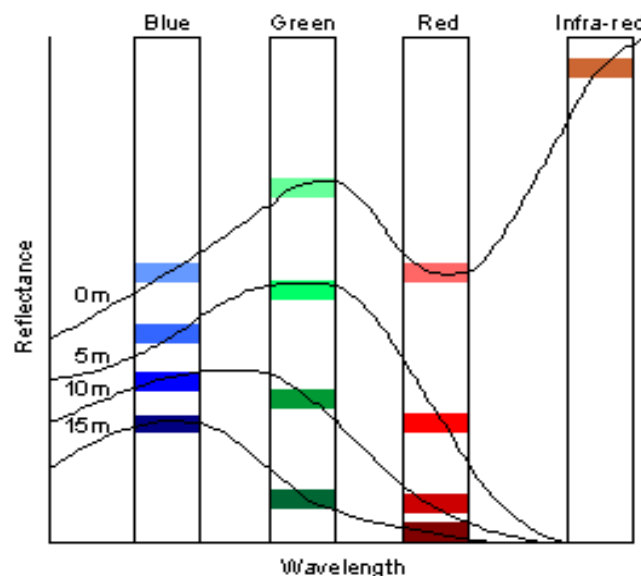


Figure 4. Spectra for a benthic habitat (i.e. seagrass) (Green et al., 2000).

Figure 4 also proves how the spectra of the same stratum at a depth of 5 m, for example, will be very different to that at 15 m. Similarly, the spectral signature of one substrate at one depth could be very similar to the profile of another stratum at a different depth. The spectral radiances are therefore influenced both by the reflectance of the substrata and by depth (as well as by scattering by the sediment load of the water), and will create confusion when attempting to use visual inspection or multispectral classification to map habitats. Therefore, for benthic habitat mapping it is important to remove the influence of water depth.

As found in literature, there are various techniques to correct for depth. Nevertheless, the removal of the influence of depth on bottom reflectance would require two main variables, a measurement of depth for every pixel, and a knowledge of the attenuation characteristics of the water column (e.g. concentrations of dissolved organic matter). As these two variables are difficult to obtain in most areas, Lyzenga (1978, 1981) proposed a simple image-based approach to compensate for the effect of variable depth when mapping bottom features (water column correction). This method was then expanded by Mumby et al. (1998).

The main idea of this water column correction method is that Instead of predicting the reflectance of the seabed, the method produces a 'depth-invariant bottom index' from each pair of spectral bands. This method is only truly applicable to clear waters. However, where water properties are moderately constant across an image, the method strongly improves the visual interpretation of imagery and should improve classification accuracies (Green et al., 2000).

The **Depth Invariant Index** approach follows three steps (Lyzenga, 1981 and Mumby et al., 1998).

1. Linearization of the depth/radiance relationship;

The transformed radiance of the pixel X_i , is the natural log of the pixel radiance L_i in band i .

$$X_i = \ln(L_i) \quad \text{Equation 2}$$

2. Calculation of the attenuation coefficient between pairs of bands;

The ratios of attenuation coefficients, k , are calculated for band pairs. For this, bi-plots are created for each pair of spectral bands. The slope of the bi-plot is a representation of the attenuation coefficient for those bands. The gradient of the line is not calculated using conventional least squares regression analysis because the result will depend on which band is chosen to be the dependent variable. Therefore, rather than calculating the mean square deviation from the regression line in the direction of the dependent variable, the regression line is placed where the mean square deviation (measured perpendicular to the line) is minimised. The following equations were used from (Green et al., 2000):

$$\frac{k_i}{k_j} = a + \sqrt{(a^2 + 1)} \quad \text{Equation 3}$$

where:

$$a = \frac{\vartheta_{ii} - \vartheta_{jj}}{2\vartheta_{ij}} \quad \text{Equation 4}$$

and:

$$\vartheta_{ij} = \overline{X_i X_j} - (\overline{X_i} * \overline{X_j}) \quad \text{Equation 5}$$

where ϑ_{ii} is the variance of band i , ϑ_{jj} is the variance of band j and ϑ_{ij} is the covariance of both bands (Nurlidiasari and Buidman, 2005).

3. Generation of the depth-invariant bottom type index. Each pair of spectral bands produced a single depth-invariant band using the following equation:

$$\text{depth-invariant index} = \ln(L_i) - \left[\left(\frac{k_i}{k_j} \right) \ln(L_j) \right] \quad \text{Equation 6}$$

These three steps are represented by Figure 5, where two types of bottom habitats are considered (sand and seagrass).

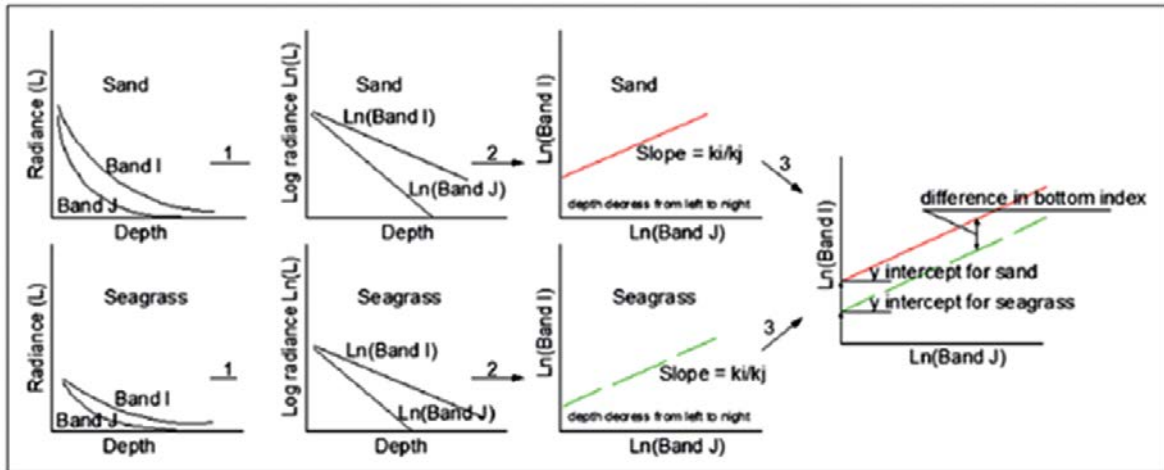


Figure 5. Construction of the depth-invariant index (Deidda and Sanna, 2012, Green et al., 2000).

In Figure 5, the first step represents the linearization of the depth/radiance relationship. Step 2 represents the calculation of the ratio between the two bands, which results in a straight line. Step 3 shows the comparison between different bottom types, showing how if a different bottom type is considered, the result will be represented by a parallel line, since they will not have the same reflectance. The slope of the two lines is the same, because the ratio of the attenuation coefficients k_i/k_j only depends on the band wavelengths and on the transparency of the water (Deidda and Sanna, 2012).

Nurlidiasari (2012) mapped coral reef using QuickBird data and estimated that water column correction using the depth invariant method increased the accuracy of coral reef mapping from 67% to 89% (Nurlidiasari and Buidman, 2005). Deidda (2012) used WorldView-2 imagery and concluded that, unlike the sunglint processing, using the coastal band for the depth invariant index produced visually different results from the blue one (Deidda and Sanna, 2012).

The exact procedure for water column correction for the study area is further explained in

Methodology and processing.

2.2.2 Classification of imagery for benthic mapping

After the pre-processing steps the classification of the images could be performed. Image classification is a crucial stage in remote sensing image analysis. There are two types of classifications, unsupervised and supervised. In this research, as there is some previous knowledge about the area due to the fieldwork campaign already done, a supervised classification could be performed. Two types of supervised classification could be done, pixel-based classification and object based classifications.

2.2.2.1 Supervised pixel-based Image classification

In a pixel-based classification spectral signatures representative of the various habitat types are fed into a classifier that assigns every pixel in the image to a habitat class (Benfield et al., 2007).

Coral reef mapping studies most commonly use the Maximum Likelihood Classification (MLC) per pixel (Andréfouët, 2003; Mumby and Edwards, 2002; Mumby et al., 1997). This decision rule utilizes mean and covariance/variance data to assign pixels to a habitat class based upon training data (Benfield et al., 2007). MLC assumes that the statistics for each class in each band are normally distributed and calculates the probability that a given pixel belongs to a specific class. A statistic distance is calculated to every pixel-based on mean values and covariance matrix of the clusters. Then, the pixel is assigned to the class to which it has the highest probability.

2.2.2.2 Object-based image classification

Recent studies employing Object-Based Image Analysis (OBIA) to map coral reefs have successfully showed an improved performance across different spatial scales (Benfield et al., 2007; Leon and Woodroffe, 2011; Phinn et al., 2012). OBIA is particularly suited for the analysis of very high resolution (VHR) images such as QuickBird or WorldView-2, where the increased heterogeneity of sub-meter pixels would otherwise confuse pixel-based classifications yielding an undesired 'salt and pepper effect' (Leon and Woodroffe, 2011). Benfield et al. (2007) showed that the classification using OBIA was up to 24% more accurate than the MLC for Landsat and up to 17% more accurate for QuickBird. This increase in accuracy when mapping coral reefs is attributed to the better representation of landforms as multi scale objects and their associated topology. Geometric and contextual attributes are more robust than highly variable pixel spectral properties making them more suitable for the analysis of very-high resolution or complex images, such as those of intertidal and underwater environments (Leon and Woodroffe, 2011).

Leon et al. (2012) used spectral and scale-dependent spatial concepts such as texture, context and shape (e.g. adjacency, compactness) to define conceptual rules relating the objects within a hierarchical structure. Phin et al. (2012) integrated existing knowledge on the biological and geomorphic structures and processes which make up coral reefs, with field survey data, high-spatial-resolution multi-spectral images and Object-Based Image Analysis (OBIA) techniques.

Object-oriented classification is composed of two steps, segmentation and classification. The segmentation stage creates the image objects that are then used for further classification. In each step of the segmentation, pairs of neighbouring image objects are merged, which result in the smallest growth of heterogeneity. If this growth exceeds a threshold defined by a break-off value (scale parameter), the process stops. By varying the scale parameter, it is possible to create image objects of different sizes. Weighting values are defined by the user (e.g. colour, shape, smoothness, compactness) (Benfield et al., 2007). This process enables groups of pixels corresponding to reef features to be identified based on their characteristic length/width (size), spectral reflectance signature (colour) and shape (compactness) (Phinn et al., 2012).

The exact classification procedure followed is further explained in

Methodology and processing.

2.2.3 Determination of water depth

Information of water depth is a fundamental environmental parameter in marine systems (Kerr, 2012), and it is important for the discrimination and characterization of coral reef habitats. Bathymetric data is ecologically important because benthic community composition varies with depth, as well as resources and disturbances. Knowledge of water depth also allows estimation of bottom albedo, which can improve habitat mapping (Mumby et al., 1998). However, accurate and high spatial resolution bathymetric data is often missing in remote coral reefs areas and is difficult and expensive to obtain.

Sonar measurements are often used for bathymetry retrieval, but they can be difficult to mobilize in remote areas and for repeated surveys. Also, bathymetric Light Detection And Ranging (LiDAR) measurements are well suited to surveying both land and shallow waters simultaneously, but can be very expensive (Collin and Hench, 2012).

Water depth can also be estimated with passive satellite imagery. Lyzenga (1978, 1981) developed a theory using passive remote sensing for determination of water depth, that was then expanded by Philpot (1989) and Maritorena et al. (1994) (Maritorena et al., 1994; Philpot, 1989). This provided a cost and time-effective solution to accurate depth estimation (Stumpf et al., 2003; Su et al., 2008).

The initial attempts for automatic estimation of water depth were based on the combination of aerial multispectral data and radiometric techniques. With the existence of high resolution imagery, the methods were expanded, as the spatial and spectral resolution was improving. Various authors have used IKONOS (Stumpf et al., 2003; Su et al., 2008), QuickBird (Lyons et al., 2011; Mishra et al., 2006) and WorldView-2 data (Bramante et al., 2013; Kerr, 2012) for bathymetry estimation. The use of two or more bands allows separation of variations in depth from variations in bottom albedo, but compensation for turbidity can be problematic (Stumpf et al., 2003).

Light is attenuated exponentially with depth in the water column, with the change expressed by Beer's Law,

$$L(z) = L(0)\exp(-kz) \quad \text{Equation 7}$$

where k is the attenuation coefficient and z is the depth.

Lyzenga (1978) expressed the relationship between observed radiance or reflectance to depth and bottom reflectance as:

$$R_w = (Ab - R') \exp(-gz) + R' \quad \text{Equation 8}$$

where R' is the water column reflectance if the water was optically deep, Ab is the irradiance reflectance of the bottom (albedo), z is the depth, and g is a function of the diffuse attenuation coefficients for both downwelling and upwelling light. Rearranging Eq. 8, depth z can be described as (Stumpf et al., 2003):

$$z = \frac{1}{g} [\ln(Ab - R') - \ln(R_w - R')] \quad \text{Equation 9}$$

The estimation of depth from a single band using Eq. 9 will depend on the albedo Ab , with a decrease in albedo resulting in an increase in the estimated depth. It assumes that the bottom is homogeneous and the water quality is uniform for the whole study area. Lyzenga (1978, 1985) further developed a technique to determine water depth if the optical properties are not uniform, showing that two bands could provide a correction for different bottom types in finding the depth, and created from Eq. 9 the following linear solution:

$$Z = a_0 + a_i X_i + a_j X_j \quad \text{Equation 10}$$

where a_0 , a_i and a_j are derived constants for the water's optical properties. X is the transformed radiance at a particular band, and since the intensity of light is assumed to be decaying exponentially with depth, radiance can be linearized as,

$$X_i = \ln[R_w(L_i) - R'(L_j)] \quad \text{Equation 11}$$

This linear transform solution has five variables that must be determined empirically (a_0 , a_i and a_j , $Rw(L_i)$ and $R'(L_j)$), and this makes the method difficult to implement.

A new technique was developed as an alternative where fewer parameters are required, it's easier to use, more robust over variable bottom habitats, and more stable over broader geographic areas. This is the **ratio transform method** (Stumpf et al., 2003).

This ratio transform method is based on absorption rates of different wavelengths. Different bands will be attenuated at different rates as energy penetrates the water column. Therefore, as the logarithmic values change with depth, the ratio will change. As depth increases, the band with a higher absorption rate (green) will decrease proportionally faster than the band with a lower absorption rate (blue). Accordingly, the ratio of the blue to the green will increase. This method is stated to compensate implicitly for variable bottom type (varying albedo), since a change in bottom albedo affects both bands similarly, but changes in depth affect the high absorption band more. Therefore, the change in ratio because of depth is much greater than that caused by change in bottom albedo, suggesting that different bottom albedos at a constant depth will still have the same ratio. Overall, varying bottom reflectances at the same depth will have the same change in ratio (Stumpf et al., 2003).

Overall, depth can then be approximated as:

$$z = m_1 \frac{\ln(nR_i)}{\ln(nR_j)} - m_0 \quad \text{Equation 12}$$

where m_1 is a tunable constant to scale the ratio to depth, n is a fixed constant, and m_0 is the offset for a depth of 0 m. The fixed value of n is chosen to assure both that the logarithm will be positive under any condition and that the ratio will produce a linear response with depth (Stumpf et al., 2003).

In contrast to the linear method, the ratio method contains only two variable parameters and can be applied quickly and effectively over large areas with clear water.

Stumpf et al. (2003) used the ratio transform method with two IKONOS wavebands, similar to QuickBird bands, and demonstrated its benefits to retrieve depths even in deep water (>25m). Other authors extended the methodology for the new bands of WorldView-2 (Kerr, 2012; Collin and Hensch, 2012). These authors concluded that the integration of the new spectral bands of WorldView-2 into the ratio algorithm facilitates more accurate optical derivation of water depth from the satellite imagery (Kerr, 2012; Bramante et al., 2013). The purple, green, yellow and NIR3 (WV2 1st-3rd-4th-8th bands), was deemed as the most reliable model attaining depths to about 30 m (Collin and Hensch, 2012). The ratios of the WV2 'coastal blue' band (band 1) to its 'yellow' band (band 4) had greater correlation with depth than the more conventional blue-green ratio (Bramante et al., 2013).

Kerr (2010) modified equation 12 to expand the number of band ratios for depth derivation. Therefore, the model for depth estimation using the increased spectral information from WV2 becomes:

$$Z^* = m_n \bar{Z}_n + m_{n-1} \bar{Z}_{n-1} + \dots + m_1 \bar{Z}_1 + m_0 \quad \text{Equation 13}$$

Where,

$$\bar{Z}_n = \frac{\ln(nR_i + e)}{\ln(nR_j + e)} \quad \text{Equation 14}$$

the constants m_n , m_{n-1} , etc... are estimated through multiple linear regression and n , $n-1$,... represent the n -th band-ratio. The constant e was added within the natural log to ensure that the minimum value for either was 1. The equation can be re-written as:

$$Z^* = \sum m_n \bar{Z}_n + m_0 \quad \text{Equation 15}$$

3 Methodology and processing

3.1 Study area

3.1.1 Description

Sint Eustatius (17°49'N, 62°98'W) is a volcanic island situated in the northern Leeward Islands portion of the West Indies, southeast of the Virgin Islands, in the Caribbean, as shown in Figure 6. The island has a surface area of about 21 km². It has a dormant Strato Volcano named Quill, which is the highest point of the island (600 m) (Roobol and Smith, 2004).

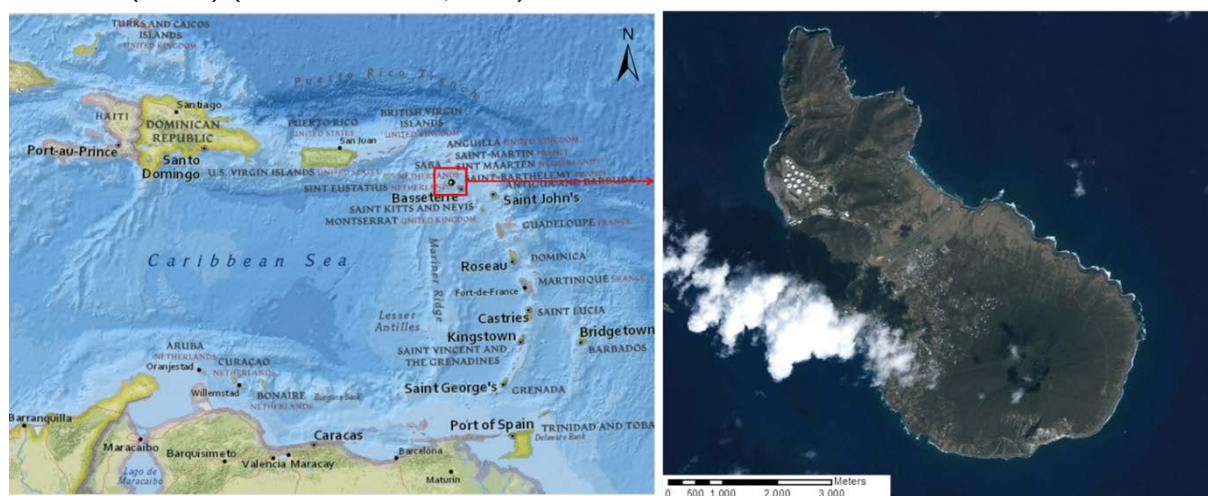


Figure 6. Location of the study area. The image in the left illustrates the general location of Statia in the Caribbean Sea. At the right, a satellite image of the island of Sint Eustatius.

St. Eustatius, also known as Statia, is a municipality of the Netherlands Antilles. Together with St. Kitts and Nevis, Statia lies on a shallow submarine plateau of maximally 180 m depth. Statia consists of three main geological units: North-western volcanic hills, the Quill volcano and the White Wall formation (Westermann and Kiel, 1961).

The trade winds blow throughout the year from directions between East-North-East and East (Vroman, 1961). Statia is situated in the hurricane zone, and the hurricane season runs from June till November. The eastern shore of the island is exposed to heavy surf. The Western shore and generally also the Southern and Northern coasts are much less exposed (Vroman, 1961). The average day-temperature throughout the year varies between 29 and 31 degrees Celsius, and the average night-temperature ranges between 23 and 25 degrees Celsius. The average sea temperature varies between 26 and 29 degrees Celsius (KlimaatInfo).

A National Marine Park was legally established in 1996. It surrounds the island and extends from the high water mark out to a depth of 30 metres. The St. Eustatius Marine Park covers an area of 27.5 km² and protects a variety of habitats, including pristine coral communities (drop off walls, volcanic 'fingers' and 'bombs', spur and groove systems), 18th century shipwrecks and modern-day artificial reefs to promote fishing and dive tourism (Bervoets, 2010). The distance of the Marine Park boundary from shore varies between 1 and 3 km. Within the Marine Park are two well-defined, managed reserves in which no fishing or anchoring are allowed, as shown in Figure 7. These reserves were established to conserve marine biodiversity, restore fish stocks and promote sustainable tourism, and protects a variety of habitats, including pristine coral reefs (Esteban, 2009). The Park is managed by a local non-governmental, non-profit foundation named the St Eustatius National Parks Foundation (STENAPA).

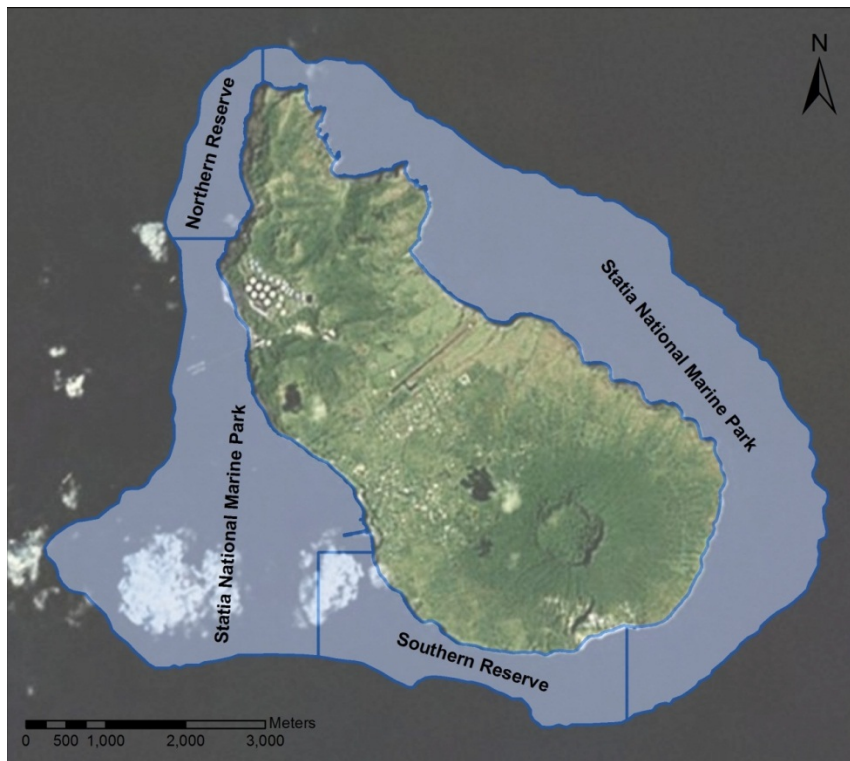


Figure 7. St. Eustatius National Marine Park and its reserves

3.1.2 Benthic habitats of St. Eustatius

A habitat classification scheme allows grouping habitat types based on common ecological or geomorphological characteristics. There are a variety of marine benthic habitat characterization schemes around the world. Here, considering the initial knowledge of the area, the previous fieldwork activities and the expected distinguishable characteristics in the images, a scheme was created by defining discrete habitat classes.

There are mainly 5 benthic habitat types in St. Eustatius:

- 1- Unconsolidated Sediment
 - 1.1 Sand
- 2- Coral Reef & Hard bottom
 - 2.1 Rubble
 - 2.2 Coral reef and gorgonian
- 3- Seagrass and algae
 - 3.1 Seagrass and algae
 - 3.2 Sargassum sp.

These habitats are complex and often mixed, and therefore its mapping classification becomes more difficult. Corals can show bleaching or could be dead, which increases its complexity for categorisation. A more detailed description of these benthic habitats is explained below (descriptions and images come from the fieldwork campaign carried out (Houtepen and Timmer, 2013) mainly):

1.1. Sand. This habitat consists only of sand areas with no coverage of benthic species. It is mostly found close to shore, but also between coral and gorgonian patches. Sand areas exhibit some variations in colour, having some areas with darker sands. Some of the sand habitats in the study area are represented in Figure 8.

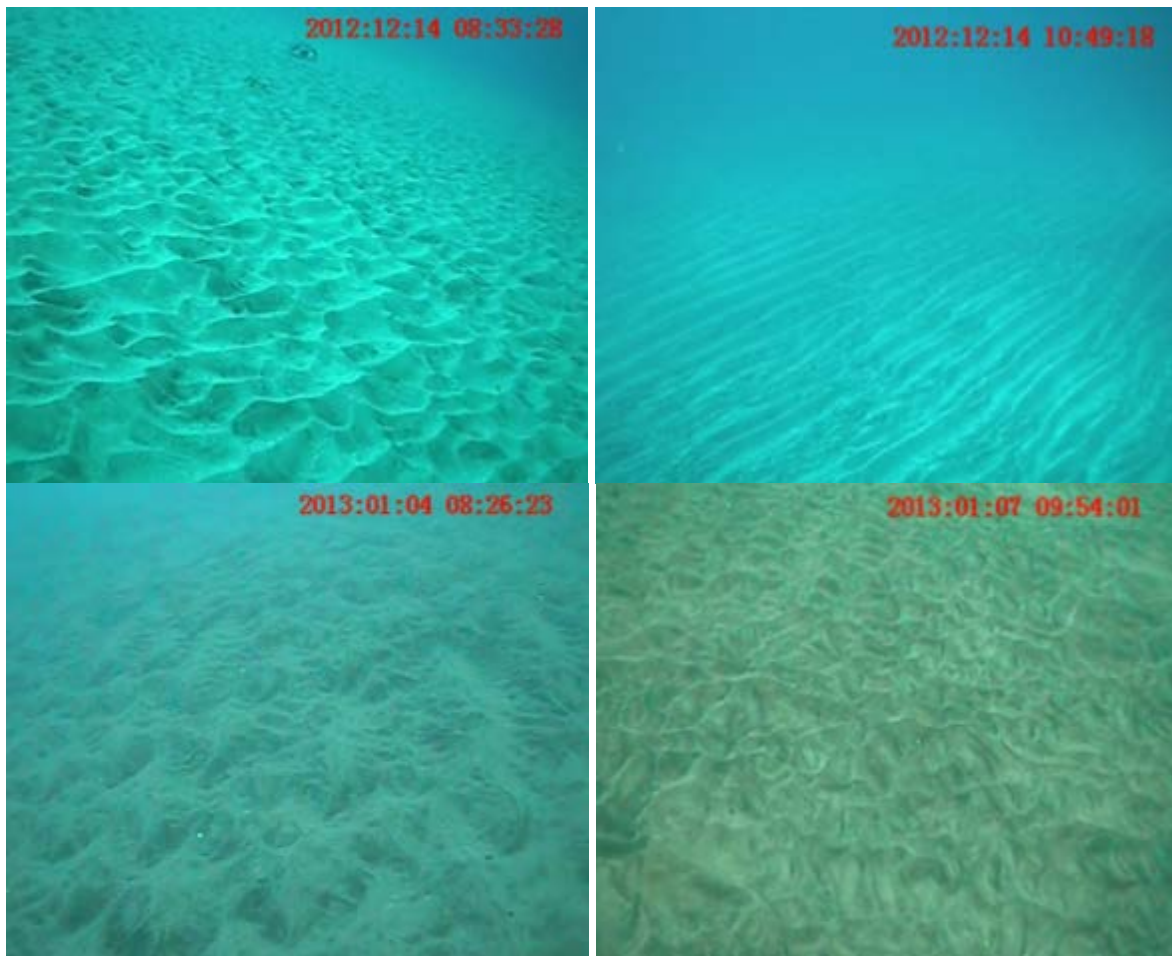


Figure 8. Bare sand areas in Statia (Houtepen and Timmer, 2013)

2.1. Rubble. Rubble habitat is quite diverse in terms of coverage percentage and species composition. It consists mainly of dead coral rubble often colonized by macroalgae. Figure 9 displays an example of rubble habitats in Statia.



Figure 9. Rubble areas (Houtepen and Timmer, 2013)

2.2. Coral. There are a variety of coral community types on Statia, from shallow sloping bottoms covered by mixed communities of coral colonies to patch reefs through volcanic boulders of various sizes to spur and groove type reefs with sandy channels divided by lava fingers. Few corals are found deeper

than 25 m (Wageningen-IMARES and Deltares, 2011). This habitat is the most species-rich and has the most diverse composition, including species of hard coral, gorgonian corals, algae and sponges. *Dictyota* sp. and *Lobophora variegata* are the main algal species. Coral communities consist of individual coral colonies (which are found in sand, rock and rubble patches) in different densities, here termed "loose reef", "intermediate reef" (found in rubble and rock fields, often sand between the coral patches) and "dense reef" (found on lava fingers and rock), as observed in the images from the fieldwork shown in Figure 10.

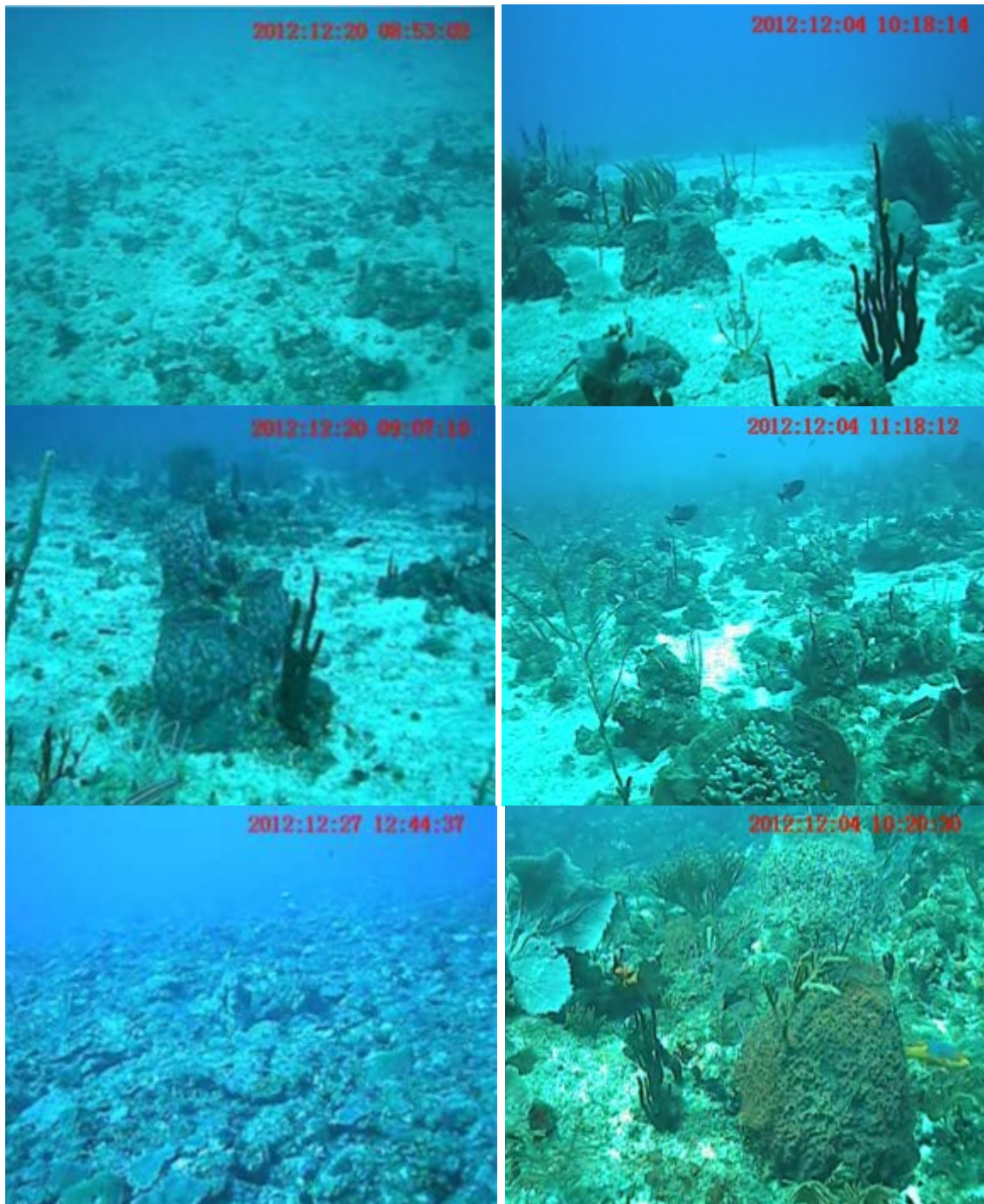


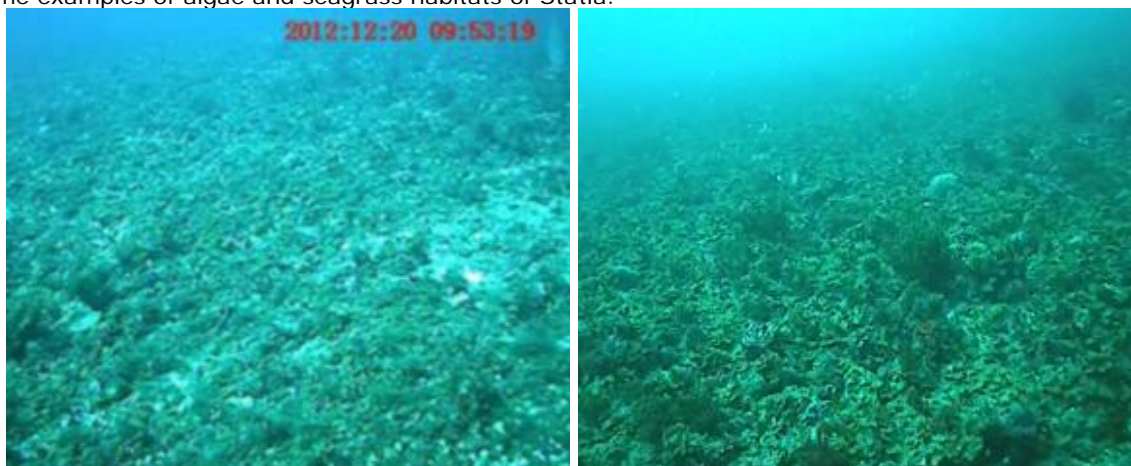
Figure 10. From top to bottom, loose, intermediate and dense reef (Houtepen and Timmer, 2013)

In this category, also gorgonian coral reefs are considered. This is a habitat dominated by different gorgonian species, including sea fans, sea pens, sea plumes and sea fingers. Examples of gorgonian corals in Statia are illustrated in Figure 11.



Figure 11. Gorgonian coral reef (Houtepen and Timmer, 2013)

3.1. Algae and seagrass. Algae and seagrass have been grouped together as it is expected that their spectral profiles will be similar. Algae refers to benthic habitats that are overgrown by different algae species. Often a transition phase between sand and reef regions. Seagrasses occur in sand patches, often alongside coral reefs. Seagrass is found from the lower intertidal zone up to about 35 m depth (Wageningen-IMARES and Deltares, 2011). This habitat is principally found in the northwest part of the island.. The dominant species of seagrasses are *Halophlia stipulacea* and *Halophila decipiens*. Seagrass beds play a vital role in maintaining the health and diversity of adjacent coral reefs. Figure 12 gives some examples of algae and seagrass habitats of Statia.



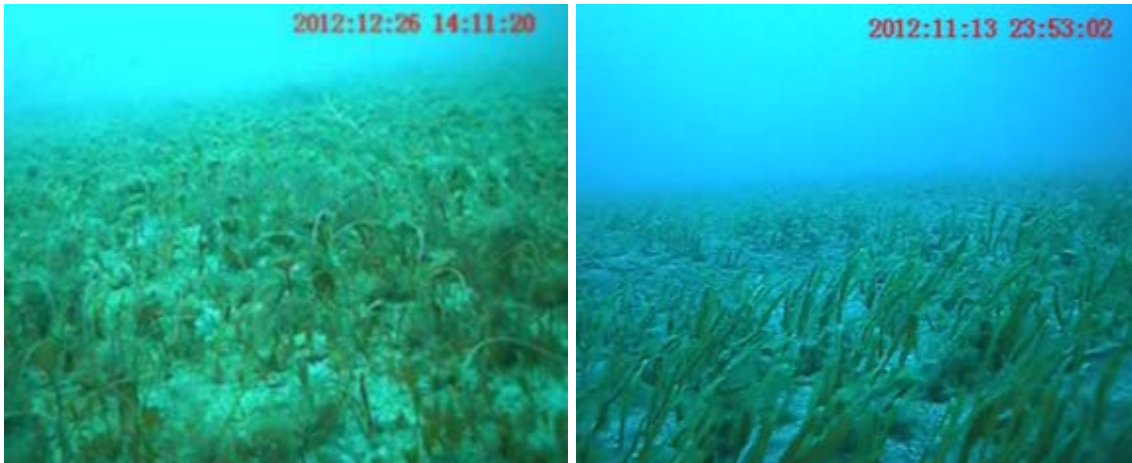


Figure 12. Algae fields (top) and Seagrass fields (bottom) (Houtepen and Timmer, 2013)

3.2. Sargassum sp. This is a species of brown algae that differs from most algae because it has flotation organs. The strands are lifted up and moving clearly with the waves. This species is mainly found on rubble and hard bottom. Some examples of images of Sargassum in Statia are shown in Figure 13.

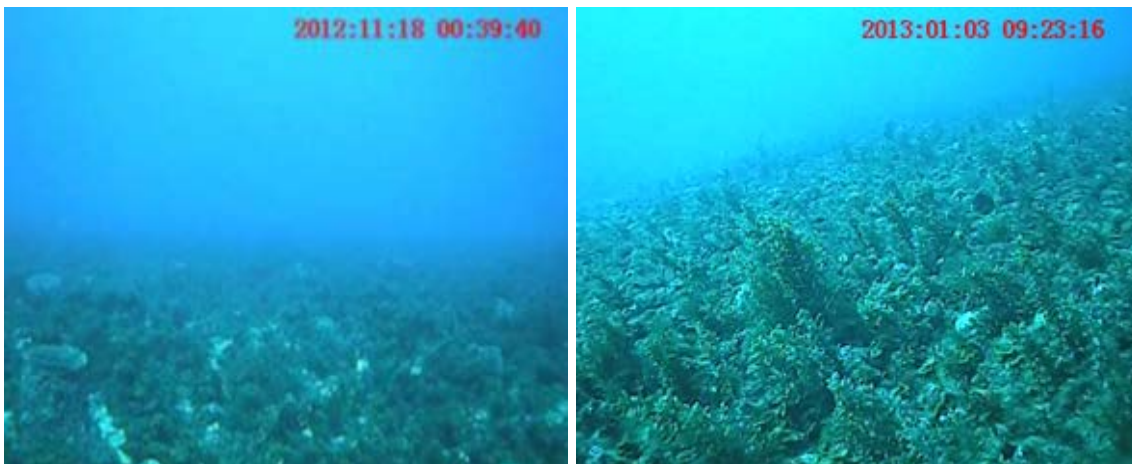


Figure 13. Sargassum sp. (Houtepen and Timmer, 2013)

Geographically, during the fieldwork campaign, the island was divided in 5 zones for the description of the main habitats (Houtepen and Timmer, 2013). Figure 14 shows this geographic division and the ground-truth data points obtained during the fieldwork.

- North-East Atlantic coast: consists of a sandy seafloor with some rubble patches on which algae grow. This beach is subject to heavy winds and waves from the East. This is likely to affect the shallow areas, limiting new benthic species recruitment and growth.
- North-West Caribbean coast: small strip of boulders close to shore on which coral species are growing, protected by the island from wind and waves. At approximately 15 m depth the habitat changes to sand, with seagrass patches from 20 m depth onwards.
- East Atlantic coast: Finger-like lava flows are a dominant feature in this area, populated by a gorgonian reef up to approximately 25 m depth. From 25 m onwards, the lava fingers are dominated by algae, including Sargassum sp.
- The South Atlantic coast is a habitat dominated by lava fingers, but in front of the White Wall area (South) more sand was found.

- West Caribbean coast: The Western seafloor changes from sandy areas in the shallow waters, at a depth of approximately 25 m, to rubble fields largely dominated by algae, but also sponges and corals occur. The transition between the two habitats is likely explained by the predominant wind and wave direction from the East. This side of the island provides the benthic habitats with most shelter.

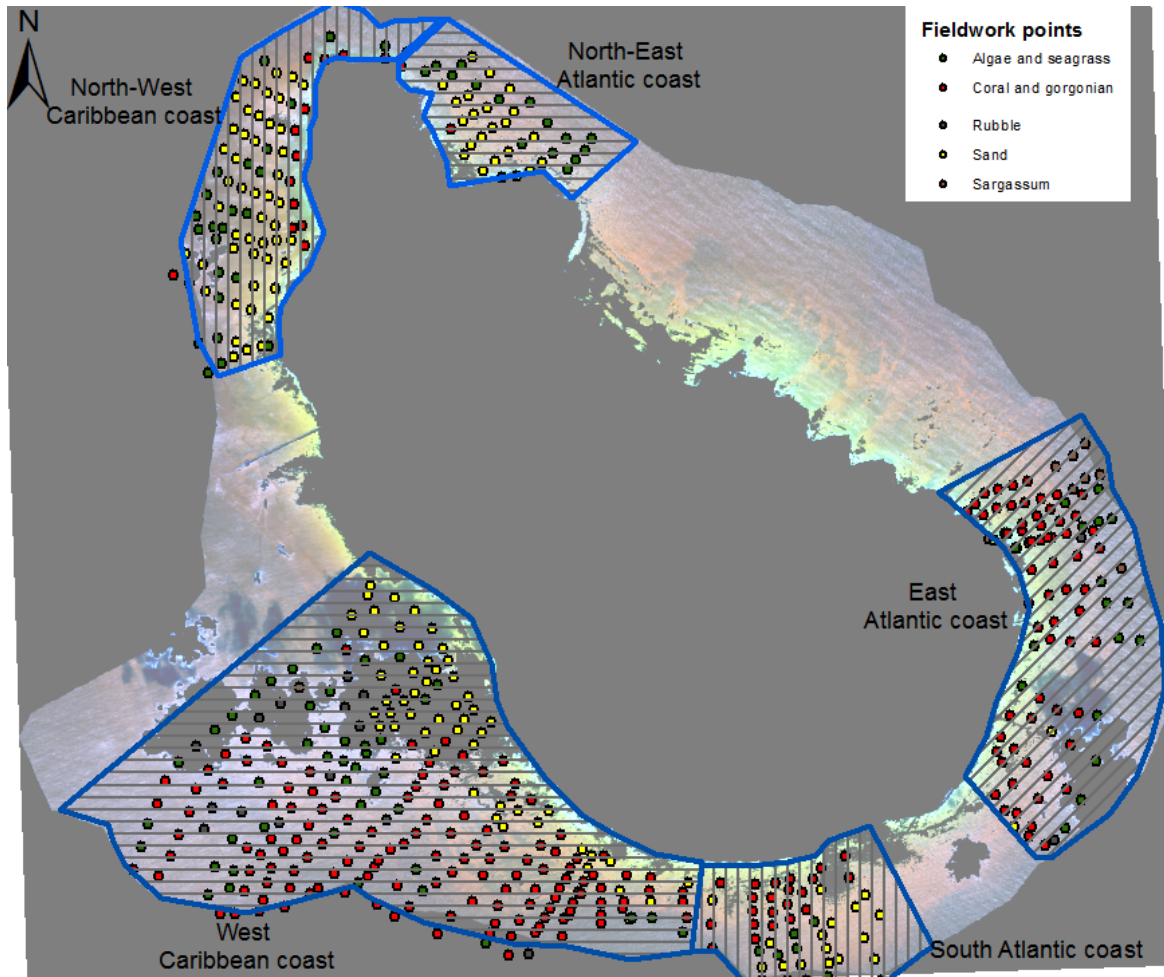


Figure 14. Representation of the 5 main zones where fieldwork was performed (based on (Houtepen and Timmer, 2013)). The dots represent the field points

3.1.3 Coral reefs status

It is reported that the coral communities in Statia are generally in a good condition, with diverse fish population and no signs of pollution (Debrot and Sybesma 2000; Klomp and Kooistra 2001). Also, it is stated that there is very little mechanical damage to coral reefs due to the fact that reefs are fairly deep and beyond the depth that vessels would damage corals and because all non-resident divers must dive with a dive guide from a local dive centre (Slijkerman et al. 2011). However, there are two factors that must be considered. First, there is significant sedimentation in the Marine Park due to erosion of cliffs and hillsides during heavy rainfall. Nevertheless, not much sediment is observed on corals due to the fact that it is dispersed by the time it reaches most of the coral reef (depths of >10m). Secondly, in 2005 there was a major coral bleaching event in the tropical Atlantic and Caribbean, with 70–80% of coral colonies bleached. Subsequent mortality resulted in a loss of the original live coral cover from about 30% to less than 15% in 2008; a 50% decrease. Macro-algal cover increased from about 40% in 2005 to

almost 60% in 2008 (Wilkinson, 2008). Since the early 1980s, significant decline in seagrass coverage is reported due to anchoring from tankers (especially in the deeper areas from 20-30 m), breakwater construction, pipeline deployment and hurricanes (especially in the late 1990s) (Slijkerman et al. 2011). The major source of land based pollution is from the Smith's Gut Landfill Site near Zeelandia Beach on the Atlantic coast. The most important threats to seagrasses are damages from boat anchors, pollution, dredging, coastal engineering and hurricanes.

The St. Eustatius National Marine Park conducted an Economic Valuation of St. Eustatius' coral reef ecosystems in 2009. The findings of this study have outlined that Statia's coral reef resources provide important goods and services to the economy of the island, with a low estimate for the value of Statia's coral reefs set at USD \$11,200,454. Therefore, as Statia has approximately 28 km² of coral reef a rough calculation gives a value of \$400 for one square meter of reef. This number highlights the importance of coral reefs to the island, it also suggests that there is an increased need for conservation, so that the value does not continue to diminish (Bervoets, 2010).

3.2 Data

- **Imagery:**

For St. Eustatius WorldView-2 (WV2) and QuickBird (QB) single date multi-spectral and panchromatic images are available. Table 1 represent their main sensor characteristics.

Table 1. Sensors main characteristics.

| Sensor | Area | Acquisition data | Max angle | Sun elevation | Cloud cover |
|------------|--------------|------------------|-----------|---------------|-------------|
| QB | St Eustatius | 06/11/2010 | 2.9 | 53.6 | 9.7% |
| WV2 | St Eustatius | 18/02/2011 | 0.4 | 55.1 | 17% |

- o WorldView-2

WorldView-2 satellite provides a high resolution 0.5 m panchromatic and 2 m 8-band multispectral imagery. WorldView-2 satellite is owned by DigitalGlobe (Longmont, CO, USA). The image was already radiometrically corrected and has 16 bitsPerPixel. The satellite orbits the earth in a sun synchronous orbit, at an altitude of 770 km and it has an orbit period of approximately 100 minutes, and a revisit frequency of 1.1 days, with a swath size of 16.4 km It has a spatial resolution for panchromatic bands of 0.46 m at nadir (0.56 m at 20° off-nadir), while multispectral imagery is captured with a resolution of 1.8 m at nadir (2.4 m off-nadir). The eight spectral bands include the four traditional visible to near infrared bands, and an additional four spectral bands (Coastal Blue (400-450 nm), Yellow (585-625 nm), Red Edge (705-745 nm) and another NIR2 (860-1040 nm) band (Chen et al., 2011).

The 8 bands are designed to improve the segmentation and classification of land and aquatic features beyond any other space-based remote sensing platform (DigitalGlobe, 2009). The additional coastal band can detect more details in water; in particular the water features (corals, seagrass, etc.) in shallow depths in addition to the blue band. Those technical advancements have resulted in better discrimination among coral reef features over local areas (Collin and Hench, 2012).

- o QuickBird

QuickBird is a high-resolution satellite that collects panchromatic imagery at 60 centimetre resolution and multispectral imagery at 2.4 and 2.8 meter resolutions. It is a product of DigitalGlobe (Longmont, CO, USA). The sensor acquires data in four spectral bands: blue (450-

520 nm), green (520-600 nm), red (630-690 nm) and NIR (760-900 nm). The swath width of the sensor is 16.5 km at nadir, or a strip at 16 km by 165 km.

Figure 15 and Table 2 illustrate the main comparisons between both satellite sensors.

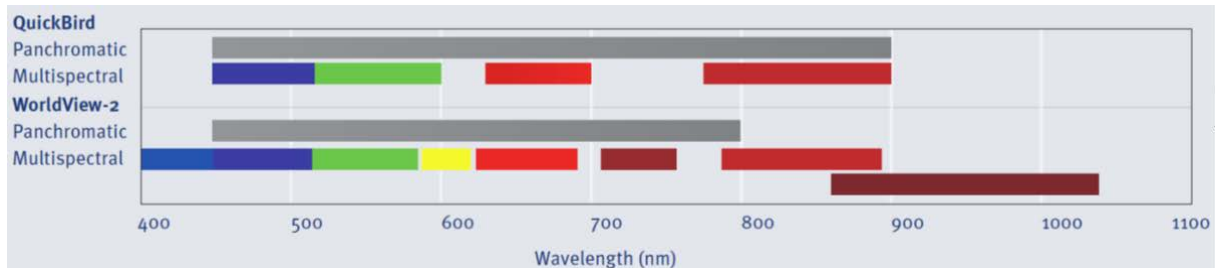


Figure 15. Graphical representation of the bands of WV2 and QB satellites. (DigitalGlobe)

Table 2. Comparison of WV2 and QB satellites (Collin and Hench, 2012)

| Waveband colors | Wavebands Numbers | Wavebands names | WV2 Wavelength range (nm) | QB Wavelength range (nm) |
|-----------------|-------------------|-----------------|---------------------------|--------------------------|
| Purple | 1 | "Coastal blue" | 400-450 | |
| Blue | 2 | Blue | 450-510 | 450-520 |
| Green | 3 | Green | 510-580 | 520-600 |
| Yellow | 4 | Yellow | 585-625 | |
| Red | 5 | Red | 630-690 | 630-690 |
| NIR1 | 6 | "Red Edge" | 705-745 | |
| NIR2 | 7 | Near Infrared 1 | 770-895 | 760-890 |
| NIR3 | 8 | Near Infrared 2 | 860-1040 | |
| | | Panchromatic | 400-800 | 450-900 |

- **Ground truth data**

A field campaign took place between October 2012 and January 2013 as part of an internship at IMARES titled "Benthic habitat mapping in the coastal waters of St. Eustatius" (Houtepen and Timmer, 2013). The main objective of this research was to find out what benthic habitats are present in the coastal waters of St. Eustatius, where they are located and what the species composition of these habitats is. For these, dropping video shots were performed every 150 meters along a transect line, running from the coastline at approximately 5 meters depth to a depth of approximately 30 meters. Every point where the camera was dropped, a GPS-waypoint was made and the footage was recorded. The depth, waypoint name and first judgment of habitat were noted after every drop.

As a result, a table was obtained with 600 points, their location, depth, substrate, vegetation and coverage percentage. For every waypoint there are videos available. Figure 16 shows a representation in Google Earth of these data.

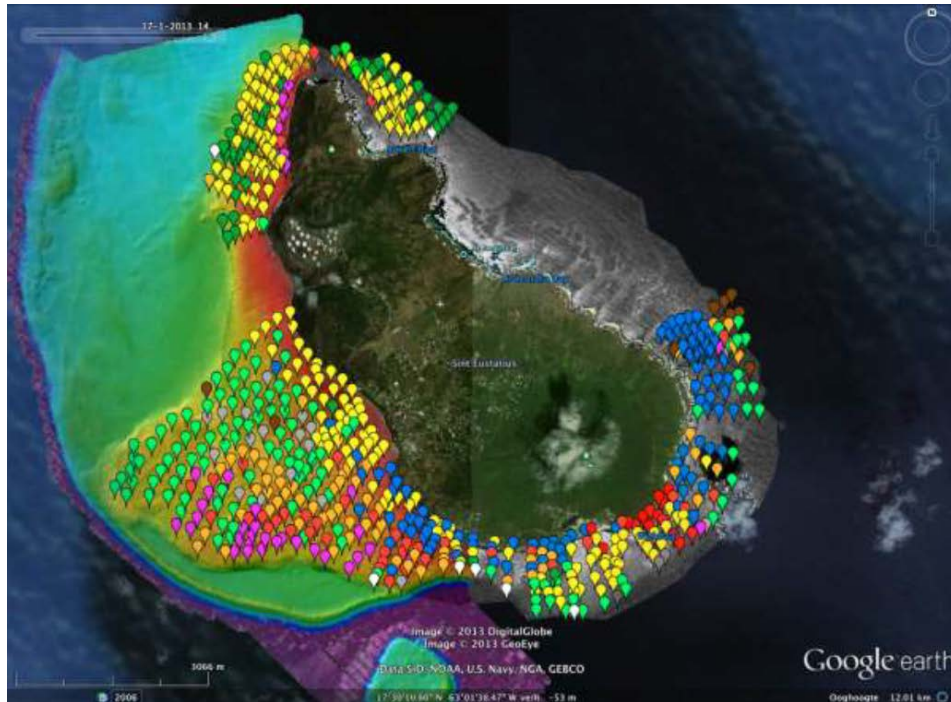


Figure 16. Field data points displayed over a depth map of coastal waters around Statia (Houtepen and Timmer, 2013). Colored dots are respectively: sand (yellow); rubble (grey); reef 0-33% (orange), reef 33- 66% (red); reef 66-100% (purple), gorgonian reef (blue); algal fields (light green); Sargassum sp. (brown) and seagrass (dark green).

- **Bathymetric data**

There are two sets of bathymetric data available for this research:

- Bathymetric data obtained from The Netherlands Hydrographic Service (TNHS) (Defense). This data is only available for the Western part of the island. It consists of a XYZ file with 4.703.598 depth points. This data was further process to obtain a Digital Elevation Model (DEM), as described in section 3.3.
- Depth data from the field campaign. Every drop shot of the field data includes its depth. To measure the depth, first a depth gauge attached to the camera was used. After this gauge was lost, the sonar fish finder from the boat used for the field campaign was employed.

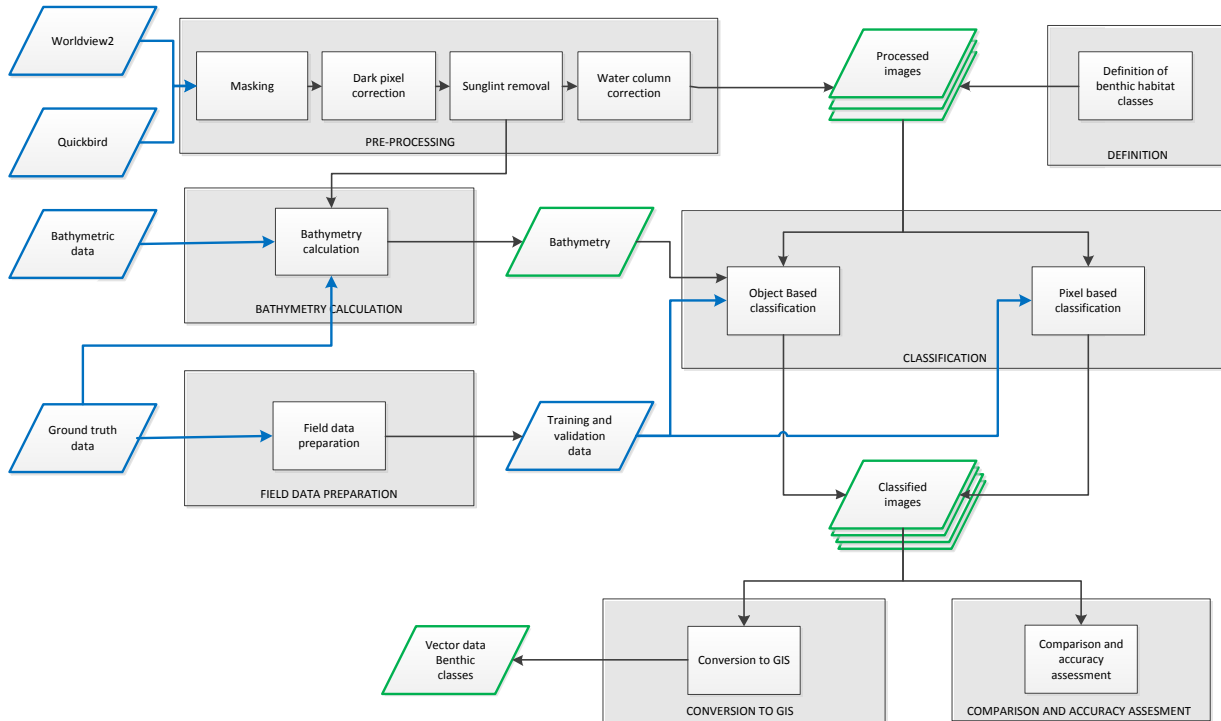
- **Benthic Habitat Map**

There is a Benthic Habitat Map available for Statia, created by Staatsbosbeheer (a Dutch organisation to manage and conserve Dutch nature reserves) in 2008 and validated by STENAPA at a limited number of points. It includes a classification of coral, sand, rock/rubble and seagrass. This benthic habitat map is included in Appendix 3. The classification of coral and sand includes low, medium and high probability. This classification was performed using a QuickBird image without further corrections and using histogram classification of ArcGIS.

Based on this classification map by STENAPA, satellite imaging and bathymetric data, a second habitat map was developed by IMARES for the environmental impact assessment of the St. Eustatia harbour extension (Slijkerman et al. 2011). From this classification a rough calculation was made on the total surface per habitat per depth category. These are included in Appendix 3. These classifications could be used in further analysis for comparison.

3.3 General Methodology

The flowchart of the general methodology of this MSc thesis is represented in Figure 17.



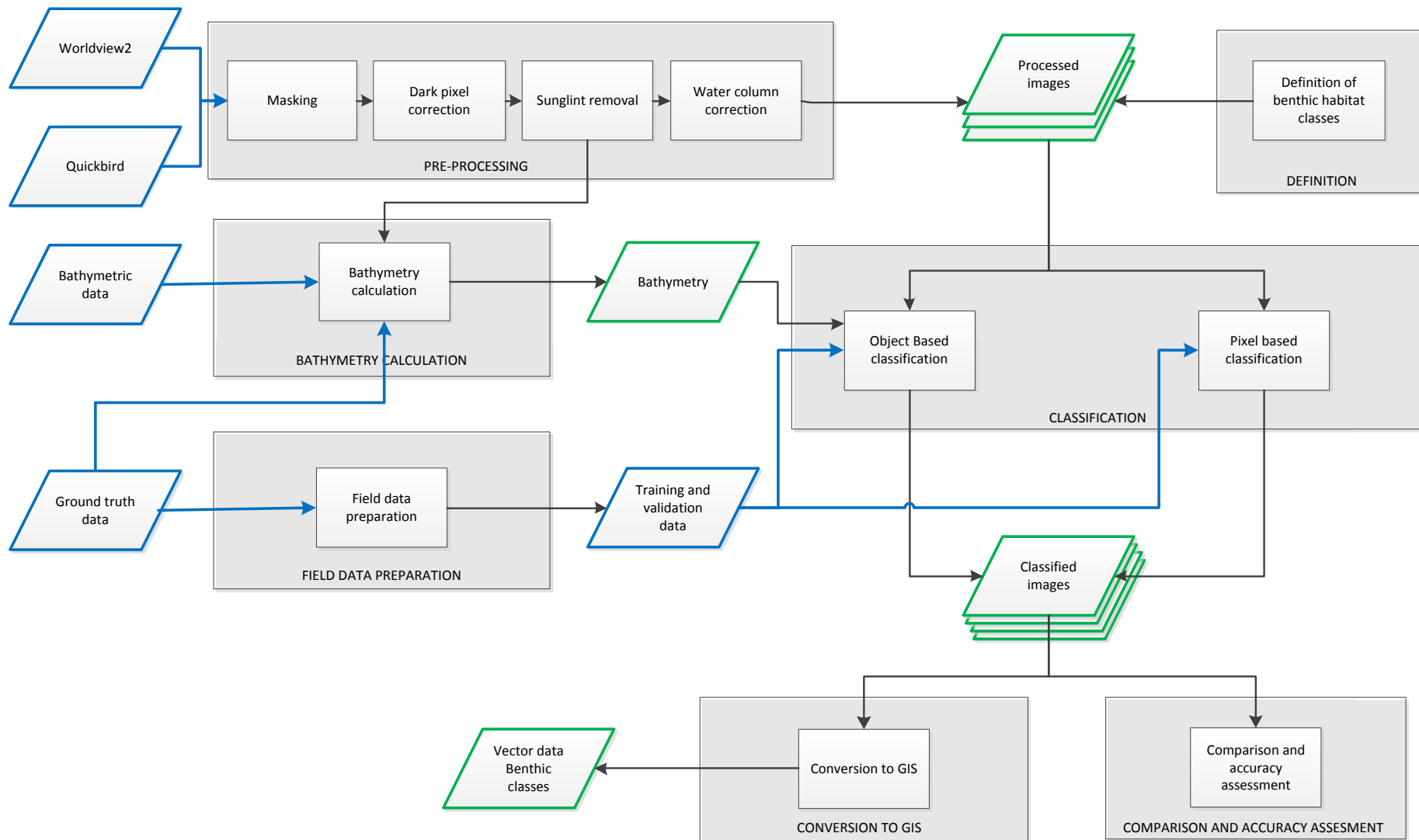


Figure 17. Methodology flowchart. Blue boxes indicate available data, green boxes are outputs and black boxes are processes.

The methodology is based on the following working steps, as observed in the flowchart (Figure 17). All imagery and data was re-projected to the same coordinate system, WGS 84 / UTM zone 20N.

3.3.1 Preparation of field data

The table containing the 600 points (drops) from the field campaign (Houtepen and Timmer, 2013), their location, depth, substrate, vegetation and coverage percentage was prepared for its use in this research. There were no images available for the first 68 drops and their classification was not accurate, therefore they were removed. Also, points for which classification was not sure were also eliminated from the table. A final simplified table was prepared for the benthic classification using the bottom type (substratum) and the bottom community (vegetation type) only when it had more than 33% coverage. Visual inspection of the recordings was also performed to confirm the classification. In case of doubt, a marine ecologist expert (Erik Meesters, IMARES) was consulted and a reclassification was made. With this final table a feature class was created with all the fieldwork points. This final table with 524 records is included in Appendix 2.

The final data points were randomly divided into two sets to be used in the classification, the training and the validation data. Therefore, each data set contained 262 points. However, some of this data points were located outside the image or in masked areas, and were not used during the classification.

3.3.2 Pre-processing imagery

Satellite sensors record the intensity of electromagnetic radiation as digital number (DN) values. The DN value of each image is specific to the type of sensor and the atmospheric condition during the image acquisition. The first step in the methodology is to pre-process the images to obtain the radiance.

WorldView-2 and QuickBird products are delivered as radiometrically corrected image pixels. Top of the Atmosphere (TOA) spectral radiance is defined as the spectral radiance entering the telescope aperture. The conversion from radiometrically corrected image pixels to TOA spectral radiance is a simple process, based on a technical note from Digital Globe for the QuickBird (Kause, 2005) and for the WorldView-2 imagery (Updike and Comp, 2010).

The equation applied is the following:

$$L = \frac{absCalFact_{Band} * q_{pixel,band}}{\Delta\lambda_{Band}} \quad \text{Equation 16}$$

where L is the satellite radiance ($W m^{-2} sr^{-1} \mu m^{-1}$), $absCalFactor_{Band}$ is the absolute radiometric calibration factor ($W m^{-2} sr^{-1} count^{-1}$) for a given band (provided in the .IMD files), $q_{Pixel,Band}$ are radiometrically corrected image pixels (counts) and $\Delta\lambda_{Band}$ is the effective bandwidth of each band (μm), as referred by Digital Globe.

WV2 and QB images were converted directly from DN to TOA Spectral Radiance.

3.3.2.1 Masking

The purpose of the masking is to consider only the area of interest, this is the shallow waters. When extracting aquatic information, it is useful to eliminate all upland and terrestrial features (Mishra et al., 2006). Therefore, all terrestrial features, boats, piers, and clouds and its shadows were masked out of the image. The process of masking follows the next steps:

1. The inland features were masked out by preparing a binary mask using ArcGIS, which was subsequently applied to all the bands.
2. Radiance values of the NIR band were used to prepare a binary mask to mask clouds and waves. However, it was found out that better results were obtained when the sunglint correction was performed before masking. Therefore, atmospheric and sunglint correction were performed first, and then another binary mask was prepared visually using ArcGIS masking the clouds, their shadows, boats and breaking waves next to the coast for each of the satellite images.
3. Previous to classification, another mask was prepared in order to mask deep waters. This mask was applied to the WorldView-2 image and was elaborated visually using ArcGIS by taking into

account the spatial extent of the QuickBird image, in order for both imagery to have a similar extent.

3.3.2.2 Atmospheric correction

The images were atmospherically corrected by applying a first-order atmospheric correction (dark pixel, or deep water subtraction) to every image. The minimum radiance value for each band was recorded and subtracted to all the pixels in that band. Radiance values of 0 were ignored in the calculation in order not to have negative values.

3.3.2.3 Sunlint removal

In both imagery used in this study (WV2 and QB) the influence of wind-driven waves could be observed, and these produce a sunlint effect at the sea surface.

The method discussed in 2.2.1.2, proposed by Hedley et al. (2005), was performed for both atmospherically corrected images.

The steps carried out were the following:

1. A sample of pixels from two homogenous areas of deep water with different sunlint effect was selected. The minimum Near Infrared (MinNIR) value in this sample was determined.
2. A linear regression of NIR brightness (x-axis) against the band signal (y-axis) was performed using the selected pixels for each band. The slope of the regression line is the output of interest for the deglint formula.
3. The deglinted radiance was calculated of all the pixels using the formula of Equation 17:

$$L'_i = L_i - b_i(L_{\text{NIR}} - \text{Min}_{\text{NIR}}) \quad \text{Equation 17}$$

3.3.2.4 Water column correction

The Depth Invariant Index method (Lyzena (1978, 1981) and expanded upon by Mumby et al. (1998)) was performed for the QB and WV2 deglinted images.

The following steps were carried out:

1. Groups of pixels are selected from the imagery using ROIs that have the same bottom type but different depths. In this case, areas of sand were selected as they were easily recognisable.
 2. The pixel values for the selected areas in all bands are converted to natural logarithms to calculate the transformed radiance ($X_i = \ln(L_i)$).
 3. Bi-plots of the transformed data are made and examined using the transformed radiances.
 4. The ratios of attenuation were obtained using the formulas included in chapter 2.2. The depth invariant Index was calculated for each pair of spectral bands producing a single depth-invariant band.
- For QB, the RGB ratios (bands 1, 2 and 3) were used to generate the depth invariant index image. However, as presented later on in Chapter 4, the ratios of the bands 2-3 and 3-1 proved to have very little linear correlation. This might be due to the larger light attenuation of band 3 (red) in the water column. Therefore, it could be expected that using the 2-3 and 3-1 attenuation ratios could only cause noise in the image. To assess this, also a depth invariant index image was created using only the bands 1-2 (Blue-green ratio), for its accuracy comparison in the image classification.
 - For WV2, to assess the possible improvement of the use of the extra "coastal blue" band (band 1) two depth invariant images were calculated, one for RGB (bands 2, 3 and 5) and one for RGC (bands 1, 3 and 5) band combinations.

3.3.3 Classification

Supervised pixel and object-based classification were performed for the images. The main steps for both of them are (Green et al., 2000):

1. Definition of habitat classes

In chapter 3.1.2., five main benthic habitat classes in the study are defined. However, the final classification was done differentiating only 4 benthic habitats. This is because during the classification process the first results did not meet the expectations. The results showed confusion between the class seagrass and coral reefs. It was difficult to differentiate the spectral profile of sargassum. Also, there were not enough field data points for the habitat type rubble to perform a successful classification, and this habitat type showed a very mixed structure. Therefore, a final classification with only 4 classes was performed:

- Coral reef and gorgonian
- Seagrass, algae and Sargassum
- Sand
- Unclassified (land, intertidal areas and clouds)

2. Selection of training areas

A training area is a group of pixels that represent a known habitat. These should be representative of the habitat class; otherwise it will cause misclassification errors.

The training areas used were defined using the training field points.

3. Evaluation of the signatures

The spectral signatures of the training areas were evaluated to avoid mistakes, by comparing them to spectral profiles of correspondent in-situ data for quality control, as it is desirable that habitat signatures derived from training samples are representative of the class in question and dissimilar to other classes, and therefore deviated spectral values within the samples were checked.

4. Selection of decision rules

A maximum likelihood classification was performed.

3.3.3.1 Pixel based classification

The input for the maximum likelihood classification were the TOA radiance images, the images atmospherically corrected, the ones also corrected for sunglint and the depth invariant images, all of them masked for deep waters. It was expected that the sunglint removal and the water column correction technique would generate a more accurate benthic habitat map for the two available satellite images. Therefore, to evaluate the improvement of the proposed methodology, a classification with and without the proposed corrections was to be performed for comparison.

Using the training samples and visual image interpretation, Regions Of Interest (ROI) of well-known ground areas were selected as training sites. The same ROIs were identified for the QB and the WV-2 images, following the classification scheme as defined in Figure 18. The signatures of the training areas were evaluated by comparing them to spectral profiles of known data. A maximum likelihood algorithm was performed using ENVI, with equal probabilities of the classes. The data scale factor was set to 1. However, this classification algorithm requires two or more image bands to produce the statistics necessary for spectral habitat separation. This limited the possibility of assessing the benefits of the water column correction using only one band ratio for QB. Therefore, a parallelepiped classification was performed for this single band image. Parallelepiped classification uses a simple non-parametric decision rule by establishing decision boundaries forming an n-dimensional parallelepiped in the image data space. The dimensions of the parallelepiped are defined based on a standard deviation threshold from the mean of each selected class. In this case, the standard deviation was set to 1.

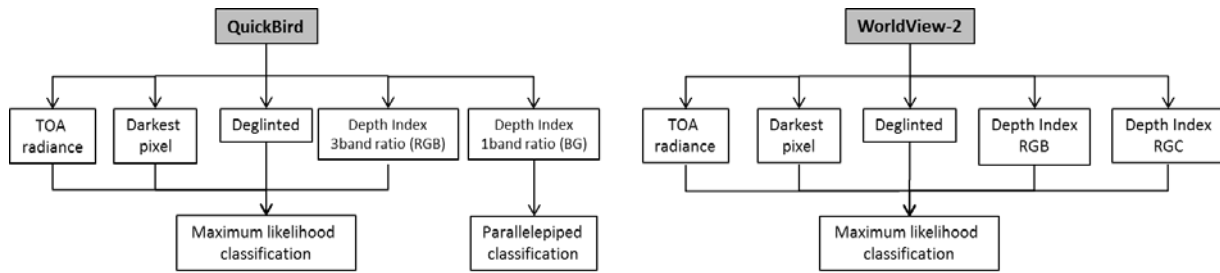


Figure 18. Pixel based classification scheme

3.3.3.2 Object Based classification

An object based classification was performed using eCognition. This consisted of two main steps:

- Segmentation: First, the images were segmented using multi-resolution criteria. The segmentation is a very important step in object based classification, and so, an iterative process was applied by adjusting the segment size, shape and compactness, re-running the segmentation, and performing a visual assessment of the results was made until a satisfactory result was obtained that matched habitat features visible in the images. This resulted in different criteria for the QB and the WV2 image due to the radiometric resolution and the range of the radiance values.
- The composition of the homogeneity criterion selected is included in Table 3.

Table 3. Homogeneity criterion selected in the object based classification

| Criteria | QB | WV2 |
|---------------------|-----|-----|
| Scale factor | 0.5 | 20 |
| Shape | 0.1 | 0.2 |
| Compactness | 0.5 | 0.5 |

It should be noted here that eCognition failed to execute the classification of the depth invariant images for QB and WV2. This could be due to the presence of long low decimal numbers (between -7 and 51 for QB and -103 to 32 for WV2) and non-existing (NaN) values. To overcome this, a low pass filter (3x3) was applied, and the image was converted to integer values (first multiplying by 1000) and then the classification was performed. However, the segmentation criteria was changed to a scale factor of 20, shape 0.1 and compactness 0.5, for these two images.

- Classification: Then, a nearest neighbour classification was performed using the mean pixel values of all the bands. Training areas for the different classes were selected using the training field data, as in the case of the pixel based classification.

The object-based classification was performed on the atmospherically corrected images, the deglnted images and the depth invariant image of the RGB band combination (as the 1-band ratio of QB and the RGC band combination for WV2 proved poorer results). The OBIA classification was not performed on the original TOA image, because in the pixel based classification the results obtained were the same as of the darkest pixel corrected image, and therefore it was estimated that it was not necessary. This classification scheme is presented in Figure 19.

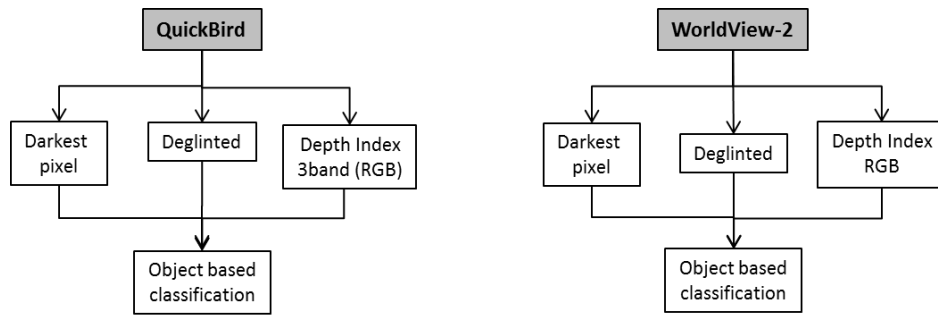


Figure 19. Object based classification scheme

3.3.4 Comparison and accuracy assessment

An accuracy assessment of the classification results was performed using the validation ground truth data. Only the validation points located in non-masked areas were used. This resulted in a different number of validation points for both images (205 for QB and 160 for WV2).

Error matrices (or confusion matrices) were calculated for all the classified images. From the confusion matrix three types of accuracies are generated, overall accuracy, users accuracy and producers accuracy. Overall accuracy represents the number of correctly classified pixels. Users accuracy is the probability that a pixel classified in the image is correctly classified when compared to field data. To calculate this, the number of pixels correctly classified as a class is divided by the total number of pixels classified in that class. Various authors had used the user's accuracy, as it is useful for assessing the accuracy of classification for the various habitat classes (Benfield et al., 2007, Mumby et al., 1997). Producers accuracy is the probability that any pixel in a given category has been correctly classified. For this, correctly classified pixels are divided by the total number of ground reference pixels in that class (Congalton, 1991).

Error of commission occurs when a pixel in a class is included when it should be excluded. Error of omission will be to exclude a pixel that should be included in the class. The Kappa coefficient is a measure of the proportional improvement over a purely random assignment of classes (Congalton, 1991).

3.3.5 Bathymetry calculation

The Ratio transform method, as explained in chapter 2.2, was performed for the calculation of the bathymetry for both images.

The next steps were followed:

1. The relative bathymetric values for both images were extracted using the expression:

$$\frac{\ln(nR_i)}{\ln(nR_j)} \quad \text{Equation 18}$$

The constant n was set to 1000 to assure the algorithm was positive (Stumpf et al., 2003). For QB, the values of R_i and R_j used in the expression were the blue band and the green band, respectively, of the deglited image.

The bathymetry was calculated using the green/blue ratio and the green/coastal ratio for the WV2 image, as these proved to be the best band ratios, so they were both finally used for the bathymetry calculation.

2. These relative bathymetric values were regressed with the ground truth data to calculate the constants m_0 and m_1 . All the field data points not located in masked areas were used.

3. The depth values were calculated for all pixel values, following the equation:

$$z = m_1 \frac{\ln(nR_i)}{\ln(nR_j)} - m_0 \quad \text{Equation 19}$$

For the accuracy assessment of the bathymetric derivation, two ground truth data sets are available, the field campaign data and the bathymetric data obtained from The Netherlands Hydrographic Service (TNHS) (Ministry of Defense). This data from THNS (only available for the Western part) was converted into a Digital Elevation Model (DEM) using the DEM lastools, a LiDAR processing toolbox. The result is shown in Figure 20.

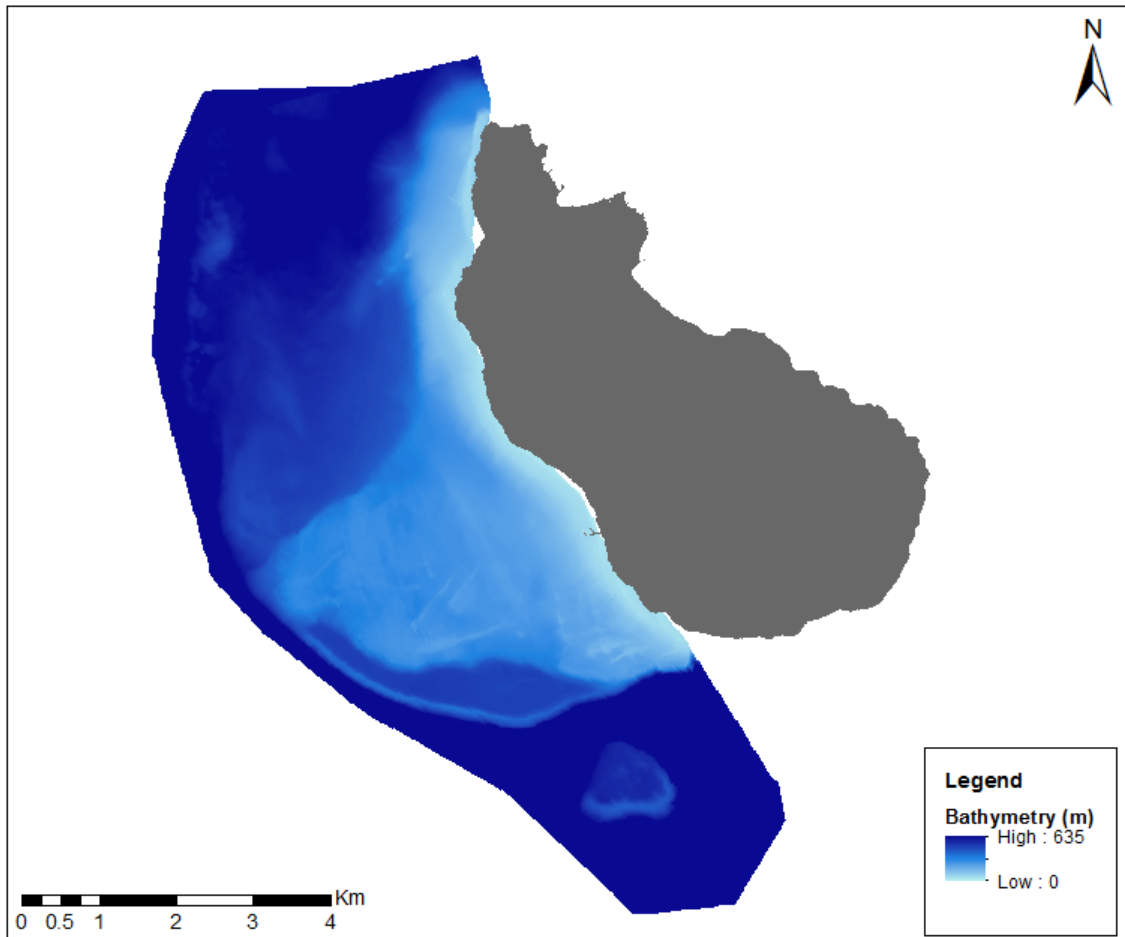


Figure 20. Bathymetry for the Western part of Statia (Ministry of Defence)

3.3.6 Conversion to GIS

Final classification results were converted into vector format.

4 Results

4.1 Sunlint removal

The deglinting process was successfully implemented on the atmospherically corrected images. Then the clouds, breaking waves and boats were masked.

Figure 21 shows an example of the deglinting method applied to the blue band of QB (NIR band regressed against the blue band). The sunlint correction for the blue band was therefore calculated using the slope of this regression and the Equation 1 in chapter 2.2.1.2, with the resulting expression: $L_i = Li - 1.7144 (LNIR - MinNIR)$, being L_i the blue band and $LNIR$ the NIR band. The minimum NIR value ($MinNIR$) was obtained from the minimum value of band 4 from the regions of interest. The same process was repeated for the other bands.

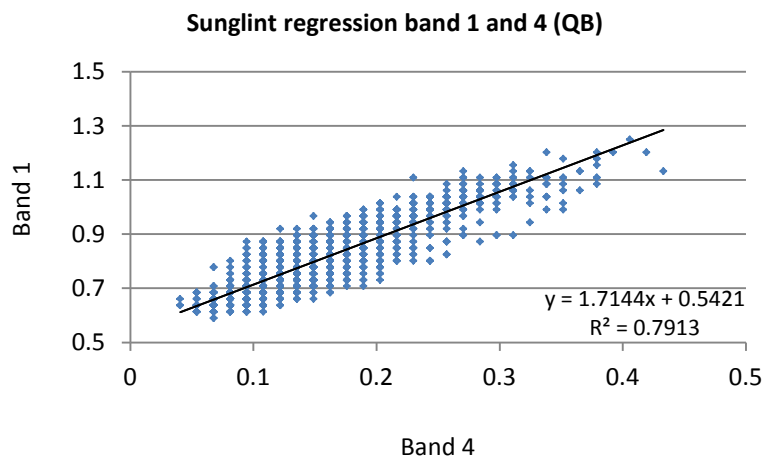
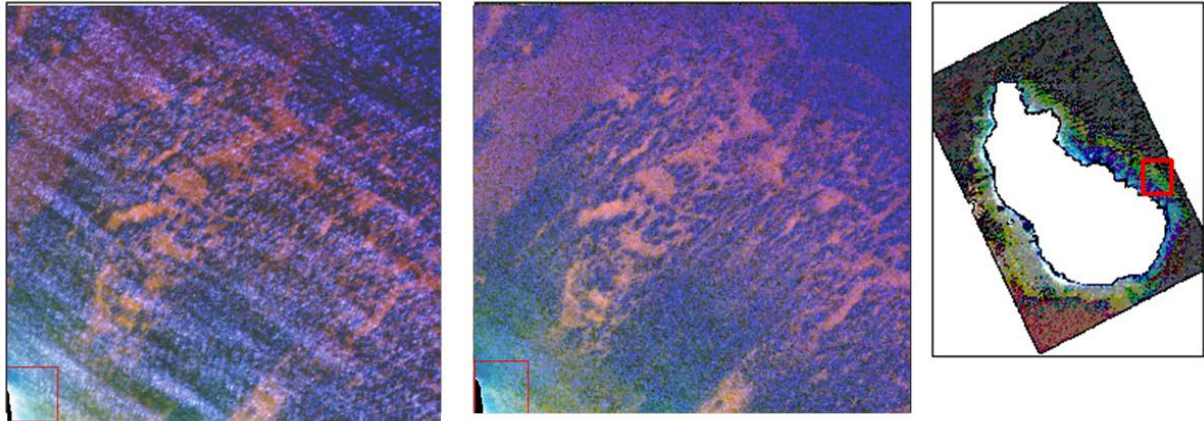


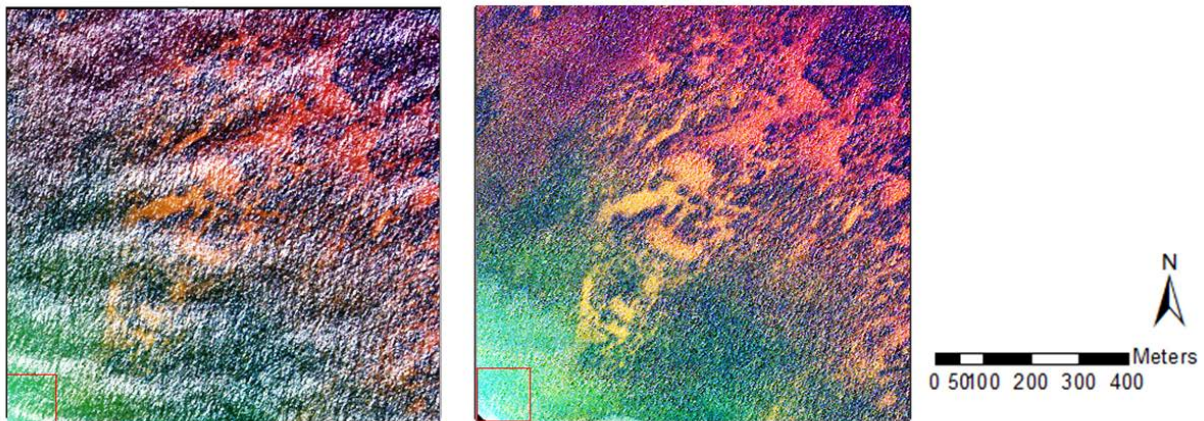
Figure 21. Bi-plot of the NIR band (band 4) and blue band (band 1) for the sunlint removal of QB

For WV2, the same process was implemented, but the bands were regressed against the band 7 (NIR2), as it is the most similar band to the NIR band of QB. In this research it was also tested to use the band 6 (red edge) instead, but the results obtained were very similar, so finally the band 7 was chosen.

Some examples of the resulting images are shown in Figure 22 for QB and WV2.



Results before (left) and after (right) the Sunglint removal method for QuickBird



Results before (left) and after (right) the Sunglint removal method for WorldView-2

Figure 22. Results before (left) and after (right) the Sunglint removal method for QB and WV2.

Because of the characteristics of this deglinting methodology, the resulting QB image has 3 bands and the WV2 image has 6 bands (NIR bands are removed). As it can be observed, the deglinted images show a clear visual improvement. Previously obscured submerged features become more visible and clearer. Therefore, it is expected that the classification accuracy will improve.

The spectral profiles for known pixels depicting algae/seagrass, sand and coral/gorgonian, for QB and WV2 is displayed in Figure 23.

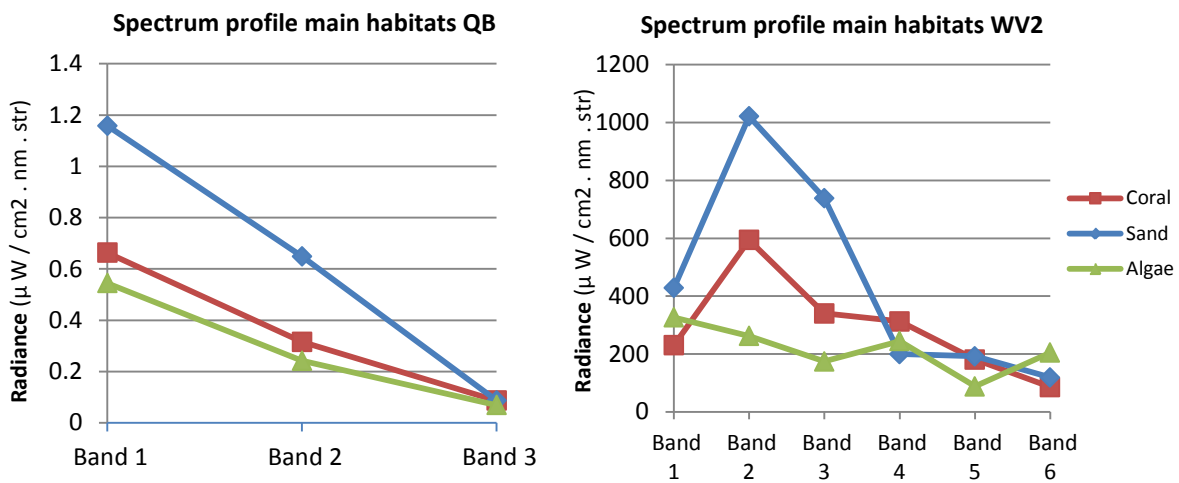


Figure 23. Spectral profile from the QB and WV2 image over different bottom types: coral, sand and algae.

4.2 Water column correction

The water column correction technique was applied on the deglinted images. For the calculation of the ratio attenuation coefficients, four regions of interest were used. These were homogeneous sand areas at various depths.

Bi-plots of the natural logarithm of the pixel values for those regions were created for each pair of spectral bands. These transformed radiance values were used in the equations included in chapter 2.2. (Equations 3, 4 and 5) to calculate the ratio of attenuation coefficients. Then, the depth invariant index was calculated for each pair of spectral bands using equation 6.

For QB, the bi-plots of the natural logarithm transformed radiance for the RGB ratios (bands 1, 2 and 3) are presented in Figure 24, and the results for the equations in Table 4.

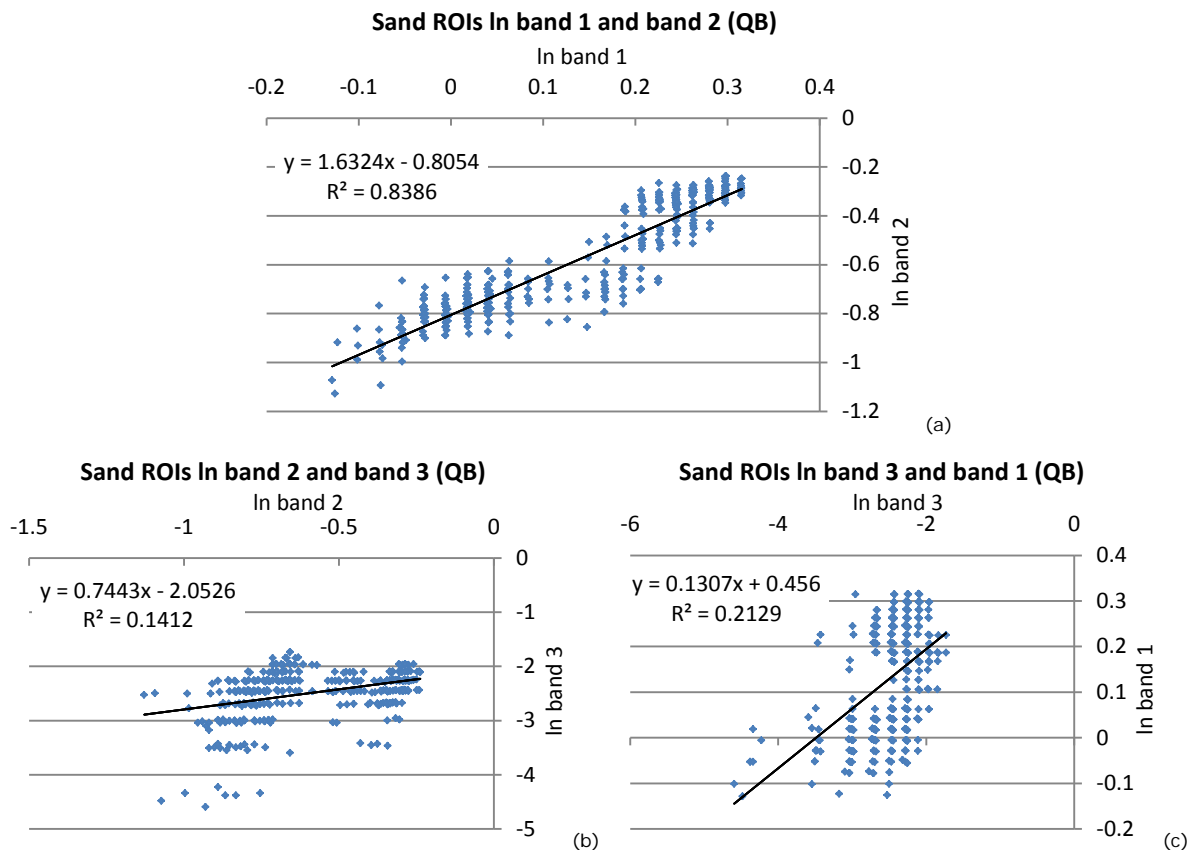


Figure 24. Scatter plots of sand substrate ROI's at various depths between band 1 and 2 (a), between band 2 and 3 (b) and between band 3 and 1 (c) for QB.

Table 4. Parameter values to calculate the ratio attenuation coefficient between bands 1 (B), 2 (G) and 3 (R) for QB.

| | Band 1 (blue) | Band 2 (green) | Band 3 (red) |
|-----------------|------------------|-------------------|-----------------|
| mean | 0.130 | -0.593 | -2.494 |
| variance | 0.015 | 0.049 | 0.192 |

| | Ratio 1/2 | Ratio 2/3 | Ratio 3/1 |
|---|--------------|--------------|--------------|
| Covariance | 0.025 | 0.036 | 0.025 |
| a | -0.667 | -1.965 | 3.520 |
| Attenuation Coefficient $\frac{k_i}{k_j}$ | 0.535 | 0.240 | 7.179 |

In the scatter plots in Figure 24 it can be observed that most of the pixel values between band 1 and 2 have a linear correlation. However, this linear correlation does nearly not exist between band 2 and 3, and is small between band 3 and 1. As discussed before, it could be possible that using the 2-3 and 3-1 attenuation ratios could only cause noise in the image. Therefore, two depth invariant index images were created, one using the three ratios and another one using only the blue-green ratio.

After calculation of the ratio attenuation coefficients (k_i/k_j), a depth invariant image was obtained by applying equation 6 of Chapter 2.2.1.3. This image was therefore corrected for the water column effect. Figure 25 shows some results of the final depth invariant index image for the three band ratio (RGB) and one band ratio (BG) of QuickBird.

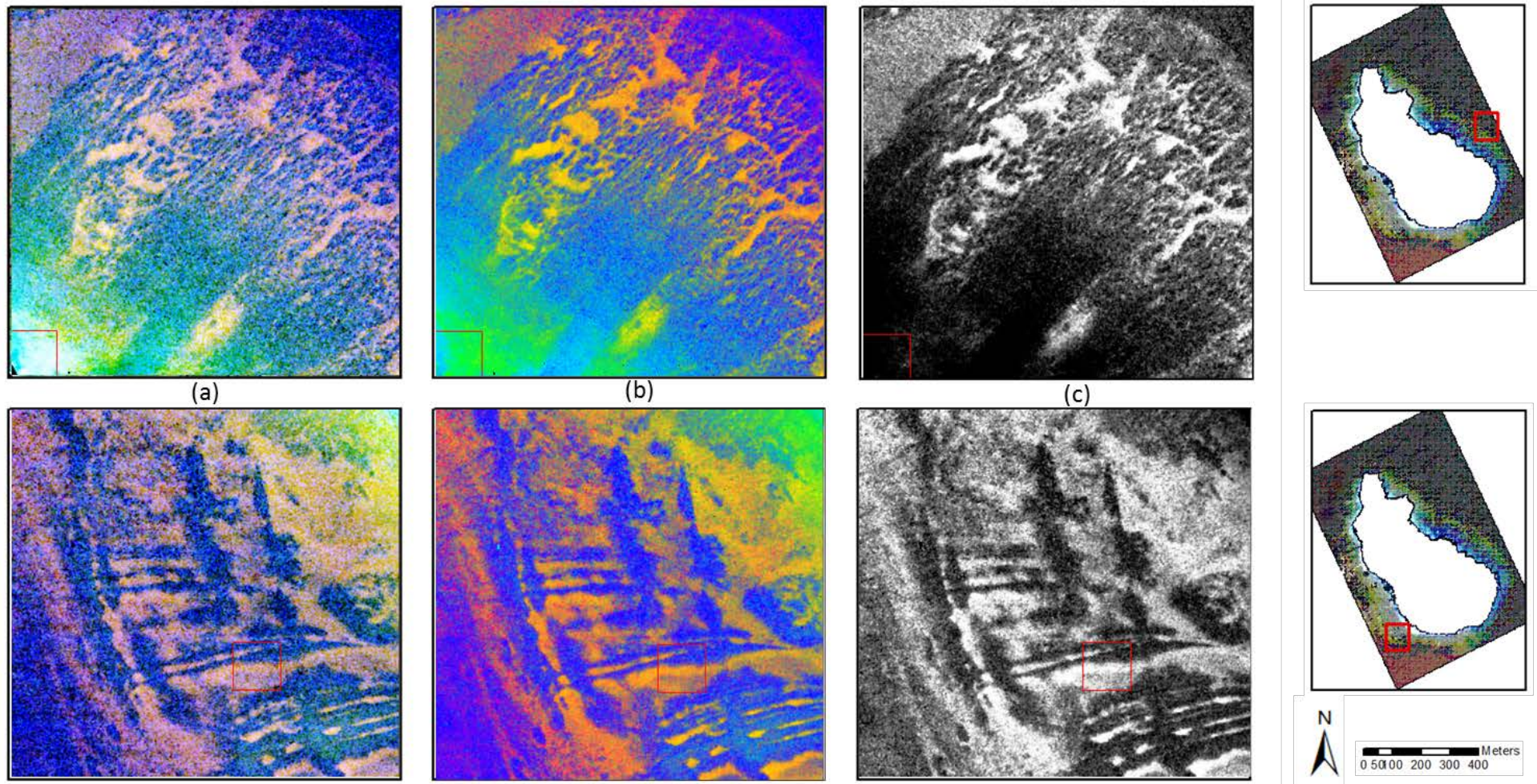


Figure 25. Two example results before (a) and after (b and c) the Depth Invariant index for QB.
 (a) Deglinted Image. (b) Three band ratio Depth Invariant index (RGB). (c) One band ratio Depth Invariant index (BG).

For WorldView-2, two depth invariant images were calculated, one for RGB (bands 2, 3 and 5) and one for RGC (bands 1, 3 and 5) band combinations. The bi-plots of the natural logarithmic transformed radiances for these two ratio combinations are presented in Figure 26 and the results for the equations in Table 5.

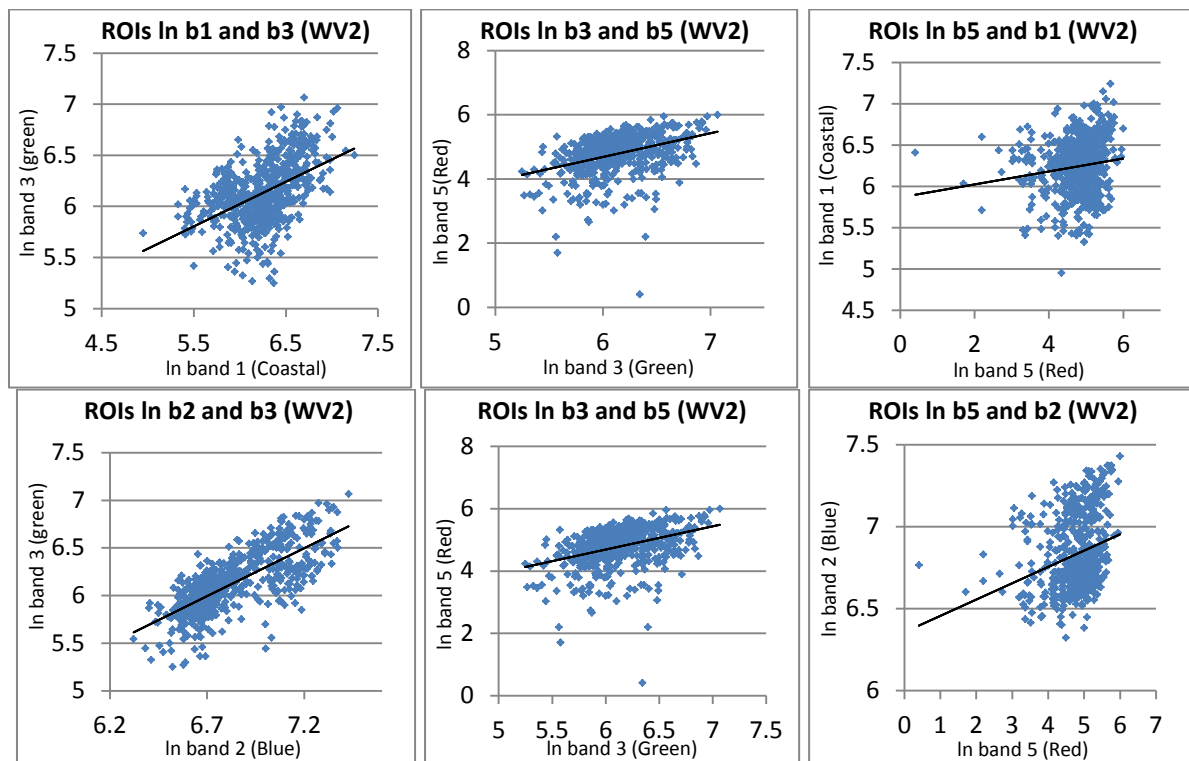


Figure 26. Scatter plots of sand substrate ROI's at various depths for the band ratios RGC (bands 1-3-5) (up) and RGB (bands 2-3-5) (down) for WV2

Table 5. Parameter values to calculate the ratio attenuation coefficient between bands 1-3-5 (coastal-green-red) and between bands 2-3-5 (blue-green-red), for WV2.

| | Band 1 (coastal) | Band 3 (green) | Band 5 (red) |
|-----------------|---------------------|-------------------|-----------------|
| mean | 6.241 | 6.127 | 4.779 |
| variance | 0.119 | 0.096 | 0.376 |

| | Ratio 1/3 | Ratio 3/5 | Ratio 5/1 |
|---|--------------|--------------|--------------|
| Covariance | 0.052 | 0.072 | 0.025 |
| a | 0.218 | -1.955 | 4.367 |
| Attenuation Coefficient $\frac{k_i}{k_j}$ | 1.242 | 0.241 | 8.846 |

| | Band 2 (blue) | Band 3 (green) | Band 5 (red) |
|-----------------|------------------|-------------------|-----------------|
| mean | 6.832 | 6.127 | 4.779 |
| variance | 0.051 | 0.096 | 0.376 |

| | Ratio 2/3 | Ratio 3/5 | Ratio 5/2 |
|---|--------------|--------------|--------------|
| Covariance | 0.051 | 0.072 | 0.030 |
| a | -0.438 | -1.955 | 5.513 |
| Attenuation Coefficient $\frac{k_i}{k_j}$ | 0.654 | 0.241 | 11.117 |

After calculation of the ratio attenuation coefficients (k_i/k_j), the two depth invariant images were created. Figure 27 displays some results of the final depth invariant index image for the RGB and RGC band ratio for WorldView-2. As it can be observed, the depth invariant images show some visual improvement, specially the RGB band ratio image.

When solving the equation for the sunglint removal method, negative values in the deglinted image were created. This is because, although submerged pixels should not result in out-of range values, areas

which are not part of the regions used in the deglinted model (e.g. isolated outlier pixels due to waves or other effects or shallow areas of sand) may produce negative values. Also, closely packed seagrass and macroalgae can absorb enough light that when the deep water signal is subtracted from total radiance, the resulting signal is negative. This issue should be considered when applying further post-processing steps, especially in the creation of the depth invariant image, as a natural logarithm of the radiance values was performed therefore creating imaginary values for these negative values (NaN values). Therefore, for the regions of interest used in the depth index method, negative radiance values were not taken into account. However, when calculating the depth invariant image, and because of the presence of these negative numbers, many NaN values were created, especially in the WorldView-2 image (probably due to the presence of more outlier values associated with the waves). This should be carefully taken into account for the later classification.

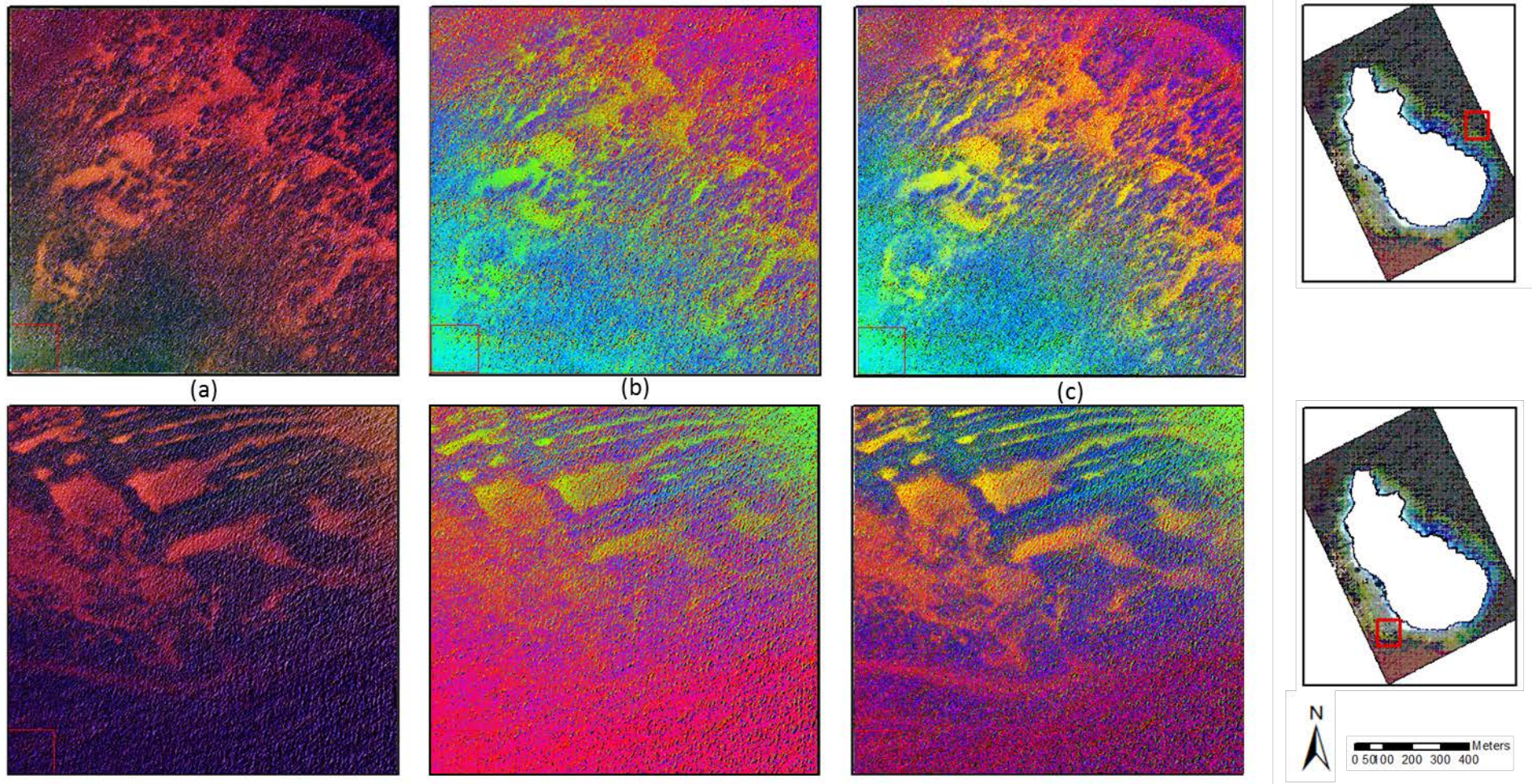


Figure 27. Two example results before (a) and after (b and c) the Depth Invariant index for the WV2 image.

(a) Deglinted Image. (b) RGC band ratio Depth Invariant index. (c) RGB band ratio Depth Invariant index.

4.3 Classification

4.3.1 Pixel-based classification

A maximum likelihood classification was implemented on the QB and WV2 preprocessed images, as explained in chapter 3.3.3.1., and following the scheme of Figure 18, using 10-20 training samples for the four main classes based on the training field data. All the bands of each image were used for the classification.

The resulting classified images are displayed in Figure 28 for QB and Figure 29 for WV2. Results of the TOA radiance image classification are not shown as they produce the same results as the atmospherically corrected image.

Close-ups of these classifications are included in Appendix 4 for a better visual interpretation.

4.3.2 Object-based classification

An object based classification using eCognition was performed, following the methodology explained in in 3.3.3.2., and following the criteria explained in Table 3. The same training field points as the ones used with the pixel based classification were used.

The resulting classification images of the object based classification are displayed in Figure 30 for QB and Figure 31 for WV2.

Close-ups of these classifications are included in Appendix 4 for a better visual interpretation.

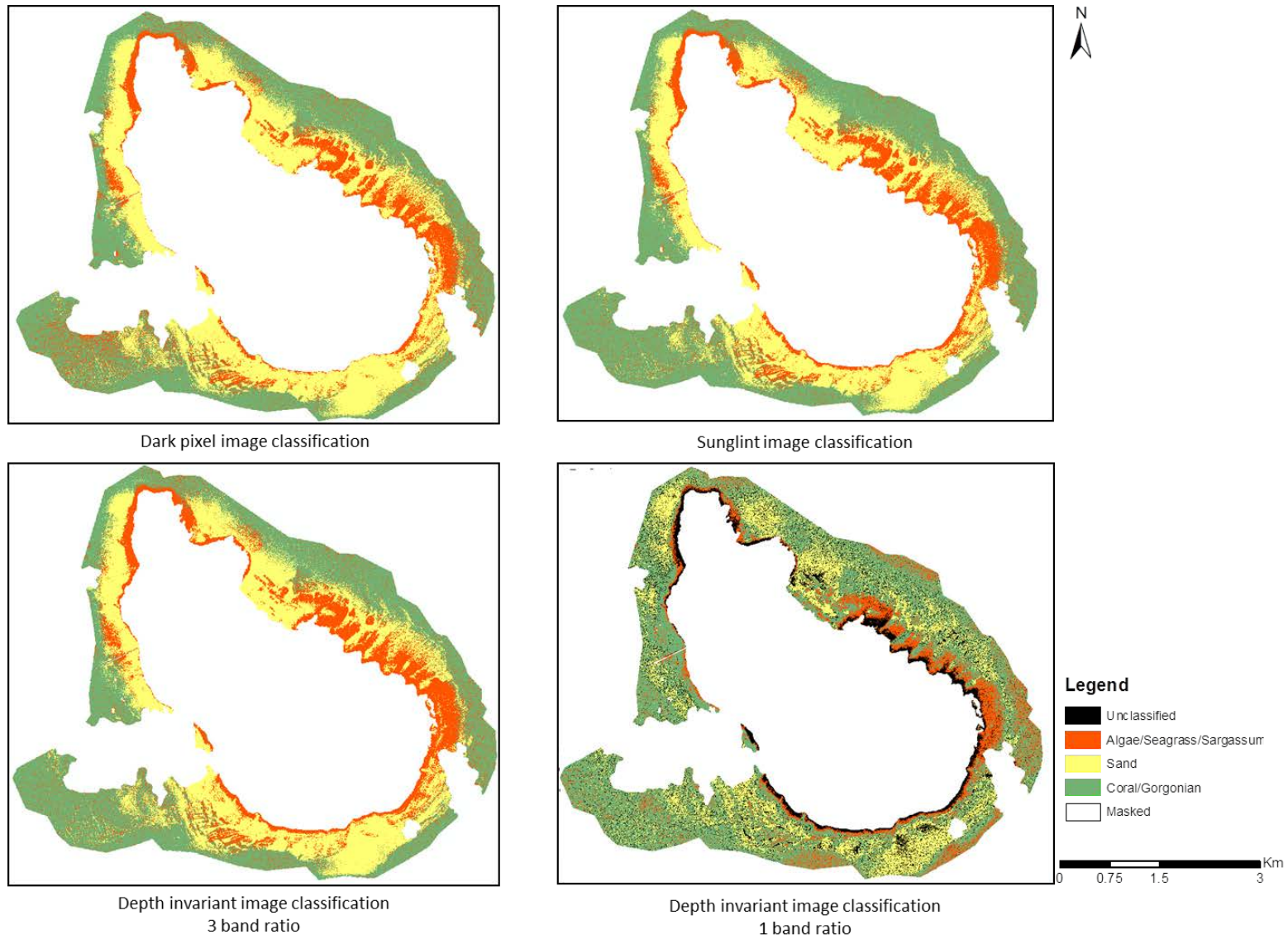


Figure 28. Pixel based classification results for QB.

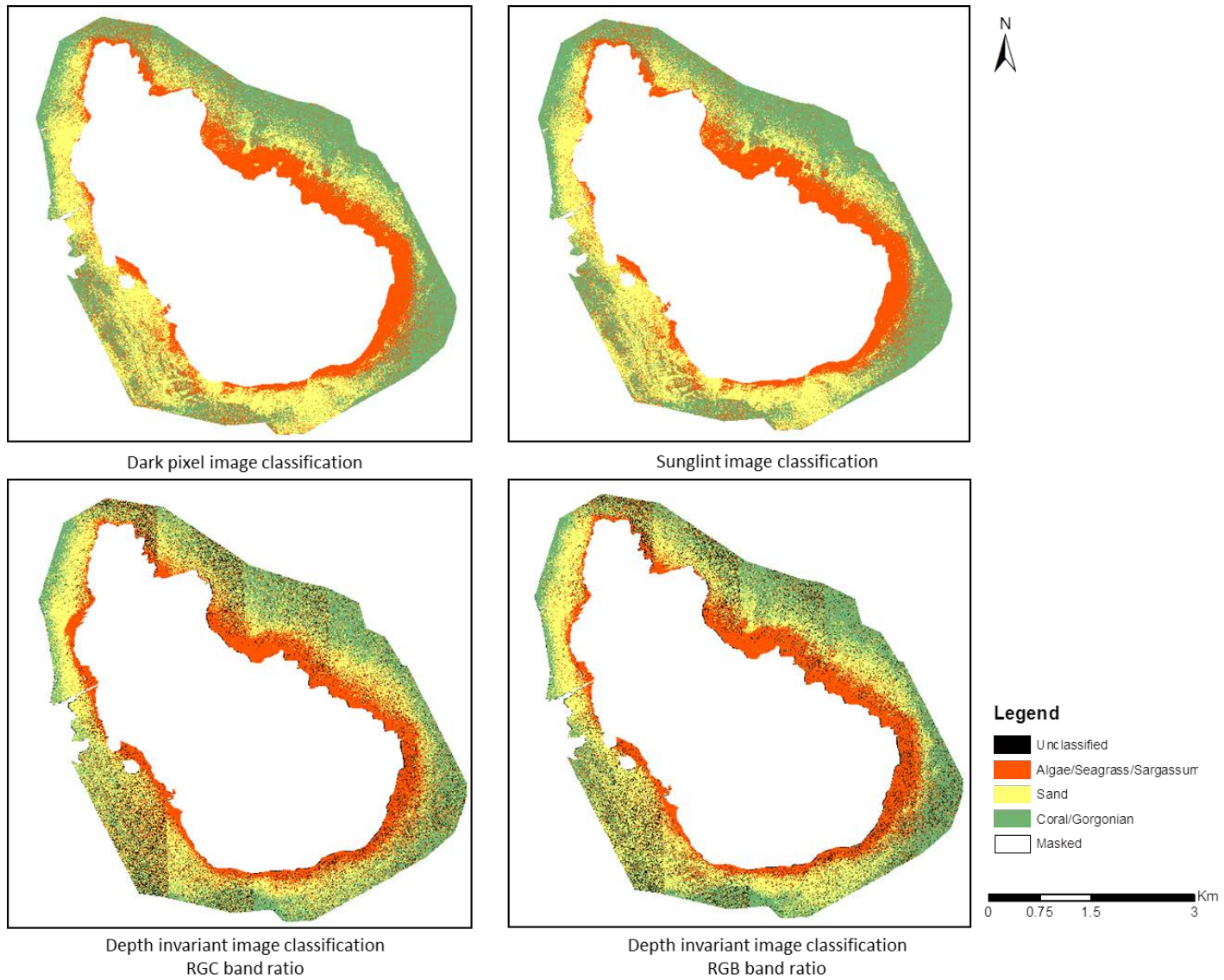


Figure 29. Pixel based classification results for WW2.

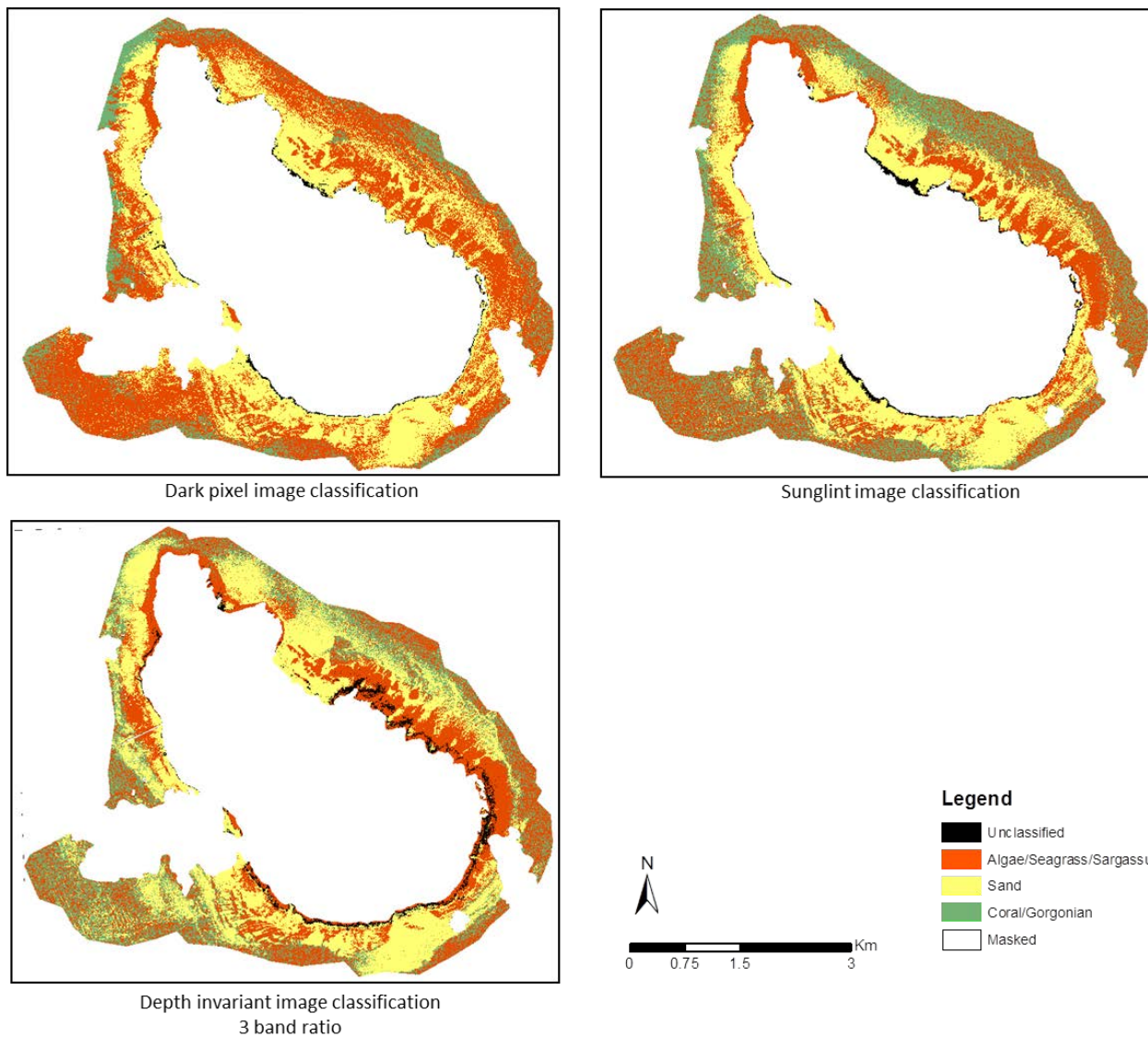


Figure 30. Object based classification results for QB.

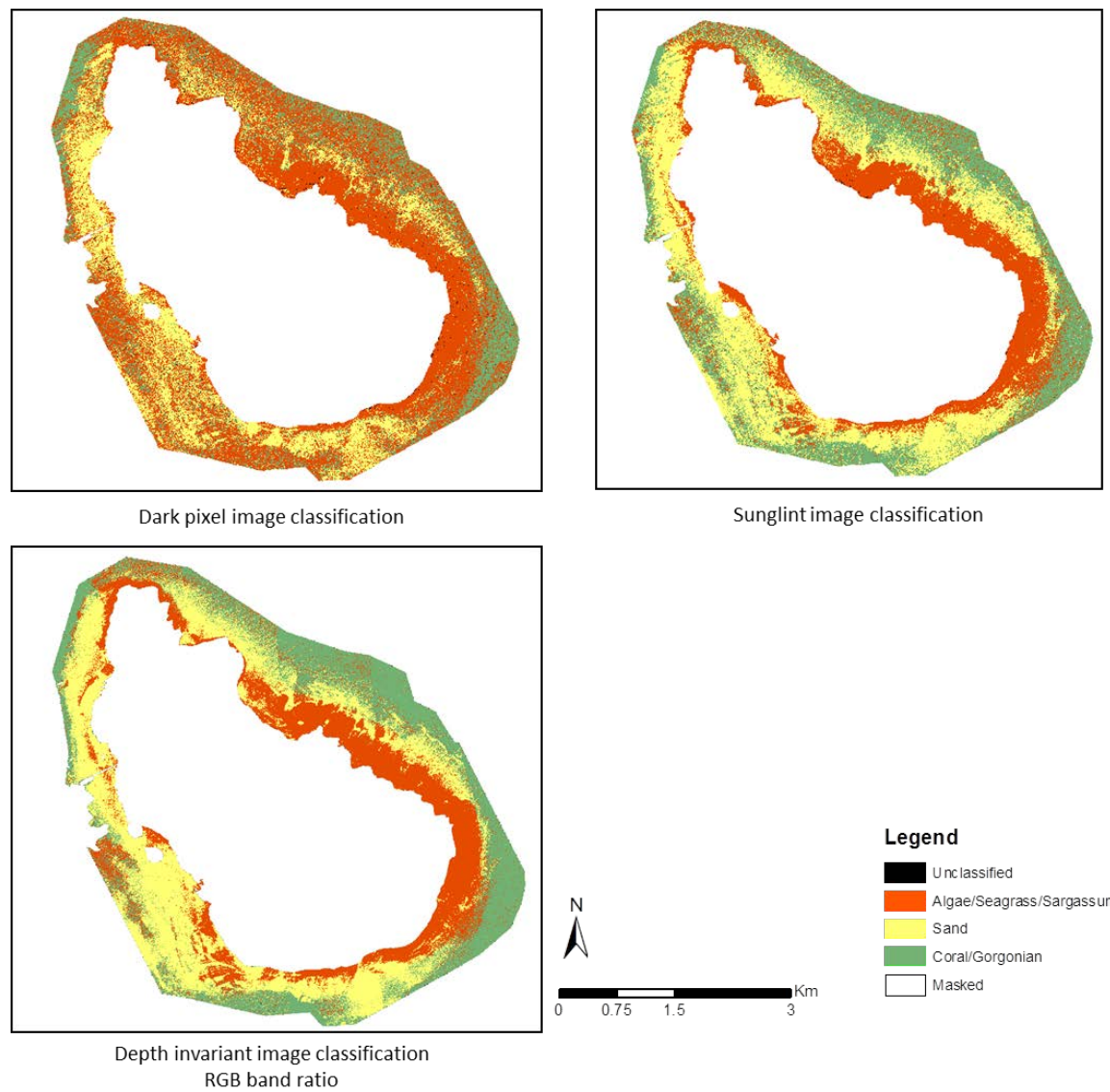


Figure 31. Object based classification results for WW2.

4.3.3 Comparison and accuracy assessment

For the validation of the classification maps, error matrices (also called confusion matrices) were derived to compare the outputs versus reference field data (Congalton, 1991). The accuracy of the resulting classified images was assessed using the validation data set.

The general results of the accuracy assessment for the pixel based classifications are presented in Table 6.

Table 6. Pixel based classification accuracies for WV2 and QB.

| QuickBird | Overall accuracy (%) | Accuracy per classes (%) | | |
|--------------------------------------|----------------------|--------------------------|----------------------|-------------|
| | | Coral/Gorg | Seagrass/Algae/Sarg. | Sand |
| TOA Radiance | 45.9 | 30.6 | 66.7 | 68.8 |
| Darkest pixel correction | 45.9 | 30.6 | 66.7 | 68.8 |
| Sunglint correction | 49.3 | 33.9 | 72.2 | 70.8 |
| Depth invariant image (3 band ratio) | 48.8 | 33.9 | 66.7 | 72.9 |
| Depth invariant image (1 band ratio) | 31.7 | 19.8 | 50.0 | 47.9 |

| WorldView-2 | Overall accuracy (%) | Accuracy per classes (%) | | |
|-----------------------------|----------------------|--------------------------|----------------------|-------------|
| | | Coral/Gorg | Seagrass/Algae/Sarg. | Sand |
| TOA Radiance | 45.6 | 48.2 | 38.7 | 45.7 |
| Darkest pixel correction | 45.6 | 48.2 | 38.7 | 45.7 |
| Sunglint correction | 51.9 | 55.4 | 51.6 | 45.7 |
| Depth invariant image (RGC) | 41.3 | 42.2 | 29.0 | 47.8 |
| Depth invariant image (RGB) | 43.8 | 48.2 | 22.6 | 50.0 |

The total results of the confusion matrices are included in Appendix 5.

The area calculated for the deglinted image for both imagery and per habitat class is shown in Table 7. As it can be observed, the total areas for both images differ, and therefore are not comparable.

Table 7. Overall area per habitat class, in hectares.

| | Area coverage (ha.) | |
|--------------------------|---------------------|-----------------|
| | QuickBird | WorldView-2 |
| Sand | 864.83 | 700.77 |
| Algae/Seagrass/Sargassum | 492.55 | 899.05 |
| Coral/Gorgonian | 1,139.95 | 694.23 |
| Total | 2,497.33 | 2,294.05 |

The results of the accuracy assessment for the object based classifications are presented in Table 8.

Table 8. Overall accuracy object based classification

| | Overall Accuracy (%) | |
|-----------------------------|----------------------|-------------|
| | QuickBird | WorldView-2 |
| Darkest pixel correction | 51.7 | 49.4 |
| Deglnted image | 53.7 | 56.9 |
| Depth invariant image (RGB) | 51.7 | 55.0 |

4.4 Bathymetry derivation

QuickBird

The relative bathymetry was obtained from the QuickBird multispectral image using the ratio between the log of the blue and green band (of the image atmospherically corrected for darkest pixel and sunglint removal). This ratio of the two logarithmic bands is shown in Figure 32a. The log transformation of the blue and green band was regressed with the ground truth data to obtain the values for the ratio

transform equation, as introduced in chapter 2.2.3 (m_1 and m_0). Only the ground truth points not corresponding to masked values were used, adding a total of 416 points.

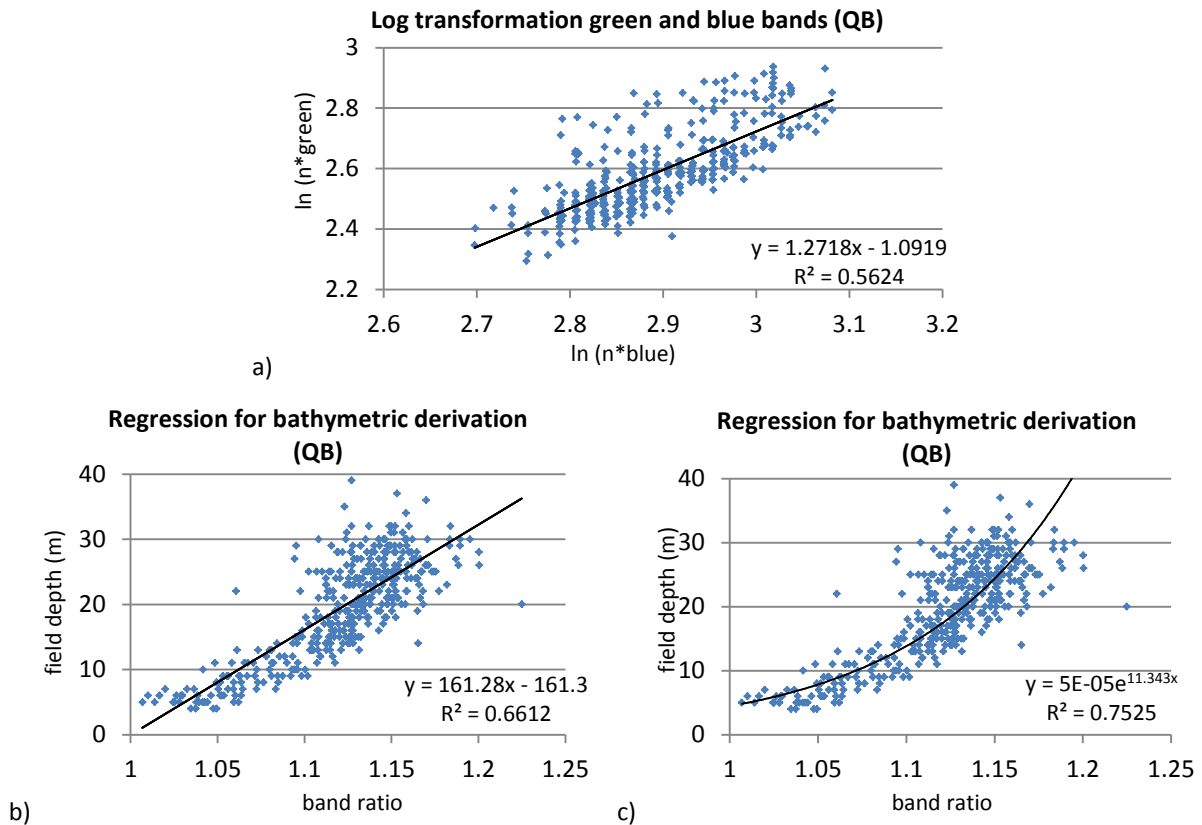


Figure 32. Log transformations of the green and blue band for QB (a). Regression bi-plot for the band ratio algorithm and depths from field data (bottom) with linear (b) and exponential (c) regression trendline

As shown in Figure 32b, the coefficient of determination, r^2 , is 0.66 (correlation coefficient $r = 0.81$). However, it can be observed that the data fit better an exponential curve (Figure 32c), with an r^2 of 0.75 ($r = 0.87$). The reason why the estimated depth better fits an exponential curve is because, as stated in (Stumpf et al., 2003), this method is best suited for bathymetry calculation in shallow waters, deeper depths tend to be underestimated and have a larger error. Therefore, to extract the values of m_1 and m_0 , a new linear regression was performed between the band ratio and the logarithmic of the field data, as shown in Figure 33.

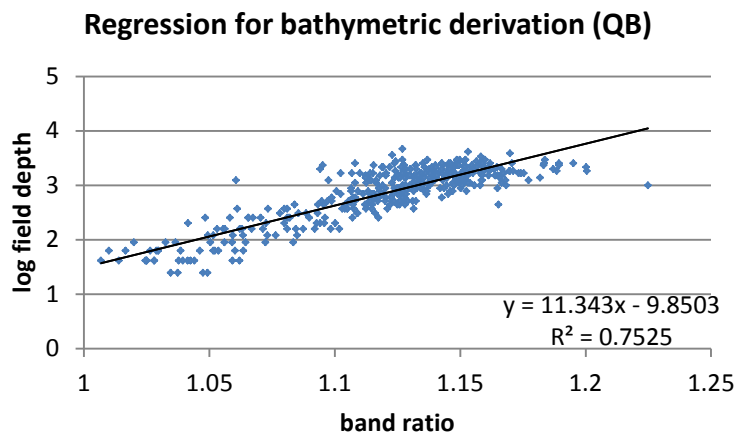
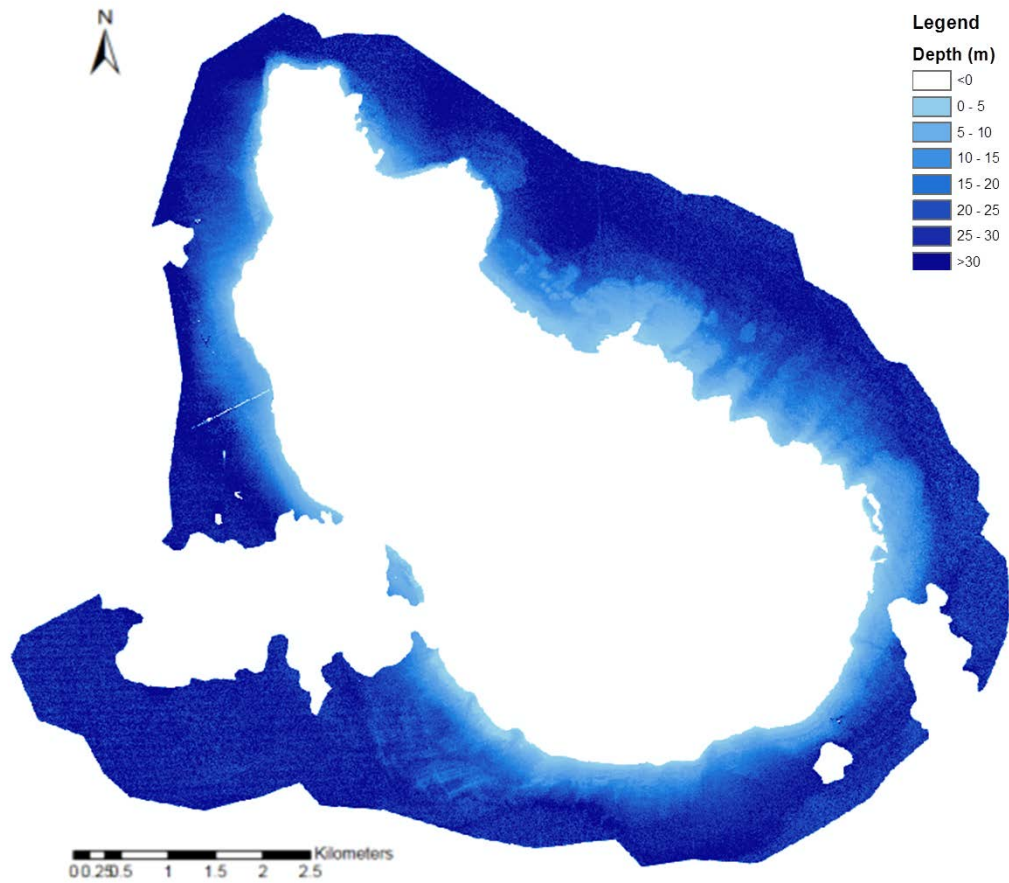


Figure 33. Regression bi-plot for the band ratio algorithm and the log of the field depth

These values of m_1 and m_0 were then used to determine the relative logarithmic depth for QB. Then, the exponent of $\log(\text{fielddepth})$ was calculated to get the backtransformed depth. The resulting bathymetry image has some noise. This is due to the fact that the ratio combination amplifies small differences more than a linear transformation, and therefore, the error variability increases with depth. To reduce this noise and improve the image, a low pass filter 3x3 was applied. The resulting bathymetry image is



shown in
Figure 34.

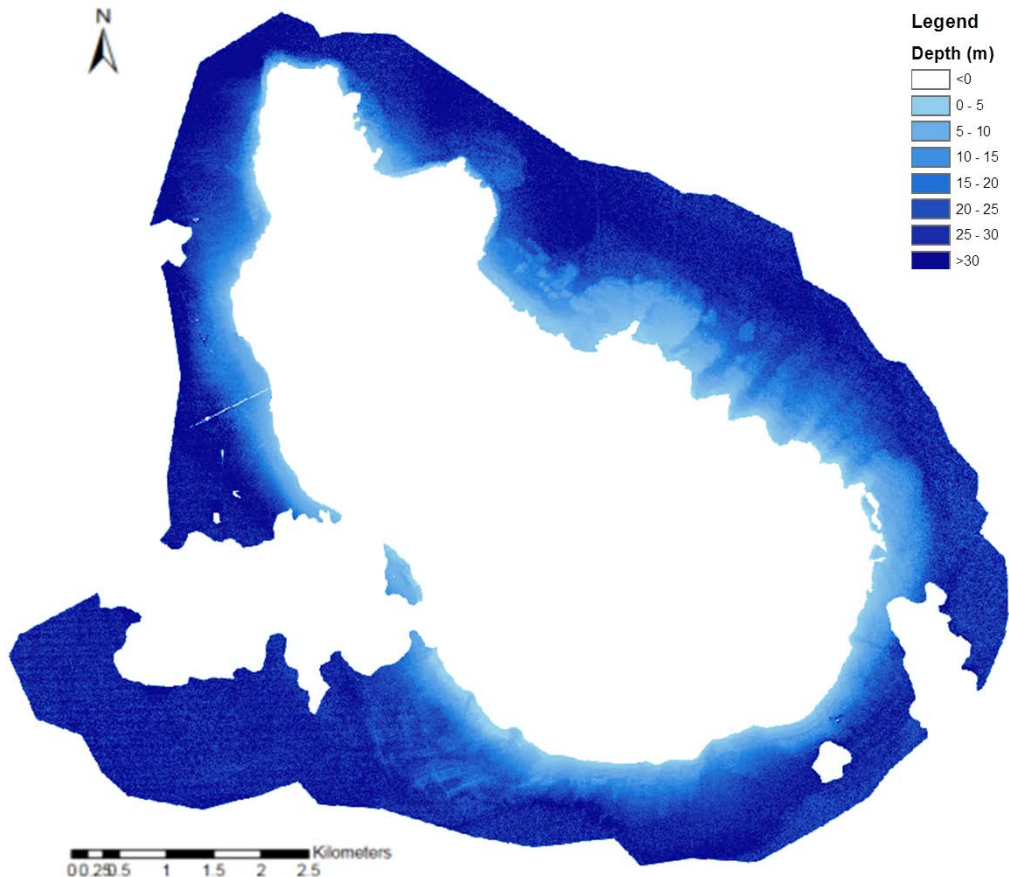


Figure 34. Estimated bathymetry for QB

Residuals were calculated by subtracting estimated depths from field depths, and these are displayed in Figure 35. It can be observed that lower depths tend to be under-estimated, while deeper depths are over-estimated.

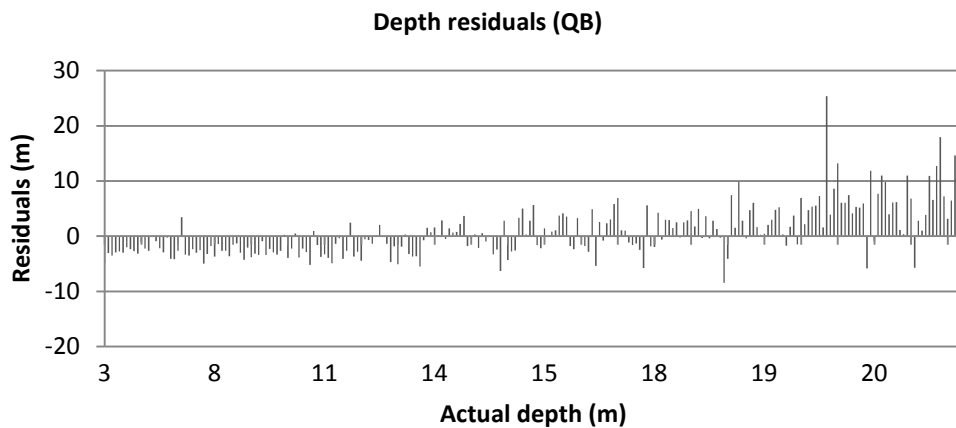


Figure 35. Histogram plot of depth residuals from the regression model versus field depth for QB.

To make an accuracy assessment using an independent set for validation, the bathymetry data of The Netherlands Hydrographic Service (TNHS) was used, although this is only available for the west side of the island. As it can be observed in Figure 36, the coefficient of determination, r^2 , is 0.64 (correlation coefficient $r=0.80$). The RMSE is of 4.76 m.

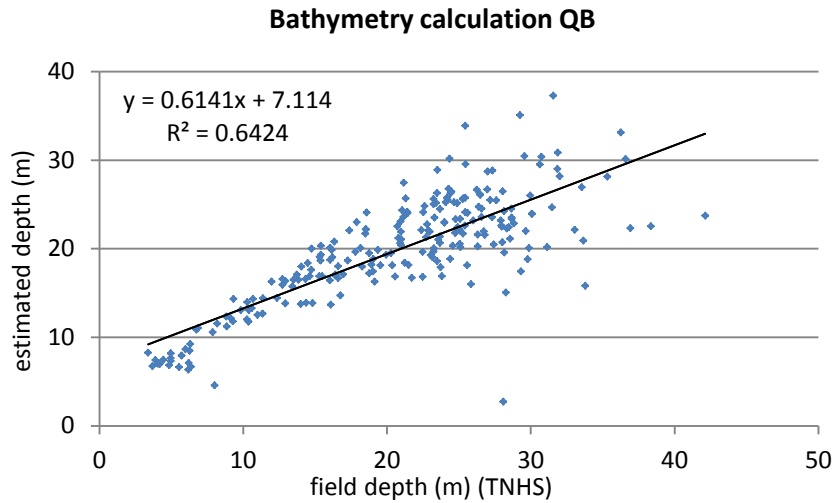


Figure 36. Validation regression bi-plot for ratio algorithm and depths from the bathymetry data of The Netherlands Hydrographic Service (TNHS) for QB.

As mentioned before, the depths are better estimated in shallow depths. To quantify this variation, the validation datasets were separated to those with a depth less than 20 m. The correlation coefficient improves for depth lower than 20 meters to $r^2=0.84$ ($r=0.92$), as shown in Figure 37, with a RMSE of 1.92 m.

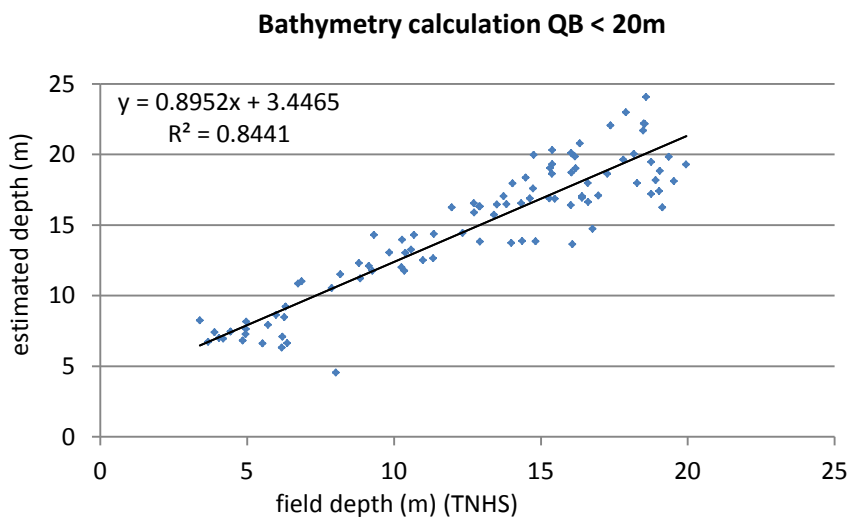


Figure 37. Validation regression bi-plot for ratio algorithm and depths from the bathymetry data of The Netherlands Hydrographic Service (TNHS) for QB. Depths lower than 20 m.

The different substrates seem to influence the values of the predicted depth. Results per habitat type are displayed in Figure 38, showing that the bathymetry estimation is best for sand areas.

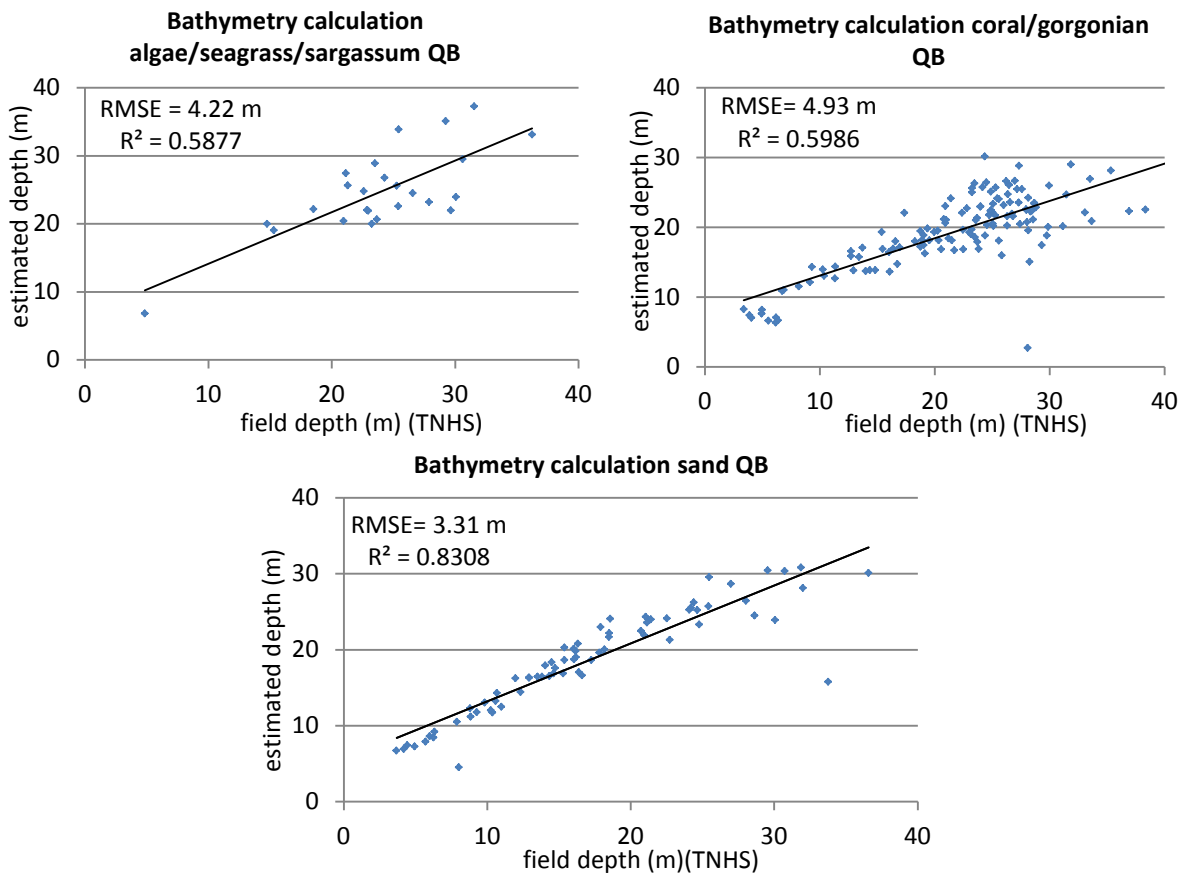


Figure 38. Relative bathymetry per habitat type regressed against the bathymetry data of The Netherlands Hydrographic Service (TNHS)

WorldView-2

For WorldView-2, as commented in chapter 3.3.5, the use of multiple linear regression was explored, including a bigger number of band ratios, as this increase in information should improve the accuracy. This was not the case in this research, probably due to the characteristics of the imagery. Finally, the bathymetry was calculated using the blue/green ratio (BG) and the coastal/green ratio (CG), as these proved to be the best band ratios for the bathymetry calculation.

These two ratios of the logarithmic bands are shown in Figure 39. The log transformation of the coastal-green and blue-green band were regressed with the ground truth data to obtain the values for the ratio transform equations, as introduced in chapter 3.3 (m_1 and m_0). Only the ground truth points not corresponding to masked values were used, with no negative values (for the log) adding a total of 370 points. Figure 40 shows this regression, obtaining the following values (Table 9):

Table 9. Tuning values for Stumpf method for WV2.

| | Coastal-Green ratio | Blue-Green ratio |
|-------|---------------------|------------------|
| m_1 | 77.131 | 148.52 |
| m_0 | 58.331 | 135.68 |

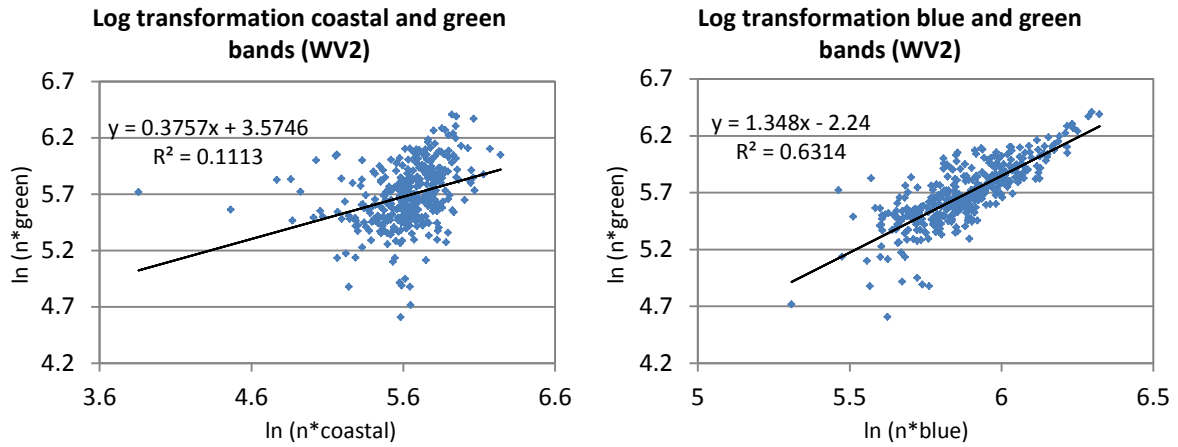


Figure 39. Log transformations of the green and coastal band (left), and of the green and blue band (right) for WV2

As it can be observed in Figure 40, the coefficient of determination (r^2) is 0.28 ($r=0.53$) for the CG ratio, and 0.41 ($r=0.64$) for the BG ratio.

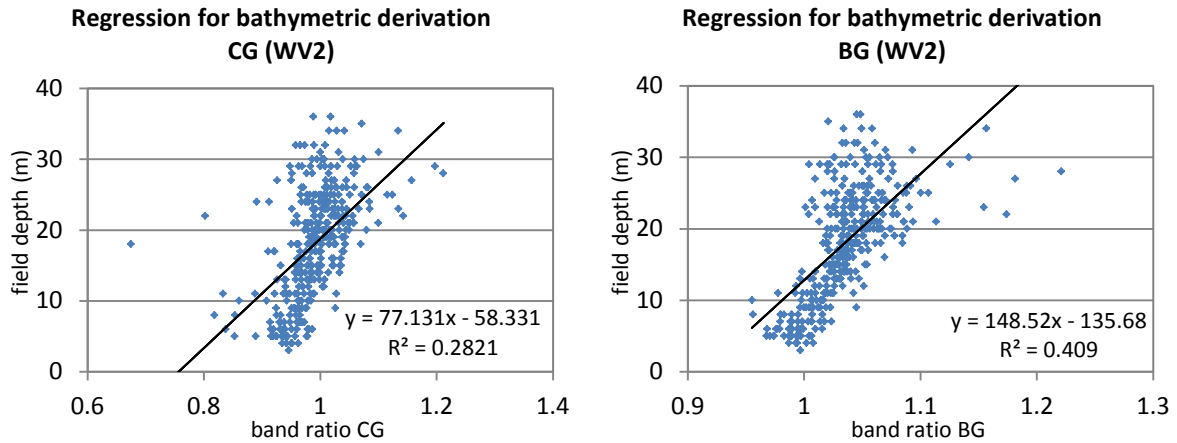


Figure 40. Regression bi-plot for the band ratio algorithm and depths from field data (right) for WV2

As in the case of QB, the estimated depth fits better a log curve (Figure 41), but the improvement on the correlation coefficients is much less (r^2 of 0.29 (CG) and 0.44 (BG)).

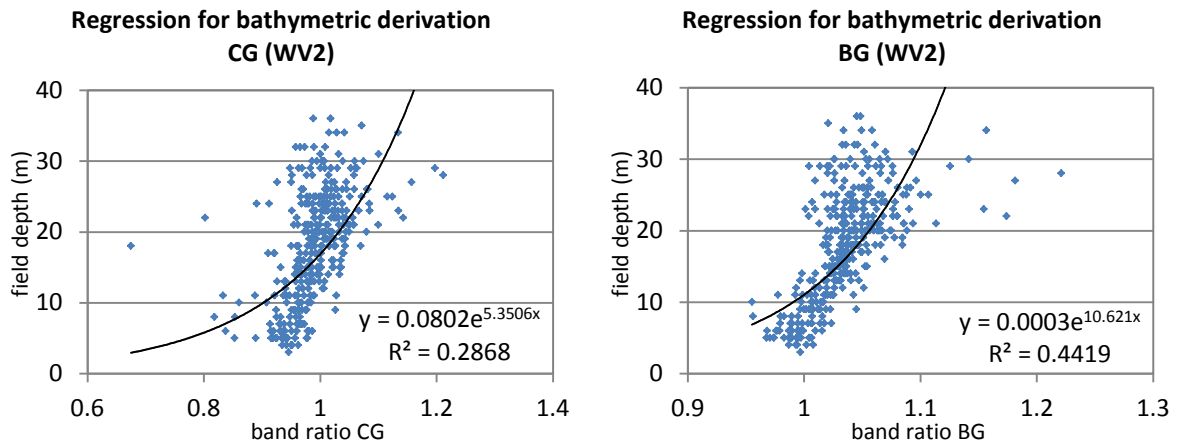


Figure 41. Regression bi-plot for the band ratio algorithm and depths from field data (right) for WV2
Linear trendline (up) and exponential trendline (bottom)

Then, with the values of m_1 and m_0 , two estimated depths were determined for WV2. A low pass filter 3x3 was applied. The resulting bathymetric images can be observed in Figure 42.

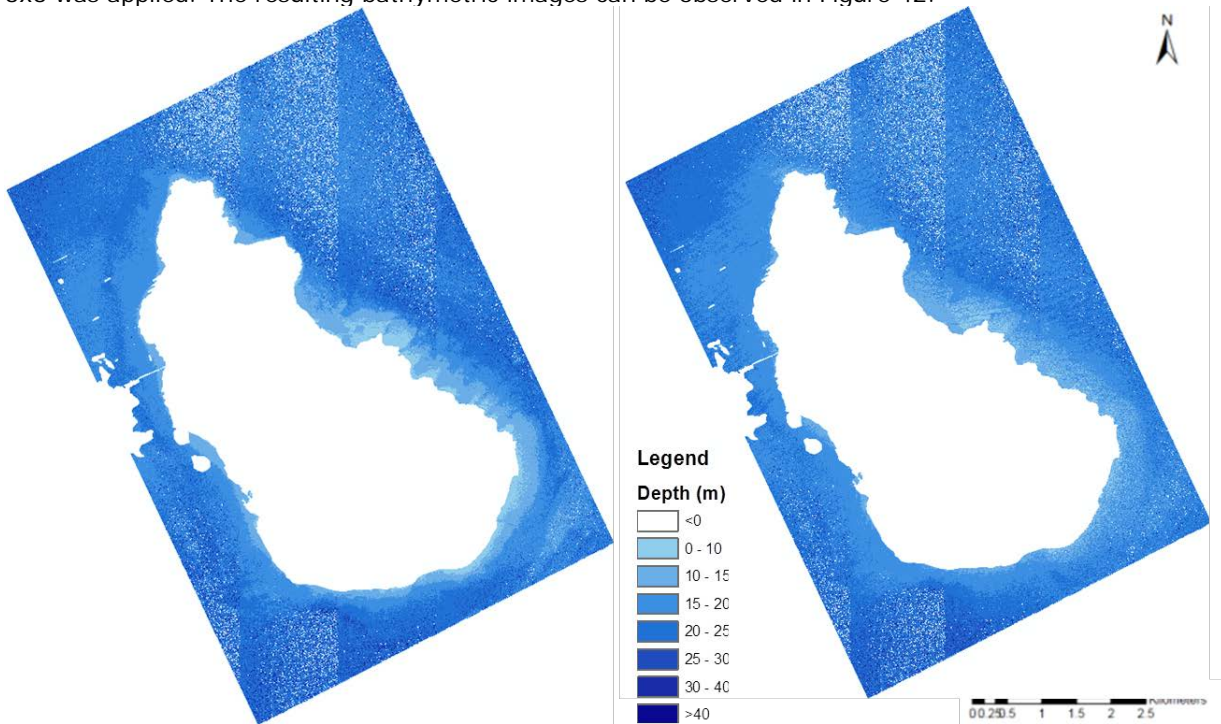


Figure 42. Estimated bathymetry for WV2. BG (left) and CG (right)

For the validation of the estimated depth, as in the case of the QB image, first a scatterplot of the regression of the estimated depth with the depth from field work for both band ratios was calculated (Figure 43). The resulting RMSE are of 5.80 m for the CG ratio and 5.11 m for the BG ratio. Again, the RMSE improve for a depth lower than 20 meters, obtaining values of 3.48 m for the CG ratio and 2.47 m for the BG ratio.

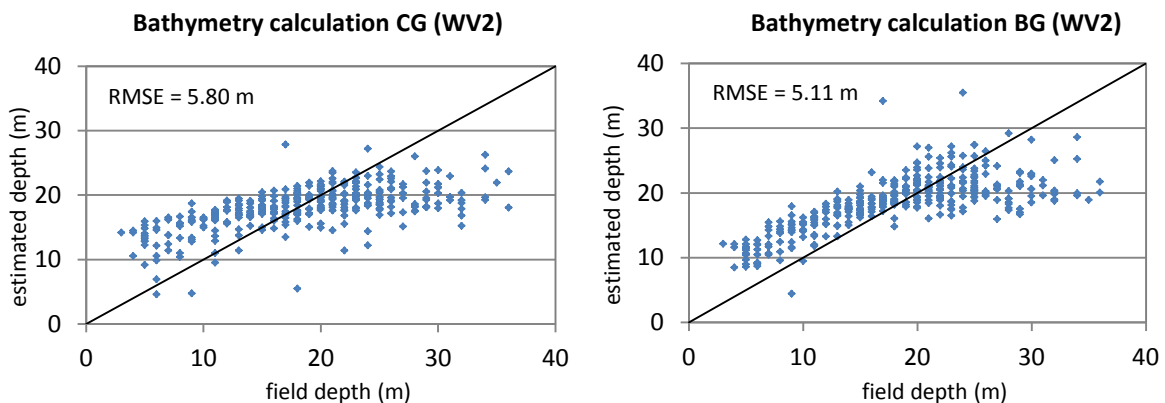


Figure 43. Validation plots for estimated depths and depths from field data (m) for WV2.

The line indicates a 1:1 correlation.

Residuals were calculated by subtracting estimated depths from field depths as displayed in Figure 44. Again, it can be observed that lower depths tend to be under-estimated, while deeper depths are over-estimated. The lower errors occur at depths between 12 and 20 m.

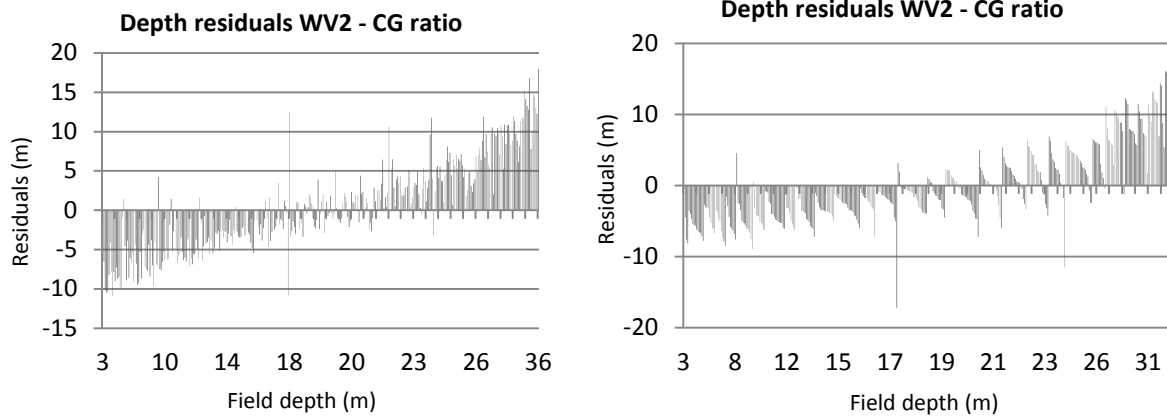


Figure 44. Histogram plot of depth residuals from the regression model versus field depth for WV2. CG ratio (left) and BG ratio (right)

To make an accuracy assessment using an independent set for validation, the bathymetry data from The Netherlands Hydrographic Service (TNHS) for the west part of the island was used. As it can be observed in Figure 45, the correlation coefficient is $r^2 = 0.32$ ($r = 0.57$) for the CG ratio and $r^2 = 0.38$ ($r = 0.61$) for the BG ratio. The RMSE is of 6.72 m for the CG ratio and 6.28 m for the BG ratio.

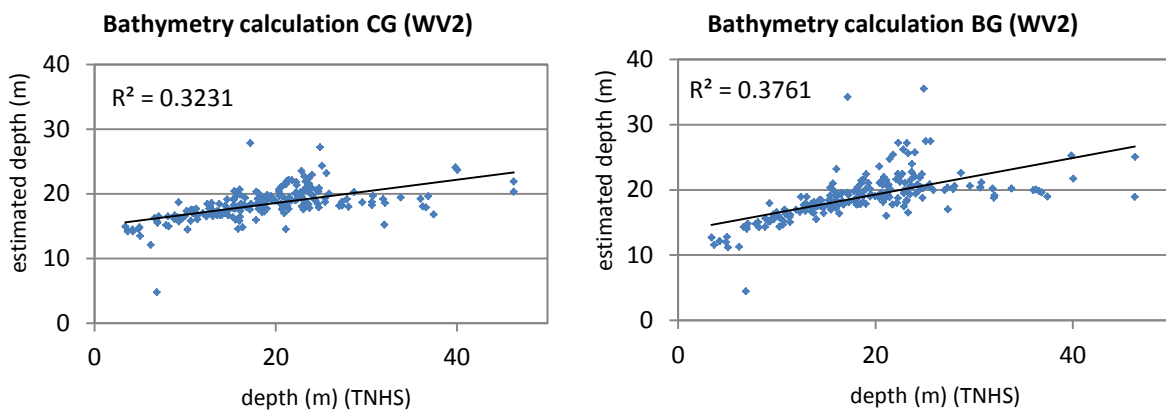


Figure 45. Validation regression bi-plot for ratio algorithm and depths from the bathymetry data of The Netherlands Hydrographic Service (TNHS) for WV2.

For shallow depths lower than 20 m, the correlation coefficient improves to $r^2 = 0.40$ and RMSE = 3.38 m for CG ratio, and $r^2 = 0.57$ and RMSE = 2.83 m for the BG ratio, as shown in Figure 46.

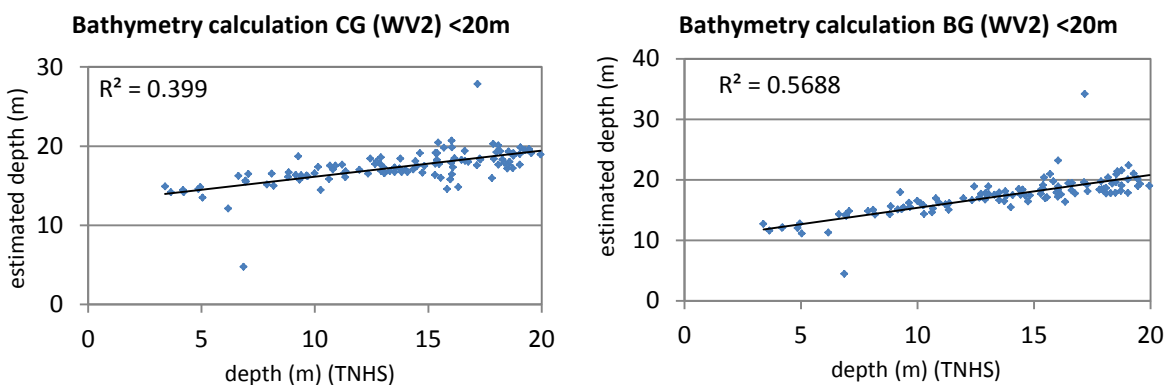


Figure 46. Validation regression bi-plot for ratio algorithm and depths from the bathymetry data of The Netherlands Hydrographic Service (TNHS) for WV2. Depths lower than 20 m.

It should be noted here that, for WV2, to obtain the estimated bathymetry from the deglnted image different band combinations were explored. First, the coastal-green-yellow-NIR3 (WV2 1st-3rd-4th-8th bands), suggested by (Collin and Hensch, 2012), was tested using a multiple linear regression. As the deglnted image has no NIR3 band, the "red edge" (band 6) was used. However, the correlations between the band ratios were very low, and the calculated depth showed no correlation with the field depth. It was also explored in this research to use the ratio of the 'coastal blue' band (band 1) to its 'yellow' band (band 4), suggested by (Bramante et al., 2013), but again no correlation was found. This results contradicted previous studies, were the expansion of the Stumpf model to a multiple linear regression provided a better resolution (Kerr, 2012).

5 Discussion

The final classification results and habitat determination are influenced by the physical characteristics of the benthic environments, the characteristics of the field data and imagery, and the methodology selected. This chapter will discuss these factors.

5.1 Remote sensing of marine environments

In general, remote sensing of water presents many challenges due to the complex physical interactions of absorption and scattering between water and light (Lyzenga, 1981; Mumby and Edwards, 2002). In the visible spectrum, longer wavelengths (green and red band ~500-750 nm) are rapidly absorbed in the water column and scattered, while shorter wavelengths (blue band ~450 nm) penetrate deeper (Lyzenga, 1981). The blue and green spectral bands provide the most important spectral information to perform submerged substrate mapping, since they are least attenuated by the water column (Herold et al., 2007). Water constituents such as dissolved organic matter or suspended particles usually strengthen the attenuation. This differential light penetration limits the potential use of remote sensing to describe submerged features, reducing the utility of the longer wavelength bands and relying more on the shorter (blue for QB and blue and coastal for WV2), which have inherently noisier signals due to atmospheric contaminations (Herold et al., 2007).

Due to the multiple spatial scales of biological and physical features on coral reefs (Purkis et al., 2007), their driving processes and the spatial variations of water depth and clarity (Phinn et al., 2012) and varying environmental conditions, the mapping of benthic habitats becomes a complex procedure.

Benthic habitats have a complex three dimensional nature and are often intermixed (e.g. sandy areas with variable algae cover). The pixels size of the WV2 and QB imagery is ~2 meters, and pixels will therefore possibly, or almost always, includes a mixture of these habitats. This complex structure impedes the differentiation between different marine habitats. In addition, different processes affect these habitats, thereby changing their spectral profiles, such as coral bleaching or death corals. As corals become stressed and lose their pigmentation, the underlying calcium carbonate skeletons become exposed and this highly reflective material can more easily be confused with the high signal return from sand and bare rock features (Mishra et al., 2006). Soon after the corals die, the remaining skeletons become covered with algae and pitted through bio-erosion (Mishra et al., 2006). These ecological changes reduce the overall albedo and may lead to confusion (Mishra et al., 2006).

5.2 General comments about the characteristics of the data

The characteristics and quality of the available data used in this research might have affected the results. A first visual inspection of the WV2 and QB images revealed a big influence of waves, resulting in a high sunglint effect at the sea surface, which impedes visual recognition of subsurface features. Logically, this affects all the benthic habitat classifications. This effect was more noticeable on the WorldView-2 image. Both images also show some clouds and breaking waves, which limited the extent of the application of the classification. Also, the waters on the study area might not be completely clear, and have some turbidity, whereas the methodology proposed in this thesis is applied to clear waters. Optical sensors have very limited value in high turbidity environments (Mumby, 2004).

Another important factor in this study was the disparities in acquisition dates between both images and the field survey. Furthermore, both images used for this study varied in acquisition dates between them. Benthic habitats could change through time, especially if a strong bleaching event or hurricane occurs, and therefore the difference in dates affects the comparison between both satellite images and the accuracy assessment using ground truth data. Environmental conditions play an important role in terms of the water properties and the spectral response of the material of interest. Seasonal changes have to be considered, since they exert control on the suspended sediments and suspended organic matter and might affect the algae habitat.

An important limitation in this research was the inadequate number of data points collected from the fieldwork. The field data collected did not represent the total coastal area of the island due to some limitations (e.g. anchoring zones). Also, the field points were not normal distributed to the depth values and were not representative of all the habitat types. There were very few field points for some of the habitat types, such as rubble, which makes the classification of this habitat very limited. Field data acquisition is also affected by the criteria and interpretation of the students that collected these data. A Random Sampling pattern strategy to be devised prior to the field work probably would have been better for this research (Congalton, 1991), although it should ensure that all the habitats were surveyed, and all the depth range. Congalton (1991) recommends that at least 50 sites of each habitat should be surveyed for accuracy assessment purposes. Green et al. (2000) mentions that an additional 30 sites should be visited for use in image classification. Due to the fact that the sampling was done using a boat, there are no sampling points collected in shallow waters (<5m). Also, there are no sampling points in waters deeper than 40 meters. All these resulted in the groundtruth points not being representative of all bottom types and biased towards specific depths. This limited the range of values available to calculate the regression coefficients. In an environment with multiple bottom types and depth variations, the standard error is amplified when limited data are collected. Finally, this limitation in groundtruth data also prevented a thorough accuracy assessment.

Further on, possible errors in the training and validation areas, due to position errors of the GPS used in the field campaign or misinterpretation of field data, will affect the classification results. The coordinates of the field data points were taken with a GPS, which has some inaccuracy associated and therefore affects the results.

After all the processing steps the presence of stripes in the WorldView-2 image became noticeable, which profoundly affected all the results, the classification and the bathymetry calculation. An example of this effect is presented in Figure 47. The reason for this could be that the image is a fusion of several tiles. However, the xml file of the image states that the image is composed of only one tile without overlap (included in appendix 1).

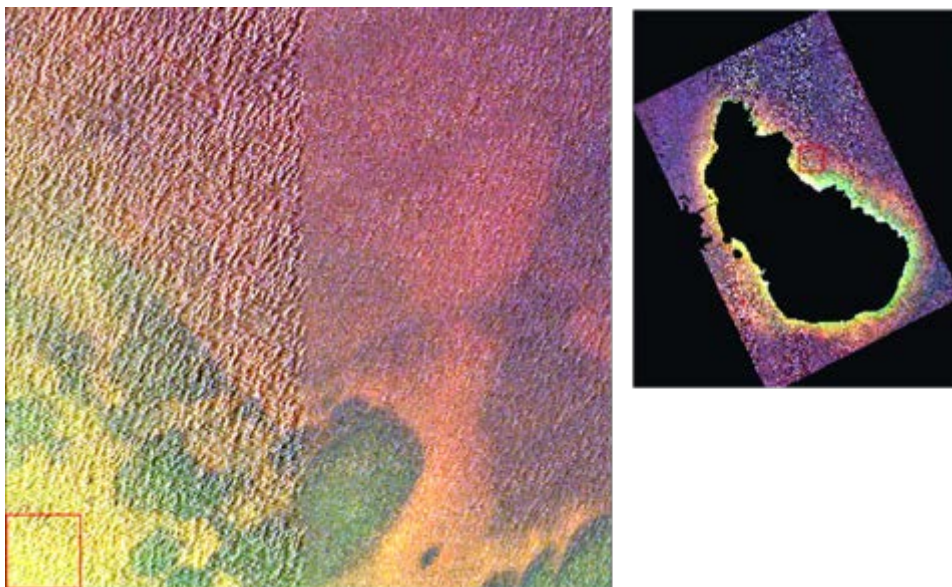


Figure 47. Example of the stripes on the WorldView-2 image.

More waves are visible on the left of the image.

5.3 Decisions or limitations in the pre-processing methods

In this research it was decided to convert the raw DN values into spectral radiances. Although all the methodology could have been performed on raw DN values, it was decided to use the radiances as spectral values were used in most previous research. This ensures that the spectral signature of the

habitats will be transferable to further research (else it will be dependent on the sensor characteristics and timing of the image). The spectral units could be used to compare images or to monitor change.

In oceanic remote sensing, the total signal received at the satellite is dominated by radiance contributed by atmospheric scattering processes and only 8-10 % of the signal corresponds to the oceanic reflectance (Kirk, 1994). Therefore, the atmospheric correction is an important preprocessing step to obtain information. In this research, a simple dark pixel subtraction was implemented. However, this method had no effect on classification accuracies over the original radiance image, and so can be discarded, as only one image per sensor is analysed. Other atmospheric correction methods that compensate for Rayleigh and aerosol scattering could be studied.

Overall, the classification accuracies were not high for all the three image processing methods, probably due to the characteristics of the data, as discussed previously. Although there was a clear visual improvement of the deglinted and depth invariant images, this improvement was not translated to a high degree to the classification accuracies. Only for the deglinted images some improvement was found.

For the pixel based classification, the deglinted images present a classification improvement over the atmospherically corrected images of about 3.4% for QB and 6.3% for WV2. This increment in accuracy was greater in WV2 probably due to the presence of more waves. However, no accuracy improvement is achieved in the depth invariant images. The reason might be the quality of the imagery or the atmospheric conditions. The major limitation of depth-invariant processing is that turbid patches of water will create spectral confusion (Green et al., 2000). As stated in Mumby et al. (1998) and Lyzenga (1981), the depth invariant index approach is only truly applicable in clear waters. However, in the Caribbean, and therefore in the study area, the waters are clear. In the creation of the Depth Invariant images, a visual inspection showed a better improvement using the blue band (RGB band ratio) instead of the coastal band (RGC band ratio). This could be because the coastal band has a lower wavelength and, therefore, is more sensitive to the atmosphere water content, which is very high on the tropics.

A summary of the classification accuracies results per processing step are displayed in Figure 48 and Figure 49.

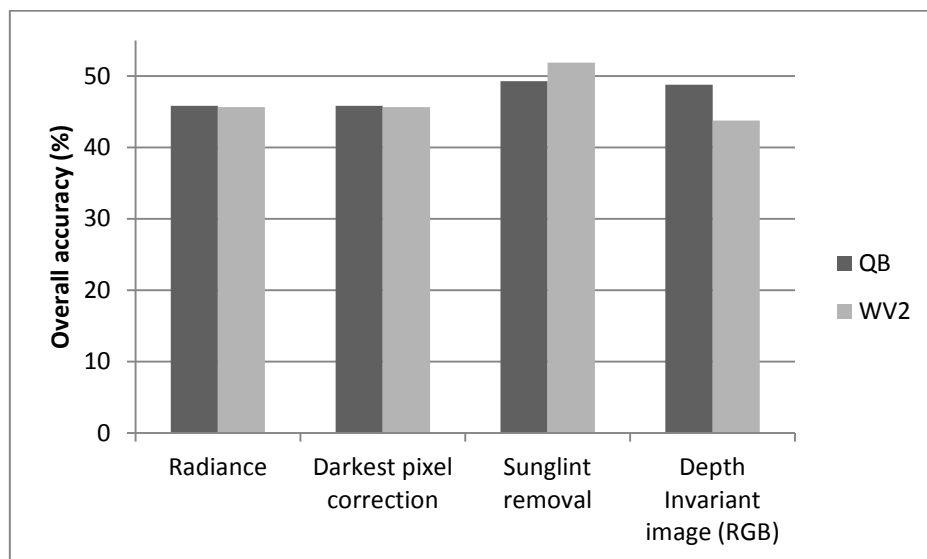


Figure 48. Pixel based classification accuracies of the three methodologies for the two sensors, QB and WV2

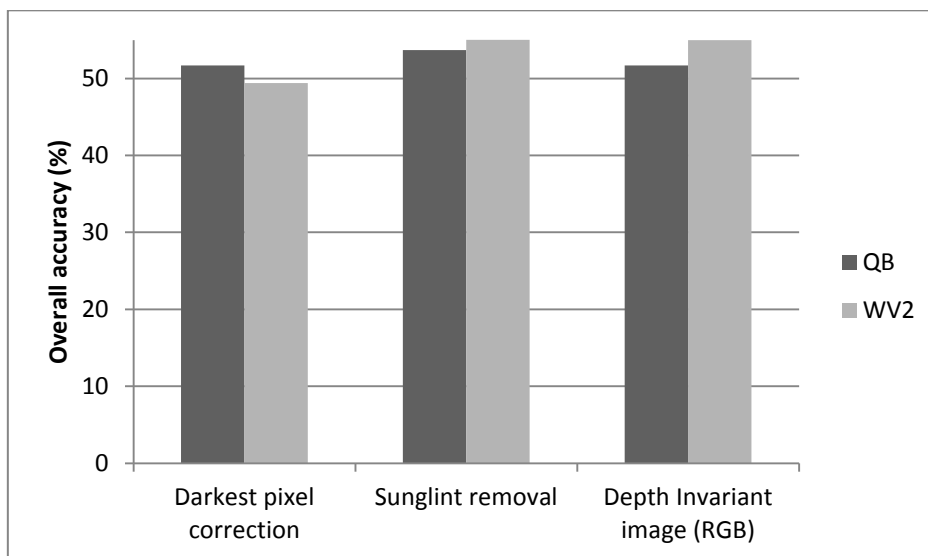


Figure 49. Object based classification accuracies of the three methodologies for the two sensors, QB and WV2

From the accuracy assessment per habitat type we can conclude that, as expected due to its spectral characteristics, the habitat class sand is best classified. However, seagrass also shows high classification accuracy. From a visual inspection of the classification images it seems that there is an overclassification of areas as seagrass, giving therefore a higher accuracy value.

5.4 Comparison between classification procedures

During the analysis of the spectral profiles there was spectral confusion between rubble, sargassum and seagrass/algae. There were also only limited number of groundtruth points of the habitat type rubble available to perform a successful classification, and this habitat type has a very mixed structure. Therefore, it was decided to perform the final classification only for three benthic habitat classes (coral, sand, and algae).

The type of selected image classification algorithm may influence the final classification results (Andréfouët, 2003; Capolsini et al., 2003). In the supervised classification, results are also affected by the interpreter's skills and decisions.

For the classification of the depth invariant image with one band ratio, it should be noted that a supervised classification of a single band is limited because the statistical separation of habitat spectra is confined to one dimension (Green et al., 2000).

In this research, classification accuracies of the object-based classification over pixel-based showed some improvement. The classification of the deglinted image improved around 4.4% for QB and 5% for WV2. The improvement was lower than expected probably due to the presence of waves in the imagery, which causes confusion in the segmentation and classification processes. Again, no improvements were found on the Depth Invariant images. The resulting object based classification images (Figure 30 and Figure 31) have more transitional boundaries than the pixel based classification.

5.5 Comparison between Sensors

Despite that the WorldView-2 sensor has a higher spectral resolution; classification accuracy results did not show clear advantage over QuickBird. Overall, the classification accuracy of the pixel-based classification of the deglinted image show better results for WV2 (51.9%) than for QB (49.3%).

Several researches have suggested that the more significant aspect to consider for better accuracy relies then on the sensor's spatial resolution (Capolsini et al., 2003; Mumby and Edwards, 2002). Here, although WV2 has a little better spatial resolution, the critical factor was the quality of the images. The

additional coastal band for WV2 also did not improve the classification, probably due to a higher effect of the atmosphere on this band.

5.6 Bathymetry calculation

A number of previous studies have demonstrated the usefulness of the Stumpf et al., (2003) method to derive bathymetry using multispectral imagery, as stated in 2.2.3. In this research the coefficients of determination (r^2) achieved are statistically significant. These r^2 obtained for a linear fit are 0.66 for QB ($r=0.81$), and 0.41 ($r=0.64$) for WV2 (BG ratio). For QB, a better estimation of the depth was calculated using an exponential regression, improving the r^2 to 0.75.

The study proved that the ratio method proposed by Stumpf et al. (2003) works better for shallow areas, as the RMSE for depths lower than 20 meters improved to 1.92 m and 2.47 m respectively. The reason is because the path length of photons increase as depth increases, thereby resulting in increased light attenuation and reduced light propagation (Mishra et al., 2006). Reduced propagation decreases the signal to noise ratio causing higher estimation error in the deep water (Mishra et al., 2006). Due to this better estimation over shallow areas, the estimated depth using the full range fits better a logarithmic relation, with an r^2 of 0.75 for QB and 0.44 for WV2 (BG ratio).

The independent validation using the depth data from The Netherlands Hydrographic Service provided a $r^2=0.75$ and RMSE = 4.76 m for QB, and $r^2= 0.38$ and RMSE= 6.72 m for WV2 (BG ratio).

Different studies have suggested the ability of the WorldView-2 sensor to derive bathymetry to a higher degree of accuracy than was previously possible with existing multispectral sensors. In this research, however, and in contrast with previous studies, the addition of more band ratios to a multiple linear regression did not result in better classification results. For WV2, the blue-green ratio performed better than the coastal-green ratio (r^2 of 0.41 and 0.28, respectively). This could be explained because the coastal band has a lower wavelength and therefore is more affected by the atmosphere.

The results in this research indicate that bathymetry accuracy varies with habitat types (sand and coral). This demonstrates that Stumpf et al. (2003)'s algorithm does not implicitly compensate for variable bottom type and albedo as was originally concluded by its authors. This limitation was already pointed out by (Clark, 2005), who found that the ratio method for bathymetry derivation is altered by varying albedos and produces inaccurate results for different substrates. This was also proved by Mishra et al. (2006), who stated that bottom reflectance is the most variable parameter and concluded that the regression coefficients for bathymetry calculation would be spurious if mixed bottom types were used because the variability in radiance from heterogeneous bottom would have a deleterious effect on the regression coefficients. Using a pre-classification and tuning the bathymetry separately for each class will, therefore, improve the depth calculation. This should be easy to implement, but was not tested in this research due to time constraints. Figure 38 showed that the bathymetry estimation was best for sandy bottoms. This could be explained as sandy areas represent a bright substrate with a higher reflectance. Coral and algae/seagrass areas show different variations in colour and pigment concentrations which create variable reflectance values and, therefore, produce lower correlation coefficients.

To record the depth of the field data, a depth gauge and later a sonar fish finder was used. These two devices have inherent inaccuracies and affect the final results.

Overall, in this research, QuickBird proved to be consistently more accurate for the bathymetry derivation than WorldView-2.

6 Conclusions and Recommendations

This research provides the baseline for future benthic habitat classification of the Dutch Caribbean islands using remote sensing; it sets a start-up methodology which may be improved in the future. In general, remotely sensed data have proved to be a useful addition to baseline reef habitat mapping. The data and results from this research can assist and be used as a reference in the selection of the appropriate techniques and sensors to further study benthic habitats and accurately derive bathymetry.

6.1 Conclusions

Based on the outcome of this study, we can now answer the research questions defined for this research.

- 1- To what extent can benthic habitats of St. Eustatius be classified and mapped using WorldView-2 and QuickBird imagery?

Overall, the total accuracies of benthic habitat mapping were reasonable for all the three image processing methods, ranging between 46% and 58%. However, the classification was performed over only three habitat classes. The preprocessing of the images showed clear visual improvement, but this was then not translated to a high degree into the classification accuracies. It has been shown that environmental conditions during image acquisition (clouds, sea state, and turbidity) strongly influence the quality of the results. Additional efforts should try to include more variables (e.g. depth and wave exposure) in the classification. This is expected to produce substantial improvements. Nevertheless, it can be concluded that this methodology offers a relatively simple and cost effective way to map and coarsely classify benthic habitats over large areas.

These findings may provide useful maps for the management and monitoring of benthic habitats on the islands of the Caribbean Netherlands and direct more detailed research. As such, remote sensing may also lead to more efficient spending of research investments.

- 2- Do the additional bands of WorldView-2 provide any benefits to classification accuracy in comparison to QuickBird bands?

The WorldView-2 image only proved a subtle improvement of the overall classification accuracies. For the pixel based classification of the deglinted image the WV2 image showed a 2.6% increase in the accuracy over QB. This increase was of 3.3% for the object based classification of the deglinted image. Within individual classes, the classification accuracy of the Worldview-2 image varied substantially. For the corals the WV2 image had the highest accuracy, namely 55% compared to 34% for the Quickbird image. The WV2 satellite provides finer spatial resolution and higher spectral information than previous satellites (like QB). Previous studies showed the improvement of coral reef mapping by using this satellite. However, due to the quality of the image, and mainly because of the presence of wind driven waves, this improvement was not so high in this research.

- 3- Does water column correction improve classification?

A water column correction was applied to normalize the influence of water depth. The results demonstrate that neither QB nor WV2 show major improvements in classification accuracy after water column correction. The accuracies for both sensors were lower than for the deglinted images.

Despite this, it must be noted here that the sunglint removal method improved the total accuracy of benthic habitat mapping, by increasing before and after deglinting 3.4% for QB and 6.3% for WV2. Therefore, it is concluded that the sunglint removal method proposed by Hedley et al. (2005) can be applied to enhance bottom type information.

- 4- What benefits to classification accuracy can the application of object-oriented classification provide over standard pixel based classification techniques?

The object-based classification of the deglinted image provided an increase of about 4.4% for QB and 5% for WV2 over the pixel based classification. It is expected that the incorporation of contextual information, especially depth, will provide better results.

Overall, it can be concluded that an object-oriented classification shows potential to improve the benthic habitat classification.

5- Can bathymetry be accurately calculated with available imagery using the ratio transform method?

In this research the effectiveness of the ratio method proposed by Stumpf et al. (2003) to calculate the bathymetry using multispectral imagery has been confirmed. The coefficients of determination (r^2) achieved are statistically significant, 0.75 for QB, and 0.41 for WV2 (BG ratio) for a linear relation. The root mean square errors are of 4.76 m for QB and 5.11 for WV2. It has been proved that this method works better for shallow areas, as the estimated depth fits better a logarithmic relation, with an r^2 of 0.75 for QB and 0.44 for WV2 (BG ratio). To prove this, a validation was made for depths lower than 20 meters, improving the coefficients of determination to 0.84 and 0.62, and the root mean square error of 1.92 and 2.47 respectively.

The results in this research indicate that some habitat types (sand and coral) were represented with greater accuracy. This demonstrates that Stumpf et al. (2003)'s algorithm does not implicitly compensate for variable bottom type and albedo as was originally concluded by its authors.

Overall, and in contrast with previous studies, better bathymetric values were obtained with QB than with WV2.

In conclusion, multispectral bathymetry mapping offers a very cost-efficient means by which users can determine depths over large areas and remote regions with little logistical support. The methodology used to retrieve the bathymetry is relatively simple and provides a good and cost effective approximation to depth calculation over large and remote areas. This method, however, requires truth data, but these could be extracted from the data available from the Netherlands Hydrographic Service or other bathymetric data available to apply the method in other Dutch Caribbean Islands.

6.2 Recommendations

During the research, limitations and dependencies have been discovered which are open to further investigation. This section is dedicated to providing recommendations for further research.

Field Data

- Field surveys must be planned carefully and due consideration must be given to the objectives of the study and the nature of habitats being surveyed. These issues will dictate most aspects of survey design, such as the sampling strategy, sampling technique, sampling unit, amount of replication, time to survey (e.g. weather conditions, date of image acquisition), ancillary data (e.g. depth, water turbidity) and the means of geographically referencing data (Green et al., 2000).
- In terms of data collection, the date of collection of the ground truth habitat points should be completed at the same time as the date of the available images as benthic habitats are in constant change. The acquisition of the field data points should take into account the spatial resolution of the imagery used, and this is especially important for the degree of accuracy of the GNSS used.
- Field data should include more points for reference and points dispersed along the entire area of study, at all depths and for all habitat types in order to reduce bias in the results and improve accuracy assessment. Additional field data would have to be collected in shallow (< 5m) and deep (>40m) waters.
- Coastal areas often possess gradients of water quality and suspended sediment concentration, and changes in these parameters across an image can lead to spectral confusion during image classification and misassignment of habitat categories (Green et al., 2000). To mitigate this effect, field data surveys should represent each physical environment present on the study area.
- Accuracies will improve using a more accurate Global Navigation Satellite System (GNSS) and/or an acoustic instrument for depth values.

Methodology

- Other methods for a better correction for waves could be studied. Lee et al. (2008) successfully applied a method proposed by Goodman et al. (2008) for sunglint removal in WorldView-2 imagery (Goodman et al., 2008; Lee, 2012).
- A more rigorous method for atmospheric correction could be applied if variables concerning the atmosphere and sea water conditions are known.
- In this research, the water column correction used did not provide any improvement. In further work, an alternative radiometric correction could be applied by combining depth data with attenuation coefficients.
- In this research, a simple image-based approach was used for the water column correction. However, other methods could be explored, although most include the need of knowledge of attenuation characteristics of the water column. Tassan (1996) has described a theoretical depth-invariant model for water of greater turbidity than specified by Lyzenga (1981). This method is mathematically complex and still requires field validation.
- A spatial filter could be applied to interpolate the gaps in the spectral data created by NaN values of the Depth Invariant images, assuming that the surrounding substrates are present in that area.
- Further improvements should be applied to study the classification of more habitat classes, including rubble and the differentiation between algae and sargassum sp. Also, the possibilities of identifying coral cover percentage classes (loose, intermediate and dense) could be studied.
- For the object based classification, data fusion approaches in which data from multiple sources are integrated into the rules have greatly improved the performance of these classification methods (Leon and Woodroffe, 2011). The incorporation of the depth derived from the remote sensing imagery should therefore improve the results (Gao, 2009). Also, considering the reef morphology and habitat zonation will increase mapping accuracies (Mumby et al., 1997;

Andréfouët, 2003; Capolsini et al., 2003). Leon and Woodroffe (2011) have concluded that the combination of optical and terrain information improved classification results around 10 %. There are some contextual rules that could be used during post-classification editing available in literature, like the ones proposed in Green et al. (2000). For example, seagrass is occasionally confused spectrally with coral reef patches particularly where the latter include significant levels of macroalgae. A decision rule could be established as seagrass is not found on the forereef, so that seagrass patches on the forereef should be recoded as coral (Green et al., 2000). In the study area of this research some of the rules that could be applied are:

- For Coral:
 - No coral is found at depths <1 m on the leeward side (East)
 - No coral is found at depths <5 m on the windward side (West)
- Seagrass is not deeper than 30 m.
- To ensure that contextual editing does not create bias or misleading improvements to map accuracy, the decision rules must be applicable throughout an image and not confined to the regions most familiar to the interpreter (Green et al., 2000). For future research, other contextual editing rules could be applied, like water exposure, distance to land, distance to river mouths or distance to known sites of corals.

Bathymetry

- Subdividing the scene into its different bottom types and tuning the algorithm's coefficients separately for each substrate could improve the bathymetric mapping. This was not tested in this research because of time constraints, but could be a topic of further research.
- Tide modifies field depth and, therefore, the time of data acquisition is important. Ground truth depth data collected nearly concurrently with the remotely sensed imagery will minimize temporal variability and will provide a better tuning of the algorithm parameters.
- For the calculation of the variables m_0 and m_1 , the use of only the depth data lower than 20 m, which gave a higher correlation, could be studied further.
- Sonar data and airborne LIDAR data are some examples of data that can be complementary for the bathymetry calculation and validation. However, as stated in section 2.2.3, these methods are expensive and difficult to use in remote areas.
- It could be further explored the use of more band ratios for WV2 imagery to perform a multiple linear regression.

General

- The identification of more effective and practical algorithms and methodologies may lead to consensus among reef scientist to follow more homogeneous approaches for coral reef habitat mapping (Green et al., 2000; Mumby et al., 1998; Andréfouët, 2003). A global methodology for other areas, that could be repeatable, will be very useful for benthic habitat mapping.
- In situ spectral measurements of benthic habitats will help to improve the classification. Benthic habitat mapping using remote sensing could benefit from using "spectral libraries" (libraries of spectral signatures containing lists of habitats and their reflectance) (Hochberg et al., 2003b).

7 List of references

- ANDRÉFOUËT, S., BERKELMANS, R., ODRIOZOLA, L., DONE, T., OLIVER, J. & MÜLLER-KARGER, F. 2002a. Choosing the appropriate spatial resolution for monitoring coral bleaching events using remote sensing. *Coral Reefs*, 21, 147-154.
- ANDRÉFOUËT, S., KRAMER, P., TORRES-PULLIZA, D., JOYCE, K. E., HOCHBERG, E. J., GARZA-PÉREZ, R., MUMBY, P. J., RIEGL, B., YAMANO, H., WHITE, W. H., ZUBIA, M., BROCK, J. C., PHINN, S. R., NASEER, A., HATCHER, B. G., MULLER-KARGER, F. E. 2003. Multi-site evaluation of IKONOS data for classification of tropical coral reef environments. *Remote Sensing of Environment*, 88, 128-143.
- ANDRÉFOUËT, S., MUMBY, P. J., MCFIELD, M., HU, C. & MULLER-KARGER, F. E. 2002b. Revisiting coral reef connectivity. *Coral Reefs*, 21, 43-48.
- BENFIELD, S. L., GUZMAN, H. M., MAIR, J. M. & YOUNG, J. A. T. 2007. Mapping the distribution of coral reefs and associated sublittoral habitats in Pacific Panama: A comparison of optical satellite sensors and classification methodologies. *International Journal of Remote Sensing*, 28, 5047-5070.
- BERTELS, L., VANDERSTRAETE, T., VAN COILLIE, S., KNAEPS, E., STERCKX, S., GOOSSENS, R. & DERONDE, B. 2008. Mapping of coral reefs using hyperspectral CASI data; a case study: Fordata, Tanimbar, Indonesia. *International Journal of Remote Sensing*, 29, 2359-2391.
- BERVOETS, T. 2010. Report on the Economic Valuation of St. Eustatius' Coral Reef Resources. St. Eustatius National Marine Park. STENAPA and DCNA.
- BRAMANTE, J. F., RAJU, D. K. & SIN, T. M. 2013. Multispectral derivation of bathymetry in Singapore's shallow, turbid waters. *International Journal of Remote Sensing*, 34, 2070-2088.
- CAPOLSINI, P., ANDRÉFOUËT, S., RION, C. & PAYRI, C. 2003. A comparison of Landsat ETM+, SPOT HRV, Ikonos, ASTER, and airborne MASTER data for coral reef habitat mapping in South Pacific islands. *Canadian Journal of Remote Sensing*, 29, 187-200.
- CESAR, H. S. J. 2000. Coral Reefs: Their Functions, Threats and Economic Value. *Collected Essays on the Economics of Coral Reefs*.: CORDIO, Kalmar University, Sweden.
- CHEN, S. C., LIEW, R. L. & KWONG, L. K. Mapping coastal ecosystems of an offshore landfill island using WorldView-2 high resolution satellite imagery. Proc. 34th, 10-15 April 2011 2011 Sydney, Australia. International Symposium on Remote Sensing of Environment.
- CLARK, R. E. 2005. *Naval satellite bathymetry: A performance assessment*. Master's Thesis.
- COLLIN, A. & HENCH, J. L. 2012. Towards Deeper Measurements of Tropical Reefscape Structure Using the WorldView-2 Spaceborne Sensor. *Remote Sens.*, 4(5), 1425-1447.
- COLLIN, A., HENCH, J. L. & PLANES, S. A novel spaceborne proxy for mapping coral cover. 9-13 July 2012 2012 Cairns, Australia. Proceedings of the 12th International Coral Reef Symposium.
- CONGALTON, R. G. 1991. A review of assessing the accuracy of classifications of remotely sensed data. *Remote Sensing of Environment*, 37, 35-46.
- COSTANZA, R., D'ARGE, R., DE GROOT, R., FARBER, S., GRASSO, M., HANNON, B., LIMBURG, K., NAEEM, S., O'NEILL, R. V., PARUELO, J., RASKIN, R. G., SUTTON, P. & VAN DEN BELT, M. 1997. The value of the world's ecosystem services and natural capital. *Nature*, 387, 253-260.
- DEBROT, A. O. & SYBESMA, J. 2000. The Dutch Antilles, Chapter 38. In C.R.C. SHEPPARD (ed.), *Seas at the Millennium: an Environmental Evaluation*, Vol. I Regional Chapters: Europe, The Americas and West Africa, 595-614. Elsevier, Amsterdam.
- DCNA. 2012. *The Dutch Caribbean Nature Alliance* [Online]. [Accessed 6th March 2013].
- DE PALM, J. P. 1985. Encyclopedie van de Nederlandse Antillen. In: DE WALBURG PERS & ZUTPHEN. (eds.).
- DEFENSE, M. O. 2013. *The Netherlands Hydrographic Service (TNHS)* [Online]. Ministry of Defense. Available: http://www.defensie.nl/english/navy/hydrographic_service/about_hydrographic_service/ [Accessed 14/05/2013].
- DEIDDA, M. & SANNA, G. 2012. Pre-processing of high resolution satellite images for sea bottom classification. *Italian Journal of Remote Sensing / Rivista Italiana di Telerilevamento*, 44, 83-95.
- DIGITALGLOBE. 2009. *8-Band Multispectral Imagery* [Online]. Available: http://www.digitalglobe.com/index.php/48/Products?product_id=27.
- DOXANIA, G., M., P., LAFAZANIA, P., PIKRIDAS, C. & TSAKIRI-STRATIA, M. 2012. Shallow water bathymetry over variable bottom types using multispectral WorldView-2 Image

- International Archives of the Photogrammetry, Remote Sensing and Spatial Information Sciences*, Volume XXXIX-B8, Melbourne, Australia.
- EAKIN, C. M., NIM, C. J., BRAINARD, R. E., AUBRECHT, C., ELVIDGE, C., GLEDHILL, D. K., MULLER-KARGER, F., MUMBY, P. J., SKIRVING, W. J., STRONG, A. E., WANG, M., WEEKS, S., WENTZ, F. & ZISKIN, D. 2010. Monitoring coral reefs from space. *Oceanography*, 23, 118-133.
- ECONOMIC-AFFAIRS, M. 2010. Biodiversity Monitoring on the BES-islands. The Hague, the Netherlands: Department of Nature, Landscape and Rural Affairs, Team International.
- EDWARDS, A. J. 1999. Applications of Satellite and Airborne Image Data to Coastal Management. In: UNESCO (ed.). Paris.
- ESTEBAN, N. 2009. St Eustatius National Parks Foundation. Annual Report 2009. STENAPA.
- ESTEBAN, N., KOOISTRA, D. & MAARTEN, O. C. S. 2005. Report on observations of coral bleaching St Eustatius Marine Park, Saba Marine Park, St Maarten Marine Park. NACRI Netherlands Antilles Coral Reef Initiative.
- FRASER, R. S., MATTOO, S., YEH, E. N. & MCCLAIN, C. R. 1997. Algorithm for atmospheric and glint corrections of satellite measurements of ocean pigment. *Journal of Geophysical Research D: Atmospheres*, 102, 17107-17118.
- GAO, J. 2009. Bathymetric mapping by means of remote sensing: Methods, accuracy and limitations. *Progress in Physical Geography*, 33, 103-116.
- GOODMAN, J. A., LEE, Z. & USTIN, S. L. 2008. Influence of atmospheric and sea-surface corrections on retrieval of bottom depth and reflectance using a semi-analytical model: A case study in Kaneohe Bay, Hawaii. *Applied Optics*, 47, F1-F11.
- GOVERNMENT, S. E. <http://www.statiagovernment.com/> [Online]. Saint Eustatius Government. [Accessed 18th April 2013].
- GREEN, E. P., MUMBY, P. J., EDWARDS, A. J. & CLARK, C. D. 2000. Remote Sensing Handbook for Tropical Coastal Management. *Coastal Management Sourcebooks 3*. Paris: UNESCO.
- HEDLEY, J. D., HARBORNE, A. R. & MUMBY, P. J. 2005. Simple and robust removal of sun glint for mapping shallow-water benthos. *International Journal of Remote Sensing*, 26, 2107-2112.
- HEDLEY, J. D., MUMBY, P. J., JOYCE, K. E. & PHINN, S. R. 2004. Spectral unmixing of coral reef benthos under ideal conditions. *Coral Reefs*, 23, 60-73.
- HEDLEY, J. D., ROELFSEMA, C. M., PHINN, S. R. & MUMBY, P. J. 2012. Environmental and sensor limitations in optical remote sensing of coral reefs: Implications for monitoring and sensor design. *Remote Sensing*, 4, 271-302.
- HERMAN, S. J. 2000. Coral Reefs: Their Functions, Threats and Economic Value. Kalmar, Sweden: CORDIO, Department for Biology and Environmental Sciences, Kalmar University.
- HEROLD, M., METZ, J. & ROMSOS, J. S. 2007. Inferring littoral substrates, fish habitats, and fish dynamics of Lake Tahoe using IKONOS data. *Canadian Journal of Remote Sensing*, 33, 445-456.
- HOCHBERG, E. J., ANDRÉFOUËT, S. & TYLER, M. R. 2003a. Sea surface correction of high spatial resolution ikonos images to improve bottom mapping in near-shore environments. *IEEE Transactions on Geoscience and Remote Sensing*, 41, 1724-1729.
- HOCHBERG, E. J., ATKINSON, M. J. & ANDRÉFOUËT, S. 2003b. Spectral reflectance of coral reef bottom-types worldwide and implications for coral reef remote sensing. *Remote Sensing of Environment*, 85, 159-173.
- HOUTEPEN, E. & TIMMER, T. 2013. Benthic habitat mapping in the coastal waters of St. Eustatius. Internship report. Aquatic Ecology and Water Quality Management. *Report nr. P462*. IMARES Wageningen University.
- JACKSON, J. E. A. 2012. Tropical Americas Coral Reef Resilience Workshop. Tupper Center, Smithsonian Tropical Research Institute, Panama City, Republic of Panama: International Union for the Conservation of Nature (IUCN).
- KAUSE, K. 2005. Radiometric Use of Quickbird Imagery. Technical note. Colorado, USA: Digital Globe.
- KAY, S., HEDLEY, J. D. & LAVENDER, S. 2009. Sun glint correction of high and low spatial resolution images of aquatic scenes: A review of methods for visible and near-infrared wavelengths. *Remote Sensing*, 1, 697-730.
- KERR, J. M. 2012. Worldview-02 offers new capabilities for the monitoring of threatened coral reefs. *Nova Southeastern University (National Coral Reef Institute)*.
- KIRK, J. T. O. 1994. Light and photosynthesis in aquatic ecosystems. *Light and photosynthesis in aquatic ecosystems*.
- KLOMP, K. D. & KOOISTRA, D. J. 2001. A post-hurricane, rapid assessment of reefs in the windward Netherlands Antilles (stony corals, algae, and fishes). Status of coral reefs in the western Atlantic: results of initial surveys, Atlantic and Gulf Rapid Reef Assessment (AGRR) program. *Atoll Research Bulletin* 496. pp. 404 – 37.
- KLIMAATINFO. *KlimaatInfo* [Online]. Available: <http://www.klimaatinfo.nl/> [Accessed 4th April 2013].

- KNOWLTON, N. & JACKSON, J. B. C. 2008. Shifting baselines, local impacts, and global change on coral reefs. *PLoS Biology*, 6, 0215-0220.
- KOSTYLEV, V. 2007. Habitat template approach to benthic habitat mapping. Natural Resources Canada Bedford Institute of Oceanography.
- LEE, K. R. 2012. *Using multi-angle Worldview-2 imagery to determine ocean depth near Oahu, Hawaii*. Naval Postgraduate School.
- LEON, J. & WOODROFFE, C. D. 2011. Improving the synoptic mapping of coral reef geomorphology using object-based image analysis. *International Journal of Geographical Information Science*, 25, 949-969.
- LUBIN, D., LI, W., DUSTAN, P., MAZEL, C. H. & STAMNES, K. 2001. Spectral signatures of coral reefs: Features from space. *Remote Sensing of Environment*, 75, 127-137.
- LYONS, M., PHINN, S. & ROELFSEMA, C. 2011. Integrating Quickbird multi-spectral satellite and field data: Mapping bathymetry, seagrass cover, seagrass species and change in Moreton Bay, Australia in 2004 and 2007. *Remote Sensing*, 3, 42-64.
- LYZENGA, D. R. 1981. Remote sensing of bottom reflectance and water attenuation parameters in shallow water using aircraft and Landsat data (Bahamas). *International Journal of Remote Sensing*, 2, 71-82.
- MARITORENA, S. 1996. Remote sensing of the water attenuation in coral reefs: A case study in French Polynesia. *International Journal of Remote Sensing*, 17, 155-166.
- MARITORENA, S., MOREL, A. & GENTILLY, B. 1994. Diffuse reflectance of oceanic shallow waters: influence of water depth and bottom albedo. *Limn. and Ocean*, 39, 1689-1703.
- MILLER, J., BATTISTA, T. & PRITCHETT, A. 2011. Coral Reef Conservation Program mapping achievements and unmet needs. Coral Reef Conservation Program (U.S.). NOAA.
- MILLER, N. 2010. Workshop report by the Research and Monitoring Expert Group. Bonaire: DCNA.
- MISHRA, D., NARUMALANI, S., RUNDQUIST, D. & LAWSON, M. 2006. Benthic habitat mapping in tropical marine environments using quickbird multispectral data. *Photogrammetric Engineering and Remote Sensing*, 72, 1037-1048.
- MOBLEY, C. D. 1994. Light and Water: Radiative Transfer in Natural Waters. *Academic Press*. San Diego, CA USA.
- MUMBY, P. J., CLARK, C. D., GREEN, E. P. & EDWARDS, A. J. 1998. Benefits of water column correction and contextual editing for mapping coral reefs. *International Journal of Remote Sensing*, 19, 203-210.
- MUMBY, P. J. & EDWARDS, A. J. 2002. Mapping marine environments with IKONOS imagery: Enhanced spatial resolution can deliver greater thematic accuracy. *Remote Sensing of Environment*, 82, 248-257.
- MUMBY, P. J., GREEN, E. P., EDWARDS, A. J. & CLARK, C. D. 1997. Coral reef habitat-mapping: How much detail can remote sensing provide? *Marine Biology*, 130, 193-202.
- MUMBY, P. J., SKIRVING, W., STRONG, A. E., HARDY, J. T., LEDREW, E. F., HOCHBERG, E. J., STUMPF, R. P. & DAVID, L. T. 2004. Remote sensing of coral reefs and their physical environment. *Marine Pollution Bulletin*, 48, 219-228.
- NACRI. 2010. *Netherlands Antilles Coral Reef Initiative* [Online]. NACRI. Available: <http://www.nacri.org/> [Accessed 15/02/2013].
- NOAA. *National Oceanic and Atmospheric Administration (NOAA)* [Online]. United States Department of Commerce. Available: <http://oceanservice.noaa.gov/facts/benthic.html> [Accessed 10th February 2013].
- NURLIDIASARI, M. & BUIDMAN, S. 2005. Mapping coral reef habitat with and without column correction using Quickbird Image. *International Journal of Remote Sensing and Earth Sciences (IJReSES)*, 2.
- OLSEN, R. C. 2007. Remote Sensing from Air and Space. *SPIE Press*. Bellingham, Washington.
- PHILPOT, W. D. 1989. Bathymetry mapping with passive multispectral imagery. *Applied Optics*, 28, 1569-1578.
- PHINN, S. R., ROELFSEMA, C. M. & MUMBY, P. J. 2012. Multi-scale, object-based image analysis for mapping geomorphic and ecological zones on coral reefs. *International Journal of Remote Sensing*, 33, 3768-3797.
- PURKIS, S. J. 2005. A "reef-up" approach to classifying coral habitats from IKONOS imagery. *IEEE Transactions on Geoscience and Remote Sensing*, 43, 1375-1390.
- PURKIS, S. J., KOHLER, K. E., RIEGL, B. M. & ROHMANN, S. O. 2007. The statistics of natural shapes in modern coral reef landscapes. *Journal of Geology*, 115, 493-508.
- ROOBOL, J. & SMITH, A. L. 2004. *Volcanology of Saba and St. Eustatius, Northern Lesser Antilles* Edita-the Publishing House of the Royal.
- SCHOENMAECKERS, B. 2011. How the Netherlands protects its coral. *Change Magazine*.
- SHARMA, S., BAHAGUNA, A., CHAUDHARY, N. R., NAYAK, S., CHAVAN, S. & PANDEY, C. N. Status and monitoring the health of coral reef using Multi-temporal remote sensing - A case study of Pirotan Coral Reef Island, Marine National Park, Gulf of Kachchh, Gujarat, India.

- Proceedings of the 11th International Coral Reef Symposium, 7-11 July 2008 2008 Ft. Lauderdale, Florida.
- STERCKX, S., DEBRUYN, W., VANDERSTRAETE, T., GOOSSENS, R. & VAN DER HEIJDEN, P. Hyperspectral data for coral reef monitoring. A case study: Fordate, Tanimbar, Indonesia. EARSel eProceedings, 2005. 18-25.
- STREHER, A. S., GOODMAN, J.A., GALVAO, L. S. 2013. Sunglint removal in high spatial resolution hyperspectral images under different viewing geometries. *Anais XVI Simpósio Brasileiro de Sensoramento Remoto - SBSR*. Foz do Iguacu, PR, Brasil.
- STUMPF, R. P., HOLDERIED, K. & SINCLAIR, M. 2003. Determination of water depth with high-resolution satellite imagery over variable bottom types. *Limnology and Oceanography*, 48, 547-556.
- SU, H., LIU, H. & HEYMAN, W. 2008. Automated derivation of bathymetric information from multi-spectral satellite imagery using a non-linear inversion model. *Marine Geodesy*, 31, 281-298.
- TASSAN, S. 1996. Modified Lyzenga's method for macroalgae detection in water with non-uniform composition. *International Journal of Remote Sensing*, 17, 1601-1607.
- UPDIKE, T. & COMP, C. 2010. Radiometric Use of WorldView-2 Imagery. In: GLOBE, D. (ed.).
- VROMAN, M. 1961. Studies on the flora of Curaçao and other Caribbean islands, volume II. Utrecht.: Natuurwetenschappelijke studiekering voor Suriname en de Nederlandse Antillen.
- SLIJKERMAN, D.M.E. MAREN, B. VAN STAPEL, J. MEESTERS, H.W.G. DAVAASUREN, N. DALFSEN, J. VAN DEBROT, A.O. 2011. Quick scan environmental impact assessment of the St. Eustatia harbour extension. IMARES report C085/11, pp. 42.
- WESTERMANN, J. H. & KIEL, H. 1961. *The Geology of Saba and St. Eustatius, with notes on the Geology of St. Kitts, Nevis and Montserrat (Lesser Antilles)*. Utrecht.
- WILKINSON, C. E. 2008. Status of Coral Reefs of the World: 2008. Townsville, Australia: Global Coral Reef Monitoring Network and Reef and Rainforest Research Center.

Quality assurance

IMARES utilises an ISO 9001:2008 certified quality management system (certificate number: 124296-2012-AQ-NLD-RvA). This certificate is valid until 15 December 2015. The organisation has been certified since 27 February 2001. The certification was issued by DNV Certification B.V. Furthermore, the chemical laboratory of the Fish Division has NEN-EN-ISO/IEC 17025:2005 accreditation for test laboratories with number L097. This accreditation is valid until 1th of April 2017 and was first issued on 27 March 1997. Accreditation was granted by the Council for Accreditation.

Justification

Report C143/13
Project Number: 430.82011.08

The scientific quality of this report has been peer reviewed by a colleague scientist and the head of the department of IMARES.

Approved: ~Name Researcher who read the report ~
~Function~

Signature:

Date: ~date~

Approved: F.C. Groenendijk, MSc.
Head of Department

Signature:

Date: 23-09-2013

Appendix 1. QuickBird and WorldView-2 files

| QuickBird | WorldView2 |
|--|--|
| <p>SATID>QB02</SATID> < MODE>FullSwath SCANDIRECTION>Forward CATID>10100100054F6500 FIRSTLINETIME>2006-11-10T15:10:04.339562Z <AVGLINERATE>1.725030000000000e+03 <EXPOSUREDURATION>5.7970000000000001e-04 <MINCOLLECTEDROWGSD>2.431000000000000e+00 <MAXCOLLECTEDROWGSD>2.431000000000000e+00 <MEANCOLLECTEDROWGSD>2.431000000000000e+00 <MINCOLLECTEDCOLGSD>2.447000000000000e+00 <MAXCOLLECTEDCOLGSD>2.448000000000000e+00 <MEANCOLLECTEDCOLGSD>2.448000000000000e+00 <MEANCOLLECTEDGSD>2.439000000000000e+00 <ROWUNCERTAINTY>3.417000000000000e+01 <COLUNCERTAINTY>3.401000000000000e+01 <MINSUNAZ>1.614000000000000e+02 <MAXSUNAZ>1.614000000000000e+02 <MEANSUNAZ>1.614000000000000e+02 <MINSUNEL>5.360000000000000e+01 <MAXSUNEL>5.370000000000000e+01 <MEANSUNEL>5.360000000000000e+01 <MINSATAZ>1.358000000000000e+02 <MAXSATAZ>1.587000000000000e+02 <MEANSATAZ>1.472000000000000e+02 <MINSATEL>8.5900000000000001e+01 <MAXSATEL>8.730000000000000e+01 <MEANSATEL>8.659999999999999e+01 <MININTRACKVIEWANGLE>-2.700000000000000e+00 <MAXINTRACKVIEWANGLE>-2.000000000000000e+00 <MEANINTRACKVIEWANGLE>-2.400000000000000e+00 <MINCROSSTRACKVIEWANGLE>1.800000000000000e+00 <MAXCROSSTRACKVIEWANGLE>2.000000000000000e+00 <MEANCROSSTRACKVIEWANGLE>1.900000000000000e+00 <MINOFFNADIRVIEWANGLE>2.900000000000000e+00 <MAXOFFNADIRVIEWANGLE>2.900000000000000e+00 <MEANOFFNADIRVIEWANGLE>2.900000000000000e+00 <PNIIRS>3.000000000000000e+00 <CLOUDCOVER>9.700000000000000e-02 <RESAMPLINGKERNEL>PS <TDILEVEL>13 <POSITIONKNOWLEDGESRC>R <ATTITUDEKNOWLEDGESRC>R <REVNUMBER>28450 </IMAGE> -<MAP_PROJECTED_PRODUCT> <EARLIESTACQTIME>2006-11-10T15:10:05.554420Z <LATESTACQTIME>2006-11-10T15:10:05.554420Z <DATUMNAME>WE <SEMIMAJORAXIS>6.378137000000000e+06 <INVERSEFLATTENING>2.982572235630000e+02 <DATUMOFFSETList> <DATUMOFFSET>0.000000000000000e+00 0.000000000000000e+00 0.000000000000000e+00 <MAPPROJNAME>UTM <MAPPROJCODE>1 <MAPZONE>20 <MAPHEMI>N <PRODUCTUNITS>M <ORIGINX>4.974420000000000e+05 <ORIGINY>1.938248399999999e+06 <ORIENTATIONANGLE>0.000000000000000e+00 <COLSPACING>2.400000000000000e+00 <ROWSPACING>2.400000000000000e+00 <PRODUCTGSD>2.400000000000000e+00 <ULX>4.974420000000000e+05 <ULY>1.938248399999999e+06 <ULH>-4.200000000000000e+01 <URX>5.070204000000000e+05 <URY>1.938248399999999e+06 <URH>-4.200000000000000e+01 <LRX>5.070204000000000e+05 <LRY>1.929968399999999e+06 <LRH>-4.200000000000000e+01 <LLX>4.974420000000000e+05 <LLY>1.929968399999999e+06 <LLH>-4.200000000000000e+01 <DEMCORRECTION>Coarse DEM <NUMGCP>0</NUMGCP> </MAP_PROJECTED_PRODUCT> </IMD> <TIL> <BANDID>Multi <NUMTILES>1 <TILESIZE>3992 <TILESIZE>3451 <TILEUNITS>Pixels <TILEOVERLAP>0</p> | <p>SATID:WV02 MODE: FullSwath SCANDIRECTION>Forward CATID>10300100081BAB00 FIRSTLINETIME: 2011-02-18 T15:07:20.621447Z <AVGLINERATE>5.000000000000000e+03 <EXPOSUREDURATION>2.000000000000000e-04 <MINCOLLECTEDROWGSD>1.848000000000000e+00 <MAXCOLLECTEDROWGSD>1.849000000000000e+00 <MEANCOLLECTEDROWGSD>1.848000000000000e+00 <MINCOLLECTEDCOLGSD>1.850000000000000e+00 <MAXCOLLECTEDCOLGSD>1.850000000000000e+00 <MEANCOLLECTEDCOLGSD>1.850000000000000e+00 <MEANCOLLECTEDGSD>1.849000000000000e+00 <ROWUNCERTAINTY>2.455000000000000e+01 <COLUNCERTAINTY>3.593000000000000e+01 <MINSUNAZ>1.449000000000000e+02 <MAXSUNAZ>1.449000000000000e+02 <MEANSUNAZ>1.449000000000000e+02 <MINSUNEL>5.510000000000000e+01 <MAXSUNEL>5.520000000000000e+01 <MEANSUNEL>5.510000000000000e+01 <MINSATAZ>2.178000000000000e+02 <MAXSATAZ>2.792000000000000e+02 <MEANSATAZ>2.414000000000000e+02 <MINSATEL>8.920000000000000e+01 <MAXSATEL>8.959999999999999e+01 <MEANSATEL>8.9400000000000001e+01 <MININTRACKVIEWANGLE>-3.000000000000000e-01 <MAXINTRACKVIEWANGLE>-1.000000000000000e-01 <MEANINTRACKVIEWANGLE>-2.000000000000000e-01 <MINCROSSTRACKVIEWANGLE>-4.000000000000000e-01 <MAXCROSSTRACKVIEWANGLE>-3.000000000000000e-01 <MEANCROSSTRACKVIEWANGLE>-4.000000000000000e-01 <MINOFFNADIRVIEWANGLE>4.000000000000000e-01 <MAXOFFNADIRVIEWANGLE>4.000000000000000e-01 <MEANOFFNADIRVIEWANGLE>4.000000000000000e-01 <PNIIRS>3.000000000000000e+00 <CLOUDCOVER>1.700000000000000e-02 <RESAMPLINGKERNEL>CC <POSITIONKNOWLEDGESRC>R <ATTITUDEKNOWLEDGESRC>R <REVNUMBER>7150 </IMAGE> -<MAP_PROJECTED_PRODUCT> <EARLIESTACQTIME>2011-02-18T15:07:21.095703Z <LATESTACQTIME>2011-02-18T15:07:21.095703Z <DATUMNAME>WE <SEMIMAJORAXIS>6.378137000000000e+06 <INVERSEFLATTENING>2.982572235630000e+02 <DATUMOFFSETList> <DATUMOFFSET>0.000000000000000e+00 0.000000000000000e+00 0.000000000000000e+00 <MAPPROJNAME>UTM <MAPPROJCODE>1 <MAPZONE>20 <MAPHEMI>N <PRODUCTUNITS>M <ORIGINX>4.973190000000000e+05 <ORIGINY>1.940608999999999e+06 <ORIENTATIONANGLE>0.000000000000000e+00 <COLSPACING>2.000000000000000e+00 <ROWSPACING>2.000000000000000e+00 <PRODUCTGSD>2.000000000000000e+00 <ULX>4.973190000000000e+05 <ULY>1.940608999999999e+06 <ULH>-4.200000000000000e+01 <URX>5.074350000000000e+05 <URY>1.940608999999999e+06 <URH>-4.200000000000000e+01 <LRX>5.074350000000000e+05 <LRY>1.928678999999999e+06 <LRH>-4.200000000000000e+01 <LLX>4.973190000000000e+05 <LLY>1.928678999999999e+06 <LLH>-4.200000000000000e+01 <DEMCORRECTION>Coarse DEM <NUMGCP>0 </MAP_PROJECTED_PRODUCT> </IMD> <TIL> <BANDID>Multi <NUMTILES>1 <TILESIZE>5059 <TILESIZE>5966 <TILEUNITS>Pixels <TILEOVERLAP>0</p> |

Appendix 2. Final table of field data points

| waypoint | depth (m) | Latitude | Longitude | habitat |
|----------|-----------|----------|-----------|-----------|
| 69 | 13 | 17.47002 | -62.94801 | coral |
| 70 | 20 | 17.46874 | -62.94729 | gorgonian |
| 71 | 23 | 17.46754 | -62.94663 | sand |
| 72 | 25 | 17.46682 | -62.94555 | rubble |
| 73 | 29 | 17.46605 | -62.94428 | coral |
| 74 | 29 | 17.4665 | -62.94355 | rubble |
| 75 | 25 | 17.4675 | -62.94522 | gorgonian |
| 76 | 22 | 17.46852 | -62.94643 | coral |
| 77 | 17 | 17.4708 | -62.94661 | gorgonian |
| 78 | 9 | 17.4724 | -62.9474 | gorgonian |
| 79 | 5 | 17.47326 | -62.94778 | coral |
| 80 | 22 | 17.46957 | -62.94466 | coral |
| 81 | 29 | 17.46733 | -62.94261 | algae |
| 82 | 27 | 17.46943 | -62.94136 | algae |
| 83 | 26 | 17.4702 | -62.94247 | coral |
| 84 | 22 | 17.47125 | -62.94393 | gorgonian |
| 85 | 17 | 17.47237 | -62.94549 | gorgonian |
| 86 | 11 | 17.47335 | -62.94647 | gorgonian |
| 87 | 5 | 17.47432 | -62.94742 | gorgonian |
| 88 | 7 | 17.47593 | -62.94662 | gorgonian |
| 89 | 11 | 17.47563 | -62.94499 | coral |
| 90 | 19 | 17.47461 | -62.94349 | sand |
| 91 | 24 | 17.4736 | -62.94206 | coral |
| 92 | 29 | 17.47224 | -62.94005 | algae |
| 93 | 27 | 17.47567 | -62.9399 | algae |
| 94 | 24 | 17.47593 | -62.94136 | gorgonian |
| 95 | 18 | 17.47622 | -62.94303 | gorgonian |
| 96 | 10 | 17.47711 | -62.94435 | gorgonian |
| 97 | 5 | 17.47814 | -62.94567 | algae |
| 98 | 5 | 17.46572 | -62.95994 | gorgonian |
| 99 | 12 | 17.46415 | -62.95962 | coral |
| 100 | 17 | 17.46278 | -62.95845 | sand |
| 101 | 21 | 17.46127 | -62.95729 | sand |
| 102 | 23 | 17.45794 | -62.9578 | sand |
| 103 | 30 | 17.45634 | -62.95733 | algae |
| 104 | 21 | 17.45959 | -62.95862 | sand |
| 105 | 18 | 17.46189 | -62.95917 | sand |
| 106 | 5 | 17.46494 | -62.9618 | gorgonian |
| 107 | 13 | 17.46327 | -62.96185 | sand |
| 108 | 18 | 17.46077 | -62.96112 | sand |
| 109 | 21 | 17.45803 | -62.96065 | sand |
| 110 | 30 | 17.45532 | -62.96028 | algae |
| 111 | 6 | 17.46415 | -62.96248 | gorgonian |
| 112 | 11 | 17.46318 | -62.96339 | gorgonian |
| 113 | 15 | 17.46182 | -62.96302 | gorgonian |
| 114 | 18 | 17.4609 | -62.96242 | algae |
| 115 | 19 | 17.45984 | -62.96187 | sand |
| 116 | 22 | 17.45775 | -62.96145 | sand |
| 117 | 26 | 17.45883 | -62.96162 | sand |
| 118 | 29 | 17.45674 | -62.96156 | sand |
| 120 | 25 | 17.45538 | -62.96259 | rubble |
| 121 | 30 | 17.45647 | -62.96329 | sand |
| 122 | 25 | 17.45771 | -62.96367 | sand |
| 123 | 20 | 17.45892 | -62.96388 | sand |
| 124 | 20 | 17.46003 | -62.96411 | seagrass |
| 125 | 18 | 17.46111 | -62.9644 | coral |
| 126 | 13 | 17.46224 | -62.96451 | coral |
| 127 | 9 | 17.46334 | -62.96436 | gorgonian |
| 128 | 5 | 17.46414 | -62.96427 | gorgonian |
| 129 | 5 | 17.46393 | -62.96545 | gorgonian |
| 130 | 10 | 17.46276 | -62.96579 | coral |
| 131 | 14 | 17.46174 | -62.9657 | gorgonian |
| 132 | 17 | 17.46067 | -62.96568 | coral |
| 133 | 20 | 17.45938 | -62.96596 | sand |
| 134 | 23 | 17.45852 | -62.9654 | algae |

| waypoint | depth (m) | Latitude | Longitude | habitat |
|----------|-----------|----------|-----------|-----------|
| 135 | 26 | 17.45765 | -62.96496 | sand |
| 136 | 29 | 17.45655 | -62.96472 | algae |
| 137 | 6 | 17.48113 | -62.94464 | algae |
| 138 | 9 | 17.48155 | -62.9433 | gorgonian |
| 139 | 15 | 17.48125 | -62.94175 | gorgonian |
| 140 | 28 | 17.48126 | -62.93998 | gorgonian |
| 141 | 29 | 17.48145 | -62.93798 | algae |
| 142 | 30 | 17.48125 | -62.93631 | algae |
| 143 | 30 | 17.48411 | -62.93714 | algae |
| 144 | 28 | 17.48414 | -62.93883 | algae |
| 145 | 20 | 17.4836 | -62.94092 | gorgonian |
| 146 | 10 | 17.48289 | -62.94295 | gorgonian |
| 147 | 6 | 17.48245 | -62.94428 | gorgonian |
| 148 | 6 | 17.48429 | -62.94488 | gorgonian |
| 149 | 9 | 17.4849 | -62.94336 | gorgonian |
| 150 | 13 | 17.48524 | -62.94195 | gorgonian |
| 151 | 22 | 17.4852 | -62.94051 | gorgonian |
| 152 | 25 | 17.48577 | -62.93921 | algae |
| 153 | 30 | 17.48667 | -62.93765 | sargassum |
| 154 | 28 | 17.48827 | -62.93919 | sargassum |
| 155 | 25 | 17.48775 | -62.94105 | gorgonian |
| 156 | 12 | 17.48731 | -62.9429 | gorgonian |
| 157 | 7 | 17.48681 | -62.94467 | gorgonian |
| 158 | 6 | 17.48849 | -62.9457 | gorgonian |
| 159 | 9 | 17.48879 | -62.94474 | gorgonian |
| 160 | 11 | 17.48903 | -62.94384 | gorgonian |
| 161 | 13 | 17.48921 | -62.94293 | gorgonian |
| 162 | 17 | 17.48942 | -62.94183 | gorgonian |
| 163 | 26 | 17.48913 | -62.94069 | rubble |
| 164 | 29 | 17.48955 | -62.93976 | coral |
| 165 | 27 | 17.49074 | -62.94106 | coral |
| 166 | 22 | 17.49041 | -62.94233 | gorgonian |
| 167 | 15 | 17.49006 | -62.94376 | gorgonian |
| 168 | 10 | 17.48972 | -62.94524 | gorgonian |
| 169 | 8 | 17.48956 | -62.9466 | gorgonian |
| 170 | 7 | 17.48922 | -62.94792 | sargassum |
| 171 | 5 | 17.46383 | -62.96703 | gorgonian |
| 172 | 9 | 17.46286 | -62.96722 | coral |
| 173 | 12 | 17.4618 | -62.96729 | coral |
| 174 | 17 | 17.46081 | -62.96722 | gorgonian |
| 175 | 20 | 17.45978 | -62.96713 | coral |
| 176 | 21 | 17.45877 | -62.96683 | algae |
| 177 | 21 | 17.45764 | -62.9667 | sand |
| 178 | 26 | 17.45662 | -62.96665 | sand |
| 179 | 34 | 17.45545 | -62.96659 | algae |
| 180 | 5 | 17.46406 | -62.96968 | gorgonian |
| 181 | 12 | 17.46274 | -62.97033 | sand |
| 182 | 18 | 17.46094 | -62.97057 | gorgonian |
| 183 | 28 | 17.45909 | -62.9705 | coral |
| 185 | 31 | 17.46043 | -62.97274 | coral |
| 186 | 23 | 17.46152 | -62.97236 | gorgonian |
| 187 | 12 | 17.46271 | -62.97264 | coral |
| 188 | 8 | 17.46342 | -62.97266 | gorgonian |
| 189 | 4 | 17.46414 | -62.97224 | sand |
| 190 | 4 | 17.46458 | -62.97515 | gorgonian |
| 191 | 7 | 17.46365 | -62.97528 | gorgonian |
| 192 | 13 | 17.46277 | -62.97522 | sand |
| 193 | 21 | 17.46158 | -62.97512 | seagrass |
| 196 | 23 | 17.4615 | -62.97689 | sand |
| 197 | 19 | 17.46167 | -62.97668 | sand |
| 198 | 17 | 17.46234 | -62.97737 | gorgonian |
| 199 | 15 | 17.46288 | -62.97728 | coral |
| 200 | 9 | 17.46372 | -62.97758 | sand |
| 201 | 6 | 17.46482 | -62.97707 | gorgonian |
| 202 | 4 | 17.4659 | -62.97826 | sand |

| waypoint | depth (m) | Latitude | Longitude | habitat |
|----------|-----------|----------|-----------|-----------|
| 203 | 8 | 17.46488 | -62.97853 | sand |
| 204 | 13 | 17.46395 | -62.979 | coral |
| 205 | 16 | 17.46283 | -62.97907 | coral |
| 206 | 19 | 17.4619 | -62.97911 | coral |
| 207 | 32 | 17.46129 | -62.97917 | coral |
| 208 | 19 | 17.46165 | -62.98202 | coral |
| 209 | 21 | 17.46196 | -62.98163 | coral |
| 210 | 20 | 17.46283 | -62.98129 | gorgonian |
| 211 | 16 | 17.46365 | -62.9808 | gorgonian |
| 212 | 14 | 17.46448 | -62.98035 | gorgonian |
| 213 | 10 | 17.46545 | -62.98001 | sand |
| 214 | 5 | 17.46638 | -62.97971 | sand |
| 215 | 5 | 17.48842 | -62.94582 | coral |
| 216 | 9 | 17.48896 | -62.94452 | gorgonian |
| 217 | 11 | 17.48923 | -62.94325 | gorgonian |
| 218 | 18 | 17.48944 | -62.94183 | coral |
| 219 | 27 | 17.48992 | -62.94049 | algae |
| 220 | 29 | 17.4903 | -62.93929 | algae |
| 221 | 30 | 17.49048 | -62.93822 | algae |
| 222 | 31 | 17.49268 | -62.93915 | algae |
| 223 | 29 | 17.49235 | -62.94048 | coral |
| 224 | 27 | 17.49181 | -62.94184 | algae |
| 225 | 20 | 17.4913 | -62.94297 | gorgonian |
| 226 | 18 | 17.49081 | -62.94411 | gorgonian |
| 227 | 11 | 17.49026 | -62.94527 | gorgonian |
| 228 | 8 | 17.48957 | -62.94642 | gorgonian |
| 229 | 7 | 17.48913 | -62.94748 | sand |
| 230 | 8 | 17.49101 | -62.94831 | gorgonian |
| 231 | 11 | 17.49151 | -62.94724 | gorgonian |
| 232 | 14 | 17.49169 | -62.94606 | gorgonian |
| 233 | 17 | 17.49181 | -62.94496 | gorgonian |
| 234 | 20 | 17.49211 | -62.94373 | gorgonian |
| 235 | 25 | 17.49237 | -62.9425 | coral |
| 236 | 27 | 17.49271 | -62.94122 | sargassum |
| 237 | 29 | 17.49355 | -62.94022 | sargassum |
| 238 | 31 | 17.49383 | -62.93902 | sargassum |
| 239 | 34 | 17.49616 | -62.94009 | sargassum |
| 240 | 30 | 17.49529 | -62.94108 | sargassum |
| 241 | 24 | 17.49452 | -62.94244 | sargassum |
| 242 | 20 | 17.49341 | -62.94472 | gorgonian |
| 243 | 16 | 17.4932 | -62.9459 | gorgonian |
| 244 | 17 | 17.4929 | -62.94702 | gorgonian |
| 245 | 13 | 17.49265 | -62.94808 | gorgonian |
| 246 | 7 | 17.49188 | -62.94891 | gorgonian |
| 247 | 6 | 17.49128 | -62.94955 | gorgonian |
| 248 | 5 | 17.46629 | -62.97877 | gorgonian |
| 249 | 9 | 17.46494 | -62.97959 | coral |
| 250 | 15 | 17.46359 | -62.98067 | coral |
| 251 | 20 | 17.46232 | -62.98153 | coral |
| 252 | 35 | 17.46043 | -62.98224 | coral |
| 253 | 21 | 17.46072 | -62.98433 | coral |
| 254 | 34 | 17.45912 | -62.98489 | rubble |
| 255 | 21 | 17.46111 | -62.98394 | coral |
| 256 | 18 | 17.46181 | -62.98356 | coral |
| 257 | 19 | 17.46249 | -62.9831 | coral |
| 258 | 15 | 17.46332 | -62.9826 | coral |
| 259 | 14 | 17.46397 | -62.98229 | coral |
| 260 | 15 | 17.46472 | -62.98179 | gorgonian |
| 261 | 13 | 17.46552 | -62.98142 | gorgonian |
| 262 | 9 | 17.46621 | -62.9809 | sand |
| 263 | 6 | 17.46685 | -62.98042 | sand |
| 264 | 6 | 17.46803 | -62.98201 | gorgonian |
| 265 | 11 | 17.46676 | -62.98253 | gorgonian |
| 266 | 15 | 17.46549 | -62.98354 | gorgonian |
| 267 | 17 | 17.46402 | -62.98417 | coral |
| 268 | 14 | 17.46285 | -62.98465 | coral |
| 269 | 21 | 17.46166 | -62.98554 | coral |

| waypoint | depth (m) | Latitude | Longitude | habitat |
|----------|-----------|----------|-----------|-----------|
| 270 | 25 | 17.46048 | -62.98619 | gorgonian |
| 271 | 36 | 17.4591 | -62.98647 | coral |
| 273 | 34 | 17.46007 | -62.98814 | algae |
| 274 | 23 | 17.46076 | -62.98789 | coral |
| 275 | 20 | 17.46158 | -62.98742 | coral |
| 276 | 19 | 17.46283 | -62.98712 | coral |
| 277 | 16 | 17.46401 | -62.98644 | gorgonian |
| 278 | 17 | 17.46508 | -62.98559 | coral |
| 279 | 17 | 17.46618 | -62.9847 | gorgonian |
| 280 | 11 | 17.46725 | -62.9837 | gorgonian |
| 281 | 9 | 17.46896 | -62.9838 | sand |
| 282 | 4 | 17.46989 | -62.98291 | sand |
| 283 | 6 | 17.47196 | -62.98549 | gorgonian |
| 284 | 10 | 17.4711 | -62.98588 | gorgonian |
| 285 | 14 | 17.47029 | -62.98666 | sand |
| 286 | 15 | 17.46937 | -62.98708 | sand |
| 287 | 18 | 17.46851 | -62.98782 | coral |
| 288 | 18 | 17.46747 | -62.98864 | coral |
| 289 | 20 | 17.46642 | -62.98966 | coral |
| 290 | 20 | 17.46551 | -62.99062 | coral |
| 291 | 26 | 17.46472 | -62.99189 | coral |
| 292 | 27 | 17.46413 | -62.99295 | algae |
| 293 | 27 | 17.46295 | -62.99407 | coral |
| 294 | 32 | 17.4623 | -62.99523 | coral |
| 295 | 32 | 17.46085 | -62.99196 | coral |
| 296 | 24 | 17.46215 | -62.9908 | coral |
| 297 | 21 | 17.46323 | -62.98918 | coral |
| 298 | 18 | 17.46521 | -62.98824 | coral |
| 299 | 19 | 17.46636 | -62.98762 | coral |
| 300 | 18 | 17.46727 | -62.98651 | gorgonian |
| 301 | 15 | 17.46881 | -62.98653 | sand |
| 302 | 13 | 17.46993 | -62.98539 | sand |
| 303 | 6 | 17.47074 | -62.98423 | gorgonian |
| 304 | 5 | 17.47371 | -62.98635 | gorgonian |
| 305 | 11 | 17.47295 | -62.98794 | gorgonian |
| 306 | 17 | 17.47137 | -62.98875 | sand |
| 307 | 19 | 17.4697 | -62.98952 | coral |
| 308 | 19 | 17.46835 | -62.9906 | gorgonian |
| 309 | 24 | 17.46672 | -62.99186 | coral |
| 310 | 25 | 17.46572 | -62.9935 | algae |
| 311 | 28 | 17.46457 | -62.995 | coral |
| 312 | 39 | 17.46322 | -62.9966 | coral |
| 313 | 30 | 17.46418 | -62.9991 | coral |
| 314 | 28 | 17.46489 | -62.99802 | algae |
| 315 | 28 | 17.4654 | -62.99728 | coral |
| 316 | 24 | 17.46603 | -62.99668 | coral |
| 317 | 25 | 17.46659 | -62.99632 | coral |
| 318 | 23 | 17.46732 | -62.99544 | coral |
| 319 | 24 | 17.46771 | -62.99435 | coral |
| 320 | 24 | 17.46851 | -62.99341 | coral |
| 321 | 20 | 17.46945 | -62.99253 | coral |
| 322 | 19 | 17.47068 | -62.99152 | coral |
| 323 | 20 | 17.47206 | -62.99102 | coral |
| 324 | 16 | 17.47303 | -62.99014 | gorgonian |
| 325 | 14 | 17.47415 | -62.98955 | coral |
| 326 | 12 | 17.47497 | -62.98869 | sand |
| 327 | 7 | 17.47584 | -62.98796 | sand |
| 328 | 6 | 17.47665 | -62.98724 | sand |
| 329 | 7 | 17.50544 | -63.00417 | sand |
| 330 | 11 | 17.50513 | -63.00536 | sand |
| 331 | 16 | 17.5047 | -63.0064 | sand |
| 332 | 25 | 17.50423 | -63.00743 | seagrass |
| 333 | 34 | 17.50359 | -63.00841 | seagrass |
| 334 | 34 | 17.50575 | -63.0091 | seagrass |
| 335 | 25 | 17.50614 | -63.00766 | seagrass |
| 336 | 14 | 17.50583 | -63.00614 | sand |
| 337 | 5 | 17.5054 | -63.00365 | algae |

| waypoint | depth (m) | Latitude | Longitude | habitat |
|----------|-----------|----------|-----------|-----------|
| 338 | 7 | 17.50754 | -63.00365 | sand |
| 339 | 12 | 17.50821 | -63.00499 | sand |
| 340 | 15 | 17.50866 | -63.00613 | sand |
| 341 | 20 | 17.50914 | -63.00744 | sand |
| 342 | 26 | 17.50967 | -63.00847 | seagrass |
| 343 | 28 | 17.51033 | -63.00969 | sand |
| 344 | 32 | 17.51101 | -63.01095 | coral |
| 345 | 32 | 17.51255 | -63.00991 | sand |
| 346 | 24 | 17.51169 | -63.0086 | sand |
| 347 | 20 | 17.51111 | -63.00739 | seagrass |
| 348 | 16 | 17.51059 | -63.00602 | seagrass |
| 349 | 13 | 17.50996 | -63.00473 | sand |
| 350 | 8 | 17.50973 | -63.00297 | sand |
| 351 | 11 | 17.51161 | -63.00213 | sand |
| 352 | 13 | 17.51196 | -63.00353 | sand |
| 353 | 14 | 17.51236 | -63.00464 | sand |
| 354 | 18 | 17.51288 | -63.00611 | sand |
| 355 | 22 | 17.51355 | -63.00753 | seagrass |
| 356 | 28 | 17.51429 | -63.00879 | seagrass |
| 358 | 6 | 17.51292 | -63.0006 | coral |
| 359 | 11 | 17.51328 | -63.00165 | sand |
| 360 | 13 | 17.5133 | -63.00276 | sand |
| 361 | 15 | 17.51317 | -63.00387 | sand |
| 362 | 17 | 17.51346 | -63.00485 | sand |
| 363 | 18 | 17.51388 | -63.00587 | sand |
| 364 | 22 | 17.51433 | -63.00699 | seagrass |
| 365 | 25 | 17.51446 | -63.0077 | seagrass |
| 366 | 36 | 17.51534 | -63.009 | seagrass |
| 367 | 32 | 17.51696 | -63.00812 | seagrass |
| 368 | 26 | 17.51604 | -63.00722 | sand |
| 369 | 22 | 17.51569 | -63.00619 | seagrass |
| 370 | 19 | 17.51545 | -63.00507 | seagrass |
| 371 | 16 | 17.51504 | -63.00388 | sand |
| 372 | 14 | 17.51448 | -63.00283 | sand |
| 373 | 10 | 17.51417 | -63.00155 | gorgonian |
| 374 | 6 | 17.51434 | -63.0008 | coral |
| 375 | 7 | 17.51605 | -63.00131 | coral |
| 376 | 14 | 17.51616 | -63.00244 | sand |
| 377 | 16 | 17.51664 | -63.00329 | sand |
| 378 | 19 | 17.51694 | -63.00439 | sand |
| 379 | 22 | 17.51739 | -63.00543 | sand |
| 380 | 26 | 17.51787 | -63.00638 | sand |
| 381 | 30 | 17.51864 | -63.00722 | sand |
| 382 | 30 | 17.52031 | -63.00663 | sand |
| 383 | 24 | 17.5196 | -63.00575 | sand |
| 384 | 21 | 17.5191 | -63.00485 | sand |
| 385 | 18 | 17.5185 | -63.0039 | sand |
| 386 | 16 | 17.51827 | -63.00251 | sand |
| 387 | 9 | 17.51775 | -63.00159 | coral |
| 388 | 8 | 17.51959 | -63.00098 | coral |
| 389 | 15 | 17.51994 | -63.00201 | sand |
| 390 | 19 | 17.52019 | -63.00334 | sand |
| 391 | 21 | 17.5208 | -63.00417 | sand |
| 392 | 25 | 17.52133 | -63.00505 | sand |
| 393 | 30 | 17.52175 | -63.00587 | sand |
| 394 | 31 | 17.52416 | -63.00562 | sand |
| 395 | 25 | 17.5232 | -63.0047 | sand |
| 396 | 22 | 17.52273 | -63.00381 | sand |
| 397 | 20 | 17.52212 | -63.00304 | sand |
| 398 | 17 | 17.52164 | -63.00215 | sand |
| 399 | 14 | 17.5215 | -63.00107 | coral |
| 400 | 12 | 17.52317 | -63.00023 | coral |
| 401 | 15 | 17.52354 | -63.00126 | seagrass |
| 402 | 18 | 17.52403 | -63.00221 | sand |
| 403 | 21 | 17.52443 | -63.00316 | sand |
| 404 | 25 | 17.52519 | -63.00404 | sand |
| 405 | 32 | 17.52536 | -63.00501 | sand |

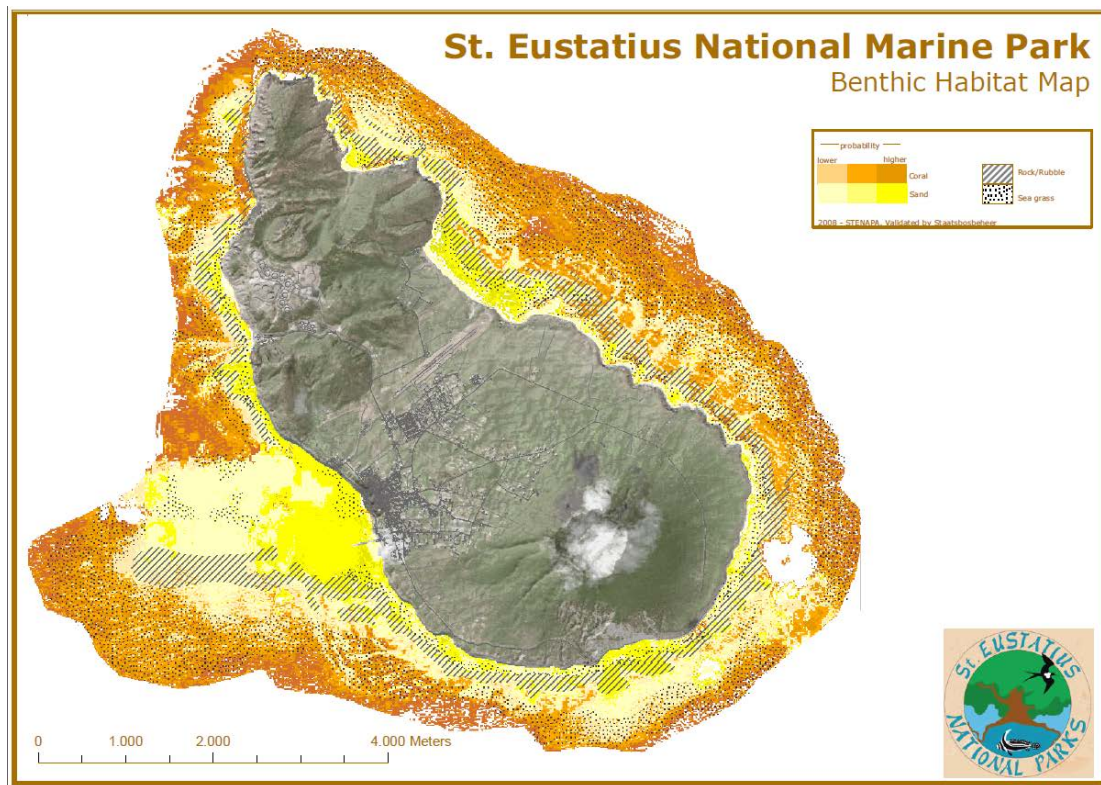
| waypoint | depth (m) | Latitude | Longitude | habitat |
|----------|-----------|----------|-----------|-----------|
| 406 | 32 | 17.5268 | -63.00332 | sand |
| 407 | 26 | 17.52592 | -63.00237 | sand |
| 408 | 21 | 17.52552 | -63.00118 | sand |
| 409 | 16 | 17.52489 | -63.00034 | sand |
| 410 | 10 | 17.52677 | -62.99862 | coral |
| 411 | 29 | 17.52691 | -62.99986 | coral |
| 412 | 29 | 17.52846 | -62.99806 | seagrass |
| 413 | 20 | 17.5271 | -62.99712 | coral |
| 414 | 31 | 17.52767 | -62.99381 | seagrass |
| 415 | 25 | 17.52675 | -62.99385 | coral |
| 416 | 18 | 17.52613 | -62.99264 | coral |
| 417 | 29 | 17.52706 | -62.99219 | sand |
| 418 | 24 | 17.52602 | -62.98985 | seagrass |
| 419 | 25 | 17.52561 | -62.99071 | sand |
| 420 | 28 | 17.52662 | -62.98701 | sand |
| 421 | 26 | 17.52608 | -62.98794 | seagrass |
| 422 | 24 | 17.52529 | -62.98861 | seagrass |
| 423 | 23 | 17.52465 | -62.98939 | sand |
| 424 | 20 | 17.52332 | -62.98845 | sand |
| 425 | 22 | 17.52373 | -62.98749 | sand |
| 426 | 25 | 17.52452 | -62.98682 | seagrass |
| 427 | 29 | 17.5254 | -62.98571 | sand |
| 428 | 30 | 17.52418 | -62.98416 | sand |
| 429 | 25 | 17.52338 | -62.98509 | seagrass |
| 430 | 22 | 17.5228 | -62.98601 | sand |
| 431 | 20 | 17.52233 | -62.98703 | sand |
| 432 | 18 | 17.52188 | -62.98798 | sand |
| 433 | 15 | 17.52124 | -62.9889 | coral |
| 434 | 14 | 17.51937 | -62.98787 | sand |
| 435 | 15 | 17.51997 | -62.98733 | sand |
| 436 | 18 | 17.5206 | -62.98648 | sand |
| 437 | 20 | 17.52125 | -62.98563 | sand |
| 438 | 23 | 17.52169 | -62.98463 | sand |
| 439 | 26 | 17.52244 | -62.98394 | sand |
| 440 | 29 | 17.52307 | -62.9826 | seagrass |
| 441 | 28 | 17.52155 | -62.98138 | seagrass |
| 442 | 24 | 17.52044 | -62.98243 | sand |
| 443 | 21 | 17.51996 | -62.9834 | sand |
| 444 | 20 | 17.51942 | -62.98443 | sand |
| 445 | 16 | 17.51877 | -62.98551 | sand |
| 446 | 14 | 17.51807 | -62.98648 | sand |
| 447 | 15 | 17.51757 | -62.985 | sand |
| 448 | 17 | 17.51763 | -62.9839 | sand |
| 449 | 19 | 17.51797 | -62.98279 | sand |
| 450 | 21 | 17.51858 | -62.98182 | sand |
| 451 | 23 | 17.51919 | -62.98102 | seagrass |
| 452 | 27 | 17.52033 | -62.97989 | seagrass |
| 453 | 30 | 17.52025 | -62.97794 | seagrass |
| 454 | 24 | 17.51939 | -62.9785 | seagrass |
| 455 | 22 | 17.51863 | -62.97925 | seagrass |
| 456 | 21 | 17.51793 | -62.9799 | seagrass |
| 458 | 8 | 17.47754 | -62.9886 | sand |
| 459 | 10 | 17.47693 | -62.98931 | sand |
| 460 | 14 | 17.47609 | -62.98989 | sand |
| 461 | 16 | 17.4753 | -62.99085 | gorgonian |
| 462 | 18 | 17.47455 | -62.99166 | sand |
| 463 | 19 | 17.47373 | -62.99211 | coral |
| 464 | 21 | 17.47293 | -62.99273 | coral |
| 465 | 24 | 17.47201 | -62.99321 | coral |
| 466 | 25 | 17.47117 | -62.99392 | coral |
| 467 | 25 | 17.47035 | -62.99462 | algae |
| 468 | 23 | 17.46952 | -62.99565 | rubble |
| 469 | 24 | 17.46865 | -62.99684 | coral |
| 470 | 24 | 17.46759 | -62.99778 | coral |
| 471 | 25 | 17.46651 | -62.99875 | coral |
| 472 | 28 | 17.46561 | -62.99987 | coral |
| 473 | 28 | 17.4646 | -63.00111 | coral |

| waypoint | depth (m) | Latitude | Longitude | habitat |
|----------|-----------|----------|-----------|-----------|
| 474 | 30 | 17.46419 | -63.00178 | coral |
| 475 | 30 | 17.46323 | -63.0038 | coral |
| 476 | 27 | 17.46461 | -63.00337 | coral |
| 477 | 24 | 17.466 | -63.00298 | coral |
| 478 | 26 | 17.4669 | -63.00187 | coral |
| 479 | 26 | 17.46788 | -63.00075 | coral |
| 480 | 25 | 17.46869 | -62.99971 | algae |
| 481 | 25 | 17.46965 | -62.99863 | coral |
| 482 | 23 | 17.47069 | -62.99755 | algae |
| 483 | 23 | 17.47172 | -62.99645 | algae |
| 484 | 23 | 17.47304 | -62.99573 | algae |
| 485 | 22 | 17.47417 | -62.99474 | sand |
| 486 | 21 | 17.47512 | -62.9935 | coral |
| 487 | 18 | 17.47597 | -62.99235 | sand |
| 488 | 15 | 17.47697 | -62.99129 | sand |
| 489 | 10 | 17.47805 | -62.98995 | sand |
| 490 | 7 | 17.47857 | -62.98895 | sand |
| 491 | 9 | 17.48013 | -62.99003 | sand |
| 492 | 13 | 17.47954 | -62.99128 | algae |
| 493 | 16 | 17.4785 | -62.99231 | sand |
| 494 | 18 | 17.47741 | -62.99346 | sand |
| 495 | 21 | 17.47657 | -62.99475 | sand |
| 496 | 23 | 17.47561 | -62.99588 | rubble |
| 497 | 23 | 17.47467 | -62.99701 | rubble |
| 498 | 22 | 17.47355 | -62.99789 | algae |
| 499 | 23 | 17.47254 | -62.99872 | algae |
| 500 | 25 | 17.47134 | -62.99957 | coral |
| 501 | 25 | 17.47047 | -63.00064 | coral |
| 502 | 24 | 17.46934 | -63.00169 | coral |
| 503 | 27 | 17.46829 | -63.00272 | coral |
| 504 | 28 | 17.46745 | -63.00374 | coral |
| 505 | 25 | 17.46621 | -63.00477 | coral |
| 506 | 23 | 17.46515 | -63.00514 | coral |
| 507 | 26 | 17.46384 | -63.00544 | coral |
| 508 | 34 | 17.46297 | -63.00578 | coral |
| 509 | 32 | 17.46291 | -63.00766 | coral |
| 510 | 22 | 17.46453 | -63.00688 | coral |
| 511 | 24 | 17.46601 | -63.00648 | coral |
| 512 | 25 | 17.46722 | -63.00559 | coral |
| 513 | 28 | 17.4684 | -63.00468 | coral |
| 514 | 24 | 17.46965 | -63.00401 | rubble |
| 515 | 23 | 17.47066 | -63.00299 | coral |
| 516 | 7 | 17.48135 | -62.99046 | sand |
| 517 | 11 | 17.48066 | -62.99137 | sand |
| 518 | 13 | 17.47983 | -62.99211 | sand |
| 519 | 17 | 17.47907 | -62.99313 | sand |
| 520 | 20 | 17.47842 | -62.99399 | sand |
| 521 | 22 | 17.47754 | -62.99502 | sand |
| 522 | 22 | 17.47659 | -62.99596 | sand |
| 523 | 24 | 17.47518 | -62.99717 | algae |
| 524 | 25 | 17.47405 | -62.9988 | algae |
| 525 | 25 | 17.47297 | -62.99988 | rubble |
| 526 | 25 | 17.47186 | -63.00129 | coral |
| 527 | 37 | 17.46293 | -63.0088 | coral |
| 528 | 30 | 17.46482 | -63.00808 | coral |
| 529 | 28 | 17.46606 | -63.00769 | coral |
| 530 | 26 | 17.46774 | -63.00662 | coral |
| 531 | 25 | 17.46934 | -63.00515 | coral |
| 532 | 24 | 17.47093 | -63.00453 | coral |
| 533 | 24 | 17.47221 | -63.00315 | coral |
| 534 | 24 | 17.47335 | -63.00153 | coral |
| 535 | 24 | 17.47445 | -63.00005 | algae |
| 536 | 24 | 17.47555 | -62.99872 | algae |
| 537 | 24 | 17.47669 | -62.99746 | rubble |
| 538 | 22 | 17.47764 | -62.99636 | rubble |
| 539 | 22 | 17.47847 | -62.99532 | rubble |
| 540 | 20 | 17.47932 | -62.99453 | gorgonian |

| waypoint | depth (m) | Latitude | Longitude | habitat |
|----------|-----------|----------|-----------|-----------|
| 541 | 15 | 17.48052 | -62.99322 | sand |
| 542 | 11 | 17.48133 | -62.99195 | sand |
| 543 | 7 | 17.48224 | -62.9908 | sand |
| 544 | 3 | 17.48386 | -62.99158 | sand |
| 545 | 9 | 17.48258 | -62.99269 | sand |
| 546 | 15 | 17.48177 | -62.99423 | seagrass |
| 547 | 20 | 17.48038 | -62.99574 | sand |
| 548 | 22 | 17.47894 | -62.99713 | rubble |
| 549 | 24 | 17.47805 | -62.99862 | rubble |
| 550 | 24 | 17.47667 | -63.0002 | algae |
| 551 | 24 | 17.4755 | -63.00165 | algae |
| 552 | 24 | 17.47413 | -63.00367 | coral |
| 553 | 24 | 17.47268 | -63.00547 | algae |
| 554 | 24 | 17.47045 | -63.00688 | coral |
| 555 | 26 | 17.46849 | -63.00769 | coral |
| 556 | 27 | 17.46645 | -63.00915 | coral |
| 557 | 31 | 17.46434 | -63.0098 | coral |
| 558 | 4 | 17.4852 | -62.99289 | sand |
| 559 | 10 | 17.48396 | -62.9941 | sand |
| 560 | 17 | 17.48267 | -62.99544 | sand |
| 561 | 22 | 17.48155 | -62.9969 | sand |
| 562 | 23 | 17.48039 | -62.99829 | rubble |
| 563 | 23 | 17.47937 | -62.99975 | algae |
| 564 | 23 | 17.47826 | -63.00132 | algae |
| 565 | 27 | 17.47538 | -63.00482 | coral |
| 566 | 26 | 17.47429 | -63.00635 | coral |
| 567 | 28 | 17.47267 | -63.00837 | coral |
| 570 | 4 | 17.48624 | -62.99447 | sand |
| 571 | 11 | 17.48528 | -62.99606 | sand |
| 572 | 20 | 17.48367 | -62.997 | sand |
| 573 | 23 | 17.48238 | -62.99831 | coral |
| 574 | 23 | 17.47966 | -63.00207 | sargassum |
| 575 | 26 | 17.47851 | -63.00363 | rubble |
| 576 | 26 | 17.47747 | -63.00538 | rubble |
| 577 | 26 | 17.47597 | -63.00645 | coral |
| 578 | 27 | 17.47489 | -63.00801 | coral |
| 579 | 27 | 17.47365 | -63.00943 | coral |
| 580 | 28 | 17.47227 | -63.01044 | coral |
| 581 | 27 | 17.47059 | -63.01104 | coral |
| 582 | 28 | 17.46895 | -63.01193 | coral |
| 583 | 28 | 17.46734 | -63.01263 | coral |
| 584 | 27 | 17.4659 | -63.01358 | coral |
| 585 | 28 | 17.46639 | -63.01554 | coral |
| 586 | 28 | 17.46816 | -63.01484 | coral |
| 587 | 29 | 17.46978 | -63.01428 | coral |
| 588 | 27 | 17.47133 | -63.01349 | coral |
| 589 | 27 | 17.47297 | -63.01282 | coral |
| 590 | 29 | 17.47432 | -63.01168 | algae |
| 591 | 27 | 17.47551 | -63.01029 | sand |
| 592 | 27 | 17.47665 | -63.00881 | algae |
| 593 | 27 | 17.47778 | -63.00743 | algae |
| 594 | 27 | 17.47921 | -63.0056 | rubble |
| 595 | 25 | 17.48032 | -63.00431 | algae |
| 596 | 22 | 17.48118 | -63.00259 | algae |
| 597 | 23 | 17.4826 | -63.00065 | rubble |
| 598 | 25 | 17.48373 | -62.99907 | algae |
| 599 | 19 | 17.48498 | -62.99787 | sand |
| 600 | 8 | 17.48645 | -62.99655 | sand |
| 601 | 5 | 17.4872 | -62.99636 | sand |

Appendix 3. Additional data

- Benthic Habitat Map from STENAPA and validated by Staatsbosbeheer



- Habitat map developed by Deltares for the environmental impact assessment of the St. Eustatia harbour extension (Deltares, 2011).
The table shows the total area per habitat in St. Eustatius per depth category.

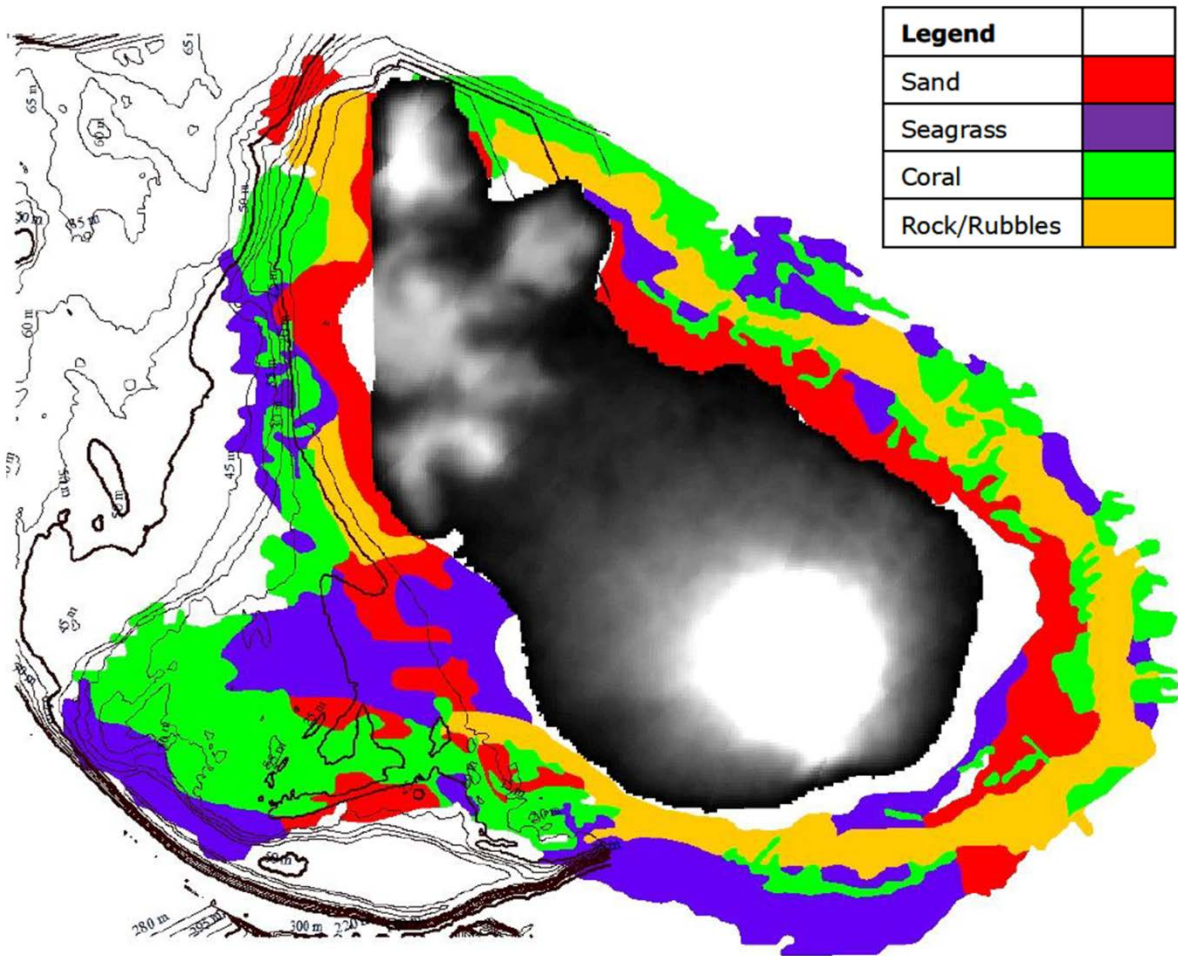
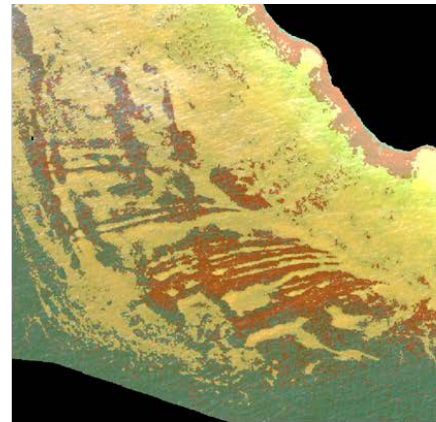
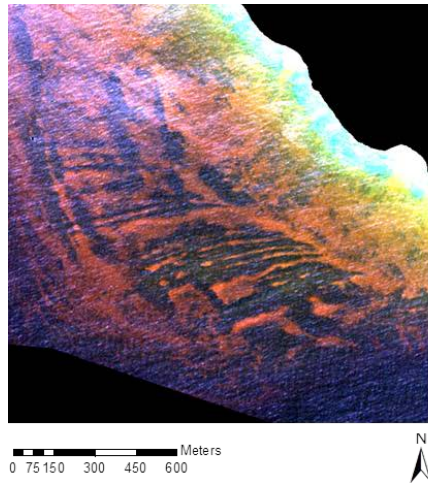


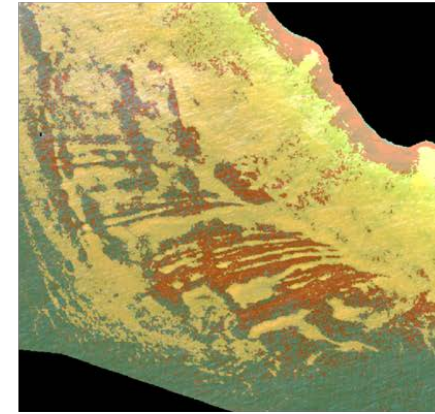
Table 4.1 total area per habitat in St. Eustatius per depth category

| Habitat | 10-25m | 25-35m | >35 | Total estimate |
|-------------|--------|--------|--------|----------------|
| Sand | 270 ha | 38 ha | | 308 ha |
| Seagrass | 520 ha | 15 ha | 500 ha | 1035 ha |
| Coral | 600 ha | 170 ha | 300 ha | 1070 ha |
| Rock/Rubble | 540 ha | | | 540 ha |

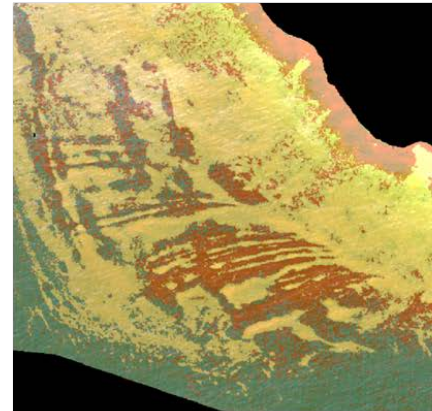
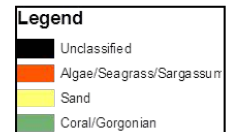
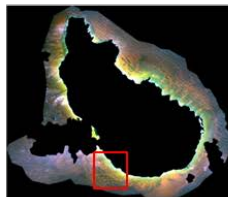
Appendix 4. Classifications zooms



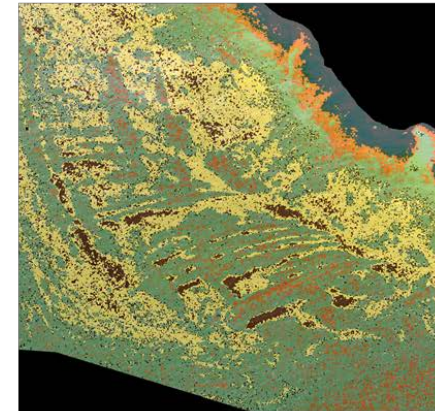
Dark pixel image classification



Sunlint image classification



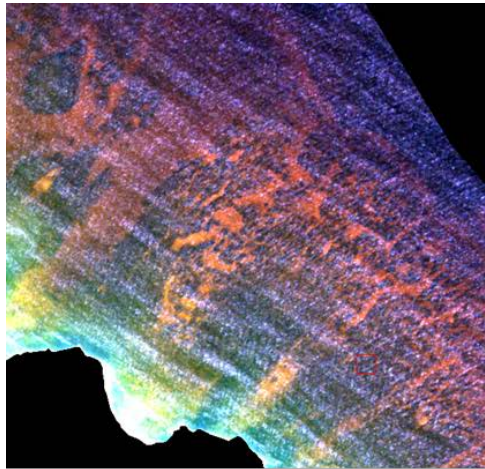
Depth invariant image classification
3 band ratio



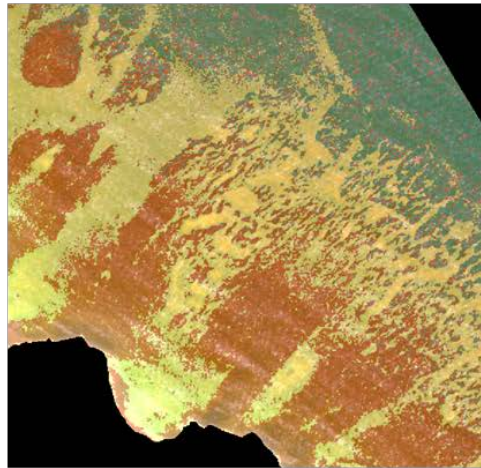
Depth invariant image classification
1 band ratio

QuickBird pixel based classification results

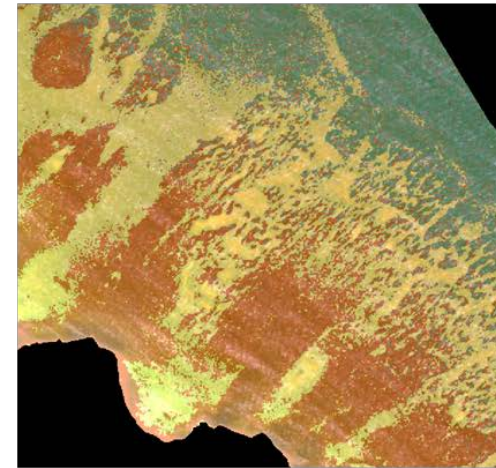
Close-up of classification results superimposed to the deglinted QuickBird image



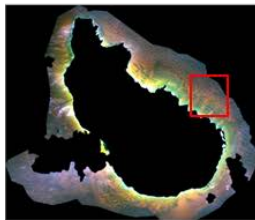
0 75 150 300 450 600 Meters



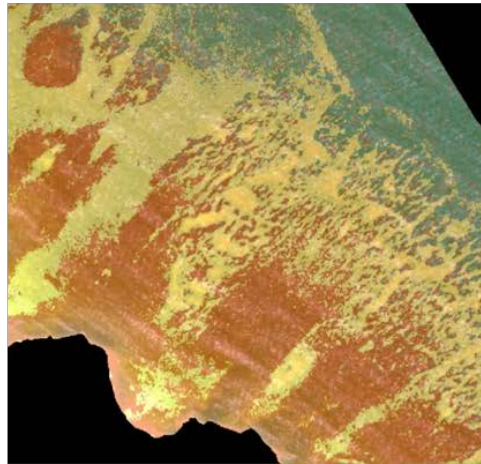
Dark pixel image classification



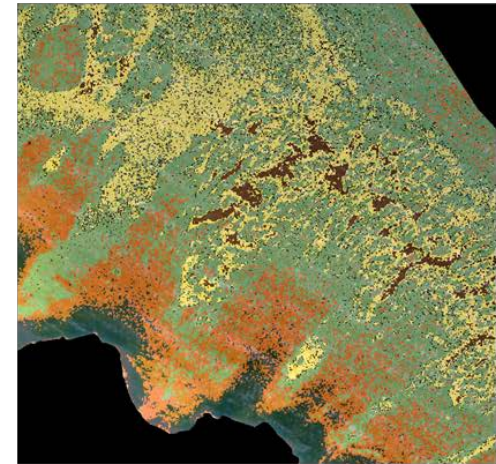
Sunglint image classification



| Legend | |
|--------|--------------------------|
| Black | Unclassified |
| Orange | Algae/Seagrass/Sargassum |
| Yellow | Sand |
| Green | Coral/Gorgonian |



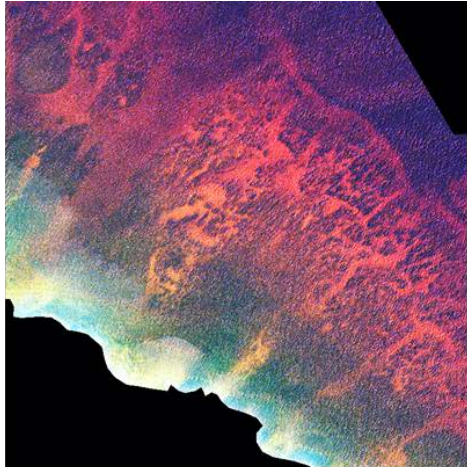
Depth invariant image classification
3 band ratio



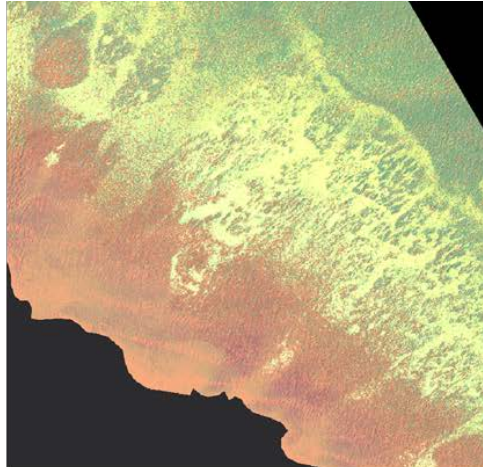
Depth invariant image classification
1 band ratio

QuickBird pixel based classification results

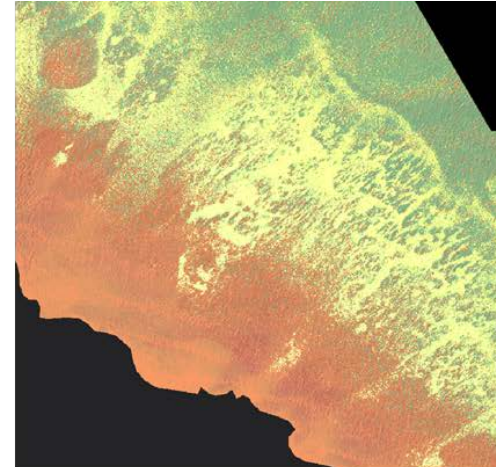
Close-up of classification results superimposed to the deglinted QuickBird image



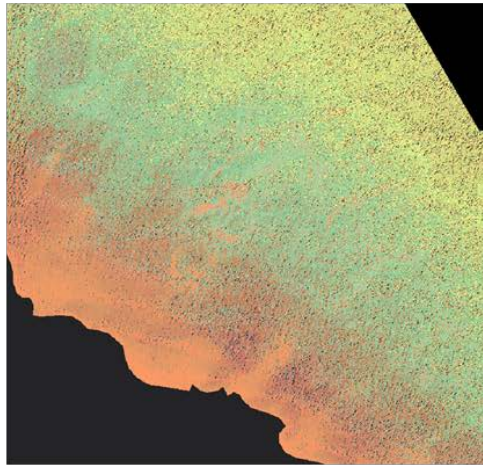
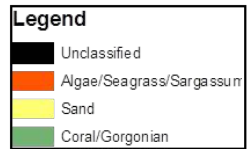
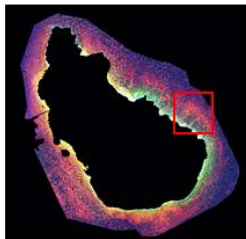
0 75 150 300 450 600 Meters



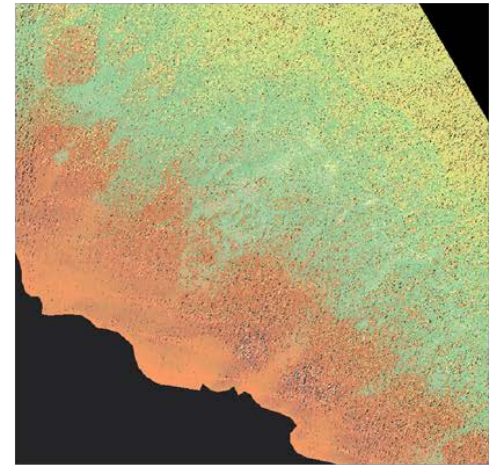
Dark pixel image classification



Sunlint image classification



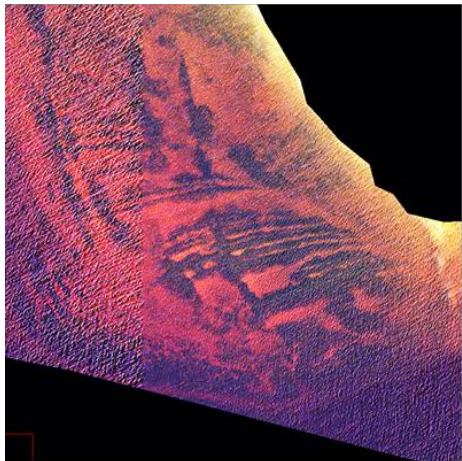
Depth invariant image classification
RGC



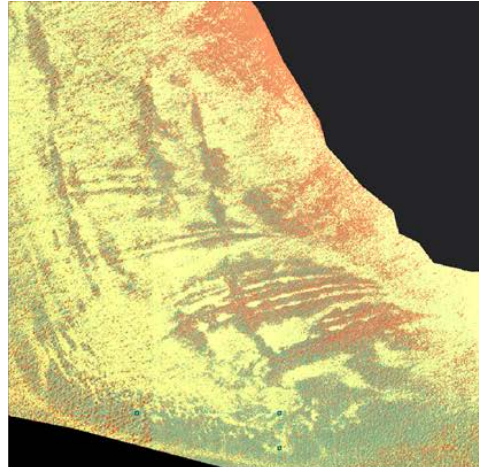
Depth invariant image classification
RGB

Worldview-2 pixel based classification results

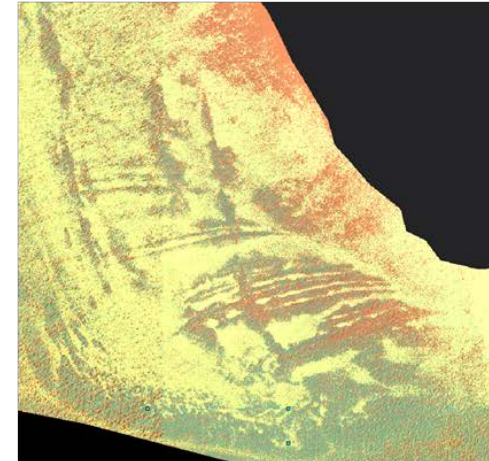
Close-up of classification results superimpose to the deglinted WV2 image



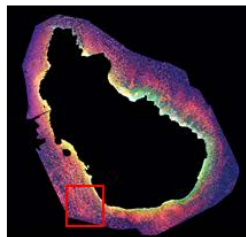
0 75 150 300 450 600 Meters



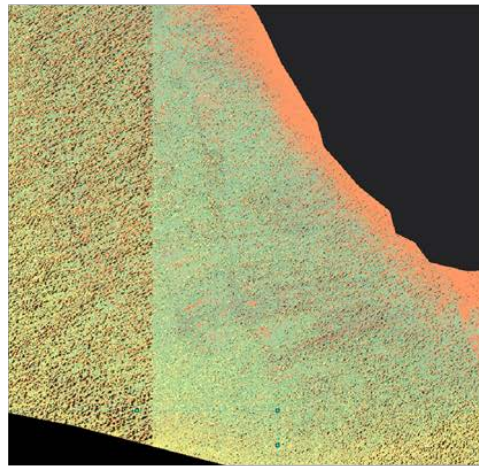
Dark pixel image classification



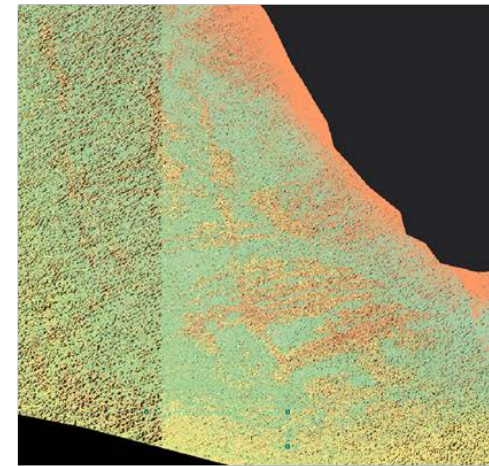
Sunlint image classification



| Legend | |
|--------|--------------------------|
| Black | Unclassified |
| Orange | Algae/Seagrass/Sargassum |
| Yellow | Sand |
| Green | Coral/Gorgonian |



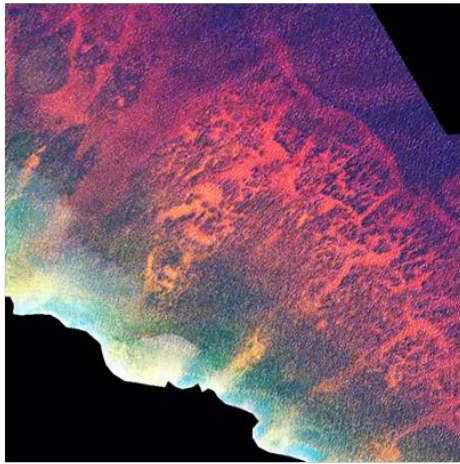
Depth invariant image classification
RGC



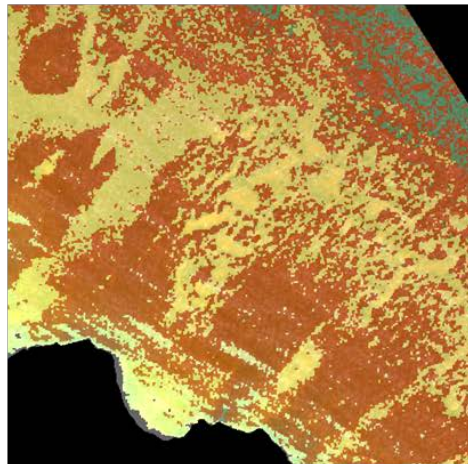
Depth invariant image classification
RGB

Worldview-2 pixel based classification results

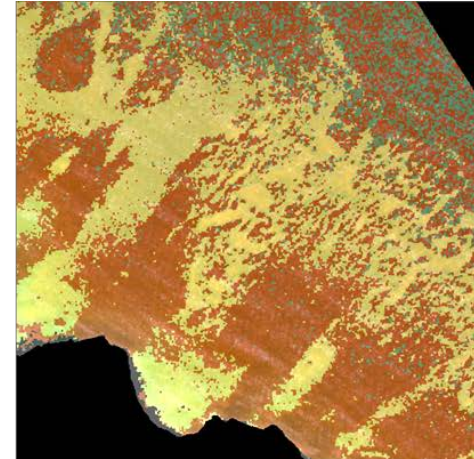
Close-up of classification results superimpose to the deglinted WV2 image



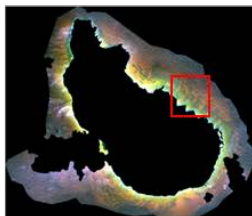
0 75 150 300 450 600 Meters



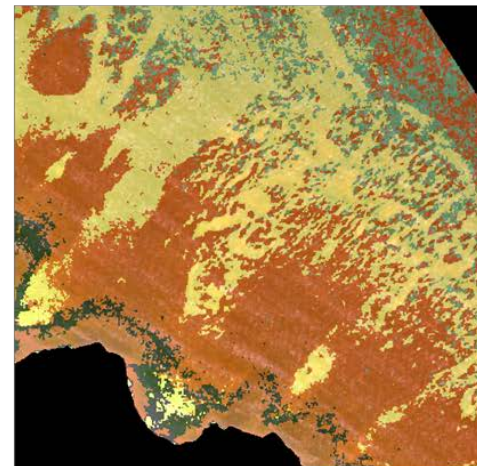
Dark pixel image classification



Sunlint image classification



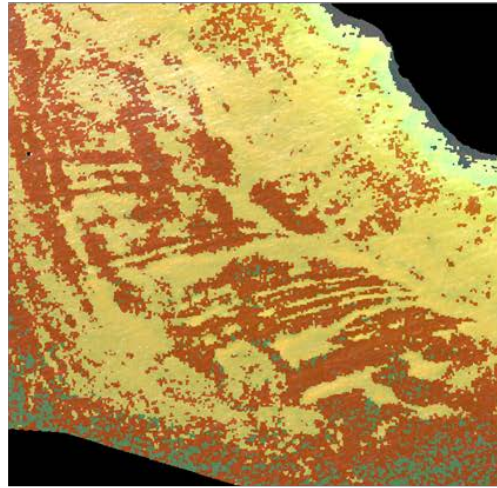
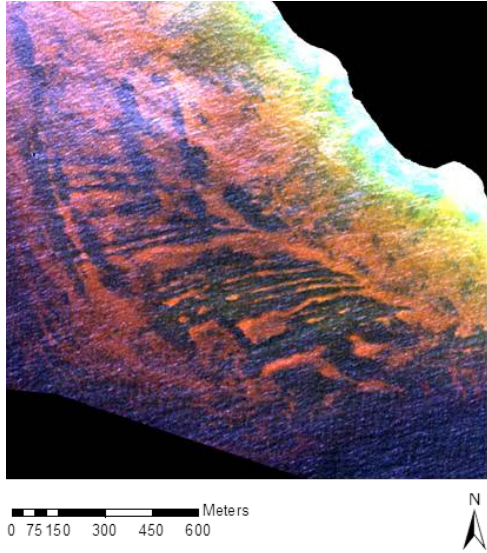
| Legend | |
|--------|--------------------------|
| Black | Unclassified |
| Orange | Algae/Seagrass/Sargassum |
| Yellow | Sand |
| Green | Coral/Gorgonian |



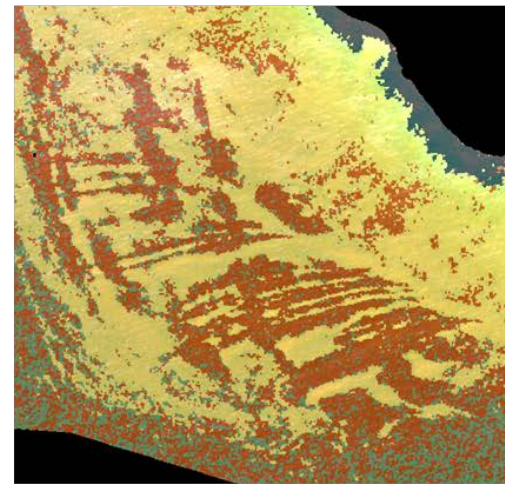
Depth invariant image classification
3 band ratio

QuickBird object based classification results

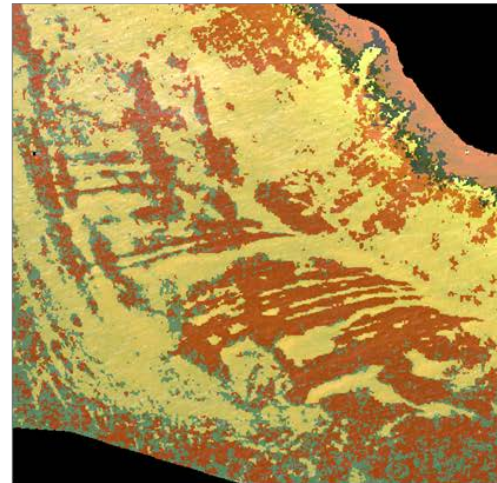
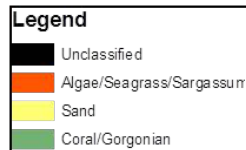
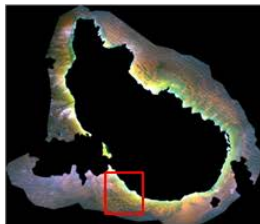
Close-up of classification results superimposed to the deglinted QuickBird image



Dark pixel image classification



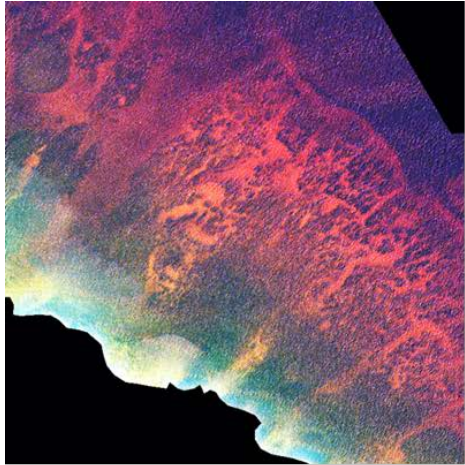
Sunlint image classification



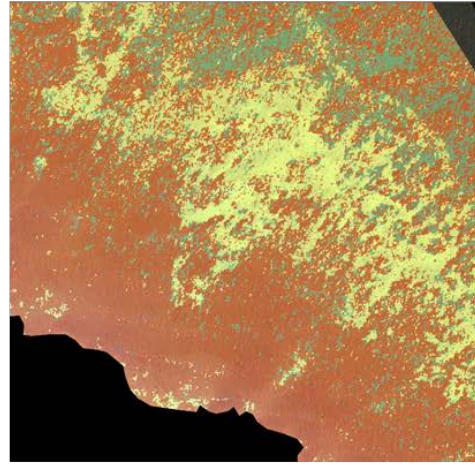
Depth invariant image classification
3 band ratio

QuickBird object based classification results

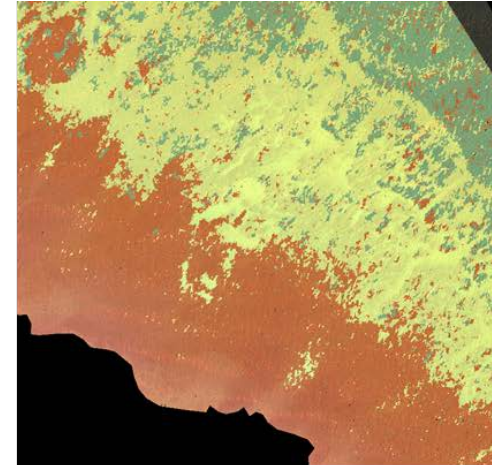
Close-up of classification results superimposed to the deglinted QuickBird image



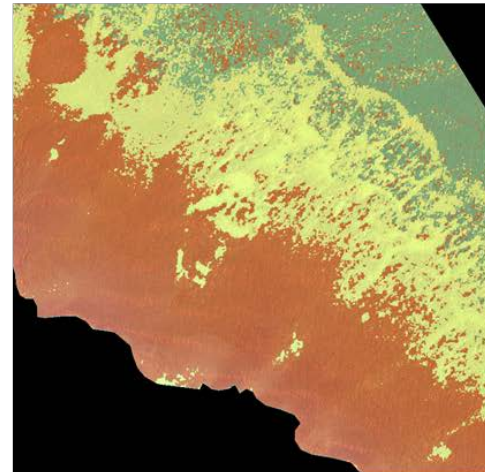
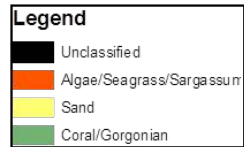
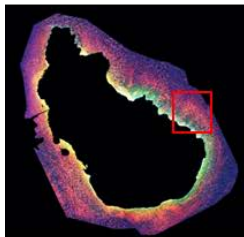
0 75 150 300 450 600 Meters



Dark pixel image classification



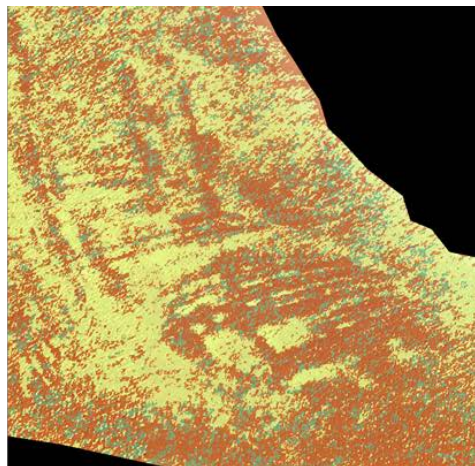
Sunlint image classification



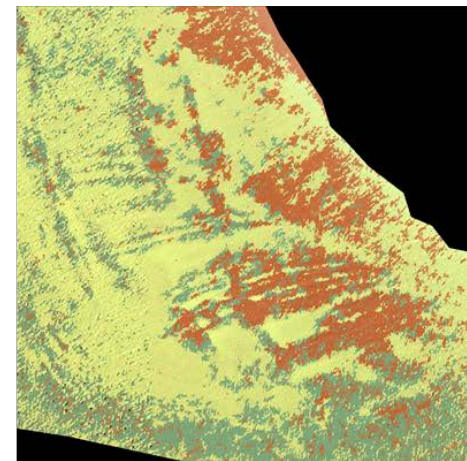
Depth invariant image classification
RGB band ratio

WorldView-2 object based classification results

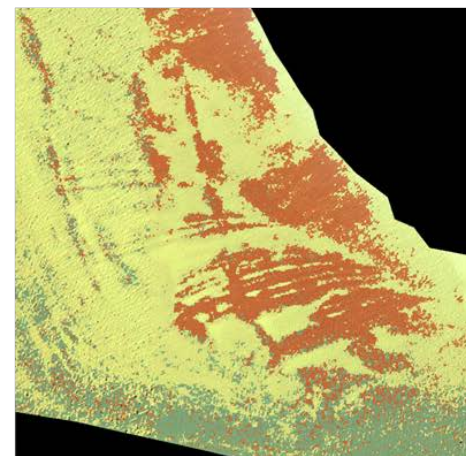
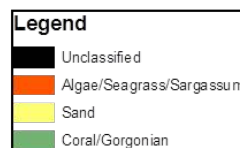
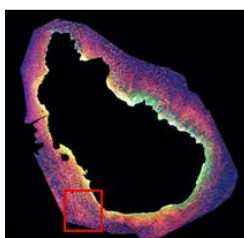
Close-up of classification results superimposed to the deglinted WorldView-2 image



Dark pixel image classification



Sunglint image classification



Depth invariant image classification
RGB band ratio

WorldView-2 object based classification results

Close-up of classification results superimposed to the deglinted WorldView-2 image

Appendix 5. Validation

This appendix contains all the validation results in the form of error matrices (which are discussed in chapter 5).

QuickBird Classification Results

- Radiance classification

Overall Accuracy = (94/205) 45.85%

Kappa Coefficient = 0.2358

| | | Ground Truth (validation points) | | | | |
|------------------|--------------------|----------------------------------|--------|--------|-------|----------|
| Classif. results | Classes | algae/seag. | coral | sand | Total | Accuracy |
| | Unclassified | 0 | 0 | 0 | 0 | 0.00% |
| | algae/seagrass | 24 | 36 | 13 | 73 | 32.88% |
| | coral | 6 | 37 | 2 | 45 | 82.22% |
| | sand | 6 | 48 | 33 | 87 | 37.93% |
| | Total | 36 | 121 | 48 | 205 | |
| | Reliability | 66.67% | 30.58% | 68.75% | | |

| Class | Commission | Omission | Prod. Acc. | User Acc. |
|----------------|------------|----------|------------|-----------|
| algae/seagrass | 67.12 | 33.33 | 66.67 | 32.88 |
| coral | 17.78 | 69.42 | 30.58 | 82.22 |
| sand | 62.07 | 31.25 | 68.75 | 39.93 |

- Darkest pixel correction

Overall Accuracy = (94/205) 45.85%

Kappa Coefficient = 0.2358

| | | Ground Truth (validation points) | | | | |
|------------------|--------------------|----------------------------------|--------|--------|-------|----------|
| Classif. results | Classes | algae/seag. | coral | sand | Total | Accuracy |
| | Unclassified | 0 | 0 | 0 | 0 | 0.00% |
| | algae/seagrass | 24 | 36 | 13 | 73 | 32.88% |
| | coral | 6 | 37 | 2 | 45 | 82.22% |
| | sand | 6 | 48 | 33 | 87 | 37.93% |
| | Total | 36 | 121 | 48 | 205 | |
| | Reliability | 66.67% | 30.58% | 68.75% | | |

| Class | Commission | Omission | Prod. Acc. | User Acc. |
|----------------|------------|----------|------------|-----------|
| algae/seagrass | 67.12 | 33.33 | 66.67 | 32.88 |
| coral | 17.78 | 69.42 | 30.58 | 82.22 |
| sand | 62.07 | 31.25 | 68.75 | 39.93 |

- Sunlint correction

Overall Accuracy = (101/205) 49.27%

Kappa Coefficient = 0.2819

| Ground Truth (validation points) | | | | | |
|----------------------------------|---------------|---------------|---------------|------------|----------|
| Classes | algae/seag. | coral | sand | Total | Accuracy |
| Unclassified | 0 | 0 | 0 | 0 | 0.00% |
| algae/seagrass | 26 | 40 | 12 | 78 | 32.88% |
| coral | 4 | 41 | 2 | 47 | 87.23% |
| sand | 6 | 40 | 34 | 80 | 42.50% |
| Total | 36 | 121 | 48 | 205 | |
| Reliability | 72.22% | 33.88% | 70.83% | | |

| Class | Commission | Omission | Prod. Acc. | User Acc. |
|----------------|------------|----------|------------|-----------|
| algae/seagrass | 66.67 | 27.78 | 72.22 | 33.33 |
| coral | 12.77 | 66.12 | 33.88 | 87.23 |
| sand | 57.50 | 29.17 | 70.83 | 42.50 |

- Depth invariant image (3 band ratio)

Overall Accuracy = (100/205) 48.78%

Kappa Coefficient = 0.2693

| Ground Truth (validation points) | | | | | |
|----------------------------------|---------------|---------------|---------------|------------|----------|
| Classes | algae/seag. | coral | sand | Total | Accuracy |
| Unclassified | 0 | 0 | 0 | 0 | 0.00% |
| algae/seagrass | 24 | 36 | 11 | 71 | 32.88% |
| coral | 6 | 41 | 2 | 49 | 82.22% |
| sand | 6 | 44 | 35 | 85 | 37.93% |
| Total | 36 | 121 | 48 | 205 | |
| Reliability | 66.67% | 33.88% | 72.92% | | |

| Class | Commission | Omission | Prod. Acc. | User Acc. |
|----------------|------------|----------|------------|-----------|
| algae/seagrass | 66.20 | 33.33 | 66.67 | 33.8 |
| coral | 16.33 | 66.12 | 33.88 | 83.67 |
| sand | 58.82 | 27.08 | 72.92 | 41.18 |

- Depth invariant image (1 band ratio)

Overall Accuracy = (65/205) 31.71%

Kappa Coefficient = 0.1104

| Ground Truth (validation points) | | | | | |
|----------------------------------|---------------|---------------|---------------|------------|----------|
| Classes | algae/seag. | coral | sand | Total | Accuracy |
| Unclassified | 2 | 13 | 14 | 29 | 0.00% |
| algae/seagrass | 18 | 64 | 9 | 91 | 19.78% |
| coral | 7 | 24 | 2 | 33 | 72.73% |
| sand | 9 | 20 | 23 | 52 | 44.23% |
| Total | 36 | 121 | 48 | 205 | |
| Reliability | 50.00% | 19.83% | 47.92% | | |

| Class | Commission | Omission | Prod. Acc. | User Acc. |
|----------------|------------|----------|------------|-----------|
| algae/seagrass | 80.22 | 50 | 50 | 19.78 |
| coral | 27.27 | 80.17 | 19.83 | 72.73 |
| sand | 55.77 | 52.08 | 47.92 | 44.23 |

Wv-2 Classification Results

- Radiance classification

Overall Accuracy = (73/160) 45.63%

Kappa Coefficient = 0.1760

Ground Truth (validation points)

| Classif. results | Classes | algae/seag. | coral | sand | Total | Accuracy |
|------------------|--------------------|-------------|--------|--------|-------|----------|
| | Unclassified | 0 | 0 | 0 | 0 | 0.00% |
| | algae/seagrass | 12 | 12 | 17 | 41 | 29.27% |
| | coral | 5 | 40 | 8 | 53 | 75.47% |
| | sand | 14 | 31 | 21 | 66 | 31.82% |
| | Total | 31 | 83 | 46 | 160 | |
| | Reliability | 38.71% | 48.19% | 45.65% | | |

| Class | Commission | Omission | Prod. Acc. | User Acc. |
|----------------|------------|----------|------------|-----------|
| algae/seagrass | 70.73 | 61.29 | 38.71 | 29.27 |
| coral | 24.53 | 51.81 | 48.19 | 75.47 |
| sand | 68.18 | 54.35 | 45.65 | 31.82 |

- Darkest pixel correction

Overall Accuracy = (73/160) 45.63%

Kappa Coefficient = 0.1760

Ground Truth (validation points)

| Class. results | Classes | algae/seag. | coral | sand | Total | Accuracy |
|----------------|--------------------|-------------|--------|--------|-------|----------|
| | Unclassified | 0 | 0 | 0 | 0 | 0.00% |
| | algae/seagrass | 12 | 12 | 17 | 41 | 29.27% |
| | coral | 5 | 40 | 8 | 53 | 75.47% |
| | sand | 14 | 31 | 21 | 66 | 31.82% |
| | Total | 31 | 83 | 46 | 160 | |
| | Reliability | 38.71% | 48.19% | 45.65% | | |

| Class | Commission | Omission | Prod. Acc. | User Acc. |
|----------------|------------|----------|------------|-----------|
| algae/seagrass | 70.73 | 61.29 | 38.71 | 29.27 |
| coral | 24.53 | 51.81 | 48.19 | 75.47 |
| sand | 68.18 | 54.35 | 45.65 | 31.82 |

- Sunlint correction

Overall Accuracy = (83/160) 51.88%

Kappa Coefficient = 0.2695

Ground Truth (validation points)

| Classif. results | Classes | algae/seag. | coral | sand | Total | Accuracy |
|------------------|--------------------|-------------|--------|--------|-------|----------|
| | Unclassified | 0 | 0 | 0 | 0 | 0.00% |
| | algae/seagrass | 16 | 15 | 18 | 49 | 32.65% |
| | coral | 4 | 46 | 7 | 57 | 80.70% |
| | sand | 11 | 22 | 21 | 54 | 38.89% |
| | Total | 31 | 83 | 46 | 160 | |
| | Reliability | 51.61% | 55.42% | 45.65% | | |

| Class | Commission | Omission | Prod. Acc. | User Acc. |
|----------------|------------|----------|------------|-----------|
| algae/seagrass | 67.35 | 48.39 | 51.61 | 32.65 |
| coral | 19.30 | 44.58 | 55.42 | 80.70 |
| sand | 61.11 | 54.35 | 45.65 | 38.89 |

- Depth invariant image (CG ratio)

Overall Accuracy = (66/160) 41.25%

Kappa Coefficient = 0.1595

| | | Ground Truth (validation points) | | | | |
|------------------|--------------------|----------------------------------|--------|--------|-------|----------|
| Classif. results | Classes | algae/seag. | coral | sand | Total | Accuracy |
| | Unclassified | 5 | 7 | 4 | 16 | 0.00% |
| | algae/seagrass | 9 | 11 | 14 | 34 | 26.47% |
| | coral | 2 | 35 | 6 | 43 | 81.40% |
| | sand | 15 | 30 | 22 | 67 | 32.84% |
| | Total | 31 | 83 | 46 | 160 | |
| | Reliability | 29.03% | 42.17% | 47.83% | | |

| Class | Commission | Omission | Prod. Acc. | User Acc. |
|----------------|------------|----------|------------|-----------|
| algae/seagrass | 73.53 | 70.97 | 29.03 | 26.47 |
| coral | 18.60 | 57.83 | 42.17 | 81.40 |
| sand | 67.16 | 52.17 | 47.83 | 32.84 |

- Depth invariant image (BG ratio)

Overall Accuracy = (70/160) 43.75%

Kappa Coefficient = 0.1797

| | | Ground Truth (validation points) | | | | |
|------------------|--------------------|----------------------------------|--------|--------|-------|----------|
| Classif. results | Classes | algae/seag. | coral | sand | Total | Accuracy |
| | Unclassified | 5 | 7 | 4 | 16 | 0.00% |
| | algae/seagrass | 7 | 10 | 14 | 31 | 22.58% |
| | coral | 6 | 40 | 5 | 51 | 78.43% |
| | sand | 13 | 26 | 23 | 62 | 37.10% |
| | Total | 31 | 83 | 46 | 160 | |
| | Reliability | 22.58% | 48.19% | 50.00% | | |

| Class | Commission | Omission | Prod. Acc. | User Acc. |
|----------------|------------|----------|------------|-----------|
| algae/seagrass | 77.42 | 77.42 | 22.58 | 22.58 |
| coral | 21.57 | 51.81 | 48.19 | 78.43 |
| sand | 62.9 | 50.00 | 50.00 | 37.10 |